

CRANFIELD UNIVERSITY

Steven Andrew Fowler

THE DEVELOPMENT OF SENSORS FOR THE DETECTION OF CLINICALLY
RELEVANT SUBSTANCES USING MOLECULAR IMPRINTING

CRANFIELD HEALTH

PhD THESIS

CRANFIELD UNIVERSITY

CRANFIELD HEALTH

PhD THESIS

Academic year 2006 – 2009

Steven Andrew Fowler

THE DEVELOPMENT OF SENSORS FOR THE DETECTION OF CLINICALLY
RELEVANT SUBSTANCES USING MOLECULAR IMPRINTING

Supervisor: Professor Sergey Piletsky
Industrial supervisor: Dr Peter Laitenberger

Presented 2009

This thesis is submitted in partial fulfilment of the requirements for the Degree of
Doctor of Philosophy (PhD)

© Cranfield University, 2009. All rights reserved. No part of this publication may be
reproduced without the written permission of the copyright holder.

Abstract

This thesis investigates the development of sensing devices based on molecularly imprinted polymers for the detection of clinically relevant analytes. Three analytes were considered, metronidazole, creatinine and propofol.

A molecularly imprinted polymer (MIP) was computationally designed for metronidazole and tested using SPE techniques. This polymer was then grafted onto a transducer surface using an immobilised initiator. Amperometric and impedance detection of metronidazole were investigated.

The capacitive detection of creatinine was reproduced from the literature (Panasyuk-Delaney et al., 2002) as this approach could be applied to other MIPs to form a universal platform for sensor development. However, the sensors produced using this methodology were difficult to reproduce and attempts to improve them were unsuccessful. A model for capacitive electrodes was developed to explain the obtained results.

To address the key challenges found in the aforementioned work, a dual polymerisable monomer was used as a conductive anchor for the amperometric and impedance detection of propofol. The developed amperometric sensors demonstrated very high sensitivity (limit of detection was below 5 μM), although the electrodes lacked in selectivity.

In conclusion, this thesis illustrates some of the key areas which need to be considered in the development of MIP-based devices and investigates some innovative solutions to these problems.

Acknowledgements

I would like to thank my supervisor, Professor S. Piletsky for all his support and guidance during this PhD. In addition, I would like to thank all of the staff within the Smart Materials group, especially Dr M. Whitcombe for his advice on chemistry, Dr K. Karim for his support and Dr E. Piletska and Dr I. Chianella for all their help in the laboratory.

I would like to extend my gratitude to Sphere Medical for their support and use of their facilities and knowledge, particularly to Dr P. Laitenberger who has always been willing to find the time to assist and guide me.

I would like to thank Health Technologies (Knowledge Transfer Network), without whom this project would not have been possible.

Penultimately, I would like to thank my friends who have helped me to maintain a modicum of sanity during this PhD. Especially those in the laboratory (Antonio, Prota, Guapa, Cookie, Ternura and ‘the Greeks’) for their humour and motivation, and Olivier for the some of the best advice I could have received.

Finally, to my family for always being there, especially Kat without whom this would not have been possible.

List of contents

Abstract	i
Acknowledgements.....	ii
List of contents	iii
List of tables	vii
List of figures	viii
Notation.....	xvi
Chapter 1 - Introduction.....	1
Chapter 2 - Review of clinical sensing devices and their technology	3
2.1 Introduction.....	3
2.2 Sensors for clinical analysis.....	3
2.3 Targets	7
2.3.1 Blood gas.....	8
2.3.2 Electrolytes.....	9
2.3.3 Metabolites.....	10
2.4 Detection Methods	15
2.4.1 Potentiometry	15
2.4.2 Voltammetry.....	16
2.4.3 Stripping Voltammetry	18
2.4.4 Amperometry.....	20
2.4.5 Impedance	20
2.5 Transducers	22
2.5.1 Material	22
2.5.2 Surface modification.....	24
2.5.3 Geometry.....	24
2.6 Recognition systems.....	25
2.6.1 Enzyme.....	25
2.6.2 Immunosensors.....	26
2.6.3 Molecularly imprinted polymers	28
2.6.4 Conclusions on clinical sensing technology.....	29

Chapter 3 - Conductometric detection of propofol using molecular imprinting	31
3.1 Introduction.....	31
3.1.1 A review of propofol and its detection	31
3.2 Investigations into the use of molecularly imprinted polymers for the detection of propofol.....	32
3.2.1 Impedance monitoring and strategies for MIP immobilisation.....	33
3.2.2 Sensors	33
3.2.3 Polymer immobilisation.....	34
3.2.4 Impedance monitoring	38
3.2.5 Investigatory procedures	39
3.3 Results of impedance monitoring for immobilised MIP	40
3.3.1 Investigation of Abtech sensors with photografted MIP films.....	40
3.3.2 Initial investigation of deposited MIP films on microchip sensors.....	42
3.3.3 Discussion of impedance monitoring using MIP-coated electrodes ...	43
3.3.4 Deposited MIP on microchip electrodes.....	44
3.3.5 Conclusion of impedance monitored MIP	44
3.4 Investigation of MIP immobilisation procedure on microchip device.....	44
3.4.1 Analysis techniques for investigating immobilised MIP	45
3.4.2 Results of measurements using MIP-coated microchip device.....	47
3.4.3 Discussion of MIP immobilisation of microchip devices.....	52
3.4.4 Conclusion of MIP immobilised on microchip device	53
3.5 Conclusions on the conductometric detection of propofol	53
Chapter 4 - Developing a molecularly imprinted polymer for the detection of antibiotics	54
4.1 Introduction.....	54
4.2 Selection of antibiotic for development in MIP based sensor	54
4.2.1 Review of MIP design	54
4.2.2 Overview of the proposed antibiotics	56
4.3 Antibiotic selection.....	60
4.3.1 Methodologies for antibiotic selection.....	60
4.3.2 Results of antibiotic selection.....	61
4.3.3 Discussion of antibiotic and monomer selection.....	64
4.3.4 Conclusion of antibiotic selection	65
4.4 Computational design and testing of MIP with selective properties for metronidazole	65

4.4.1	Investigatory techniques	65
4.4.2	Result of MIP design and testing.....	68
4.4.3	Discussion of MIP design and testing.....	74
4.4.4	Conclusion.....	74
4.5	Investigation into the detection of metronidazole using immobilised MIP.	75
4.5.1	Methodologies for the immobilisation and detection of metronidazole	75
4.5.2	Results of the immobilisation and detection of metronidazole	77
4.5.3	Discussion	85
4.5.4	Conclusion of metronidazole detection and MIP grafting	86
4.6	Chapter conclusion	87
Chapter 5 - Exploration into the capacitive detection of therapeutic compounds using molecularly imprinting technology.....		88
5.1	Introduction.....	88
5.2	Review of capacitive sensors	88
5.2.1	Capacitive devices using molecularly imprinted polymers	90
5.3	Reproduction of a capacitive MIP device for the detection of creatinine. ..	95
5.3.1	Methodology	95
5.3.2	Results of reproduced creatinine specific capacitive device.....	98
5.3.3	Discussion on the performance of the capacitive creatinine devices	104
5.3.4	Conclusion.....	106
5.4	Investigation of an improved creatinine selective device.....	106
5.4.1	Surface pre-treatment for thiol self-assembly	106
5.4.2	Improved methodology for capacitive detection of creatinine.....	107
5.4.3	Results of improved methodology for creatinine detection	108
5.4.4	Discussion of improved methodology for creatinine detection.....	109
5.4.5	Conclusion of improved methodology for the detection of creatinine	113
5.5	Conclusion of the capacitive detection of creatinine.....	114
Chapter 6 - Detection of propofol with the controlled growth of MIP onto a conducting polymer anchor.....		115
6.1	Introduction.....	115
6.2	Review of relevant compounds and their chemistry	115
6.2.1	Iniferters	115
6.2.2	N-phenylethylene diamine methacrylamide (NPEDMA).....	117
6.3	Growing polymer from an electropolymerised NPEDMA layer	120

6.3.1	Methodology of polymer immobilisation with a NPEDMA anchor .	120
6.3.2	Results of polymer immobilisation with a NPEDMA anchor.....	123
6.3.3	Discussion of polymer immobilisation with a NPEDMA anchor	126
6.3.4	Conclusion of polymer immobilisation with NPEDMA anchor	127
6.4	Impedance detection of creatinine and propofol with NPEDMA anchored MIP	127
6.4.1	Methodology for the impedance detection of creatinine and propofol	127
6.4.2	Results of the impedance detection of creatinine and NPEDMA	128
6.4.3	Discussion on the impedance detection of creatinine and propofol ..	130
6.4.4	Conclusion on the impedance detection of creatinine and propofol .	130
6.5	The electrochemical detection of propofol	131
6.5.1	Methodology for detection of propofol.....	131
6.5.2	Results of the investigation into the detection of propofol	132
6.5.3	Discussion of the electrochemical detection of propofol.....	140
6.5.4	Conclusion on the electrochemical detection of propofol	142
6.6	Investigation into the amperometric detection of propofol with a MIP covered electrode	142
6.6.1	Methodology for the amperometric detection of propofol.....	143
6.6.2	Results from the detection of propofol	144
6.6.3	Discussion of the selective detection of propofol.....	151
6.6.4	Conclusion on detection of propofol	152
6.7	Chapter conclusion	153
Chapter 7 - General conclusion and further work		155
7.1	General conclusion	155
7.2	Suggestions for further work.....	157
Reference.....		159
Publications		174

List of tables

Table 2.1 – Summary of VIA Medical’s blood gas and electrolyte monitoring systems analytes. Including the analyte range and sensitivity. {Skoog, 2000 #144}.....	6
Table 2.2 – Normal range values for blood-gas and electrolyte measurements. a {Meyerhoff, 1993 #249}, b {Pfeiffer, 1997 #71}, c {Berger, 1997 #56}, d {Eggenstein, 1999 #274} and e {Berberich, 2005 #32}.....	8
Table 2.3 – Examples of enzymes, reactions and buffer solutions used in the production of metabolite sensors {Suzuki, 2001 #34}. Activity is quoted in enzyme units per cm ²	11
Table 2.4 – A summary of stripping analysis techniques {Wang, 2000 #3}.....	19
Table 3.1 – Propofol polymerisation mixture.....	33
Table 3.2 – Composition of grafting polymerisation mixture.....	36
Table 3.3 – Protocol for deposition of NIP and MIP mixtures.	38
Table 4.1 – Table of top five computationally calculated monomers with the strongest binding for metronidazole, gentamicin and cefoxitin. <i>Value in brackets is the binding score (Kcal/mol)</i> . (DEAEM – 2-diethylaminoethyl methacrylate, EGMP – ethylene glycol methacrylate phosphate, VP – vinylpyridine, AMPSA – 2-acrylamido-2-methyl-1-propanesulphonic acid).....	61
Table 4.2 – Table of NIP compositions for highest binding monomers from computational analysis (monomer : cross-linker, 1:4.2). Initiator – 2-2-dimethoxy-2-phenylacetopenon, cross-linker – EGDMA, porogen – DMF.....	66
Table 4.3 – Table of MIP compositions based on EGMP and itaconic acid monomers for the selective binding of metronidazole. Initiator – AIBN, cross-linker – EGDMA, porogen – DMF.....	73
Table 4.4 – Composition of grafting polymerisation mixture (template : monomer : cross-linker, 2:2:17).....	76
Table 5.1 – Summary of MIP-based capacitive devices. (CV – cyclic voltammetry, MBI – mercaptobenzimidazole, DA – Dopamine, SAM – self assembled monolayer, MBA – N,N-methylenediacrylamide, AMPS – 2-acrylamido-2-methyl-1-propane sulfonic acid, <i>o</i> -PD – <i>o</i> -phenylenediamine).....	92
Table 5.2 – Composition of creatinine-imprinted polymer.....	96
Table 6.1 – Propofol polymerisation mixture.....	122

List of figures

Figure 2.1 – Illustration of complications occurring from the positioning of implanted clinical devices, a) Platelet adhesion, b) the ‘wall effect’ and c) vasoconstriction. {Frost, 2002 #128}.....	4
Figure 2.2 – Schematic of potentiometric electrochemical cell as illustrated {Wang, 2000 #3}.....	15
Figure 2.3 – Schematic of electrochemical system and its corresponding circuit.....	21
Figure 2.4 – Potential windows of platinum, mercury and carbon electrodes in various electrolytes. {Wang, 2006 #63}	23
Figure 2.5 – Two immunosensor strategies; a) sandwich technique and b) competitive technique	27
Figure 2.6 – Illustration of the preparation of molecular imprinted polymers.....	28
Figure 3.1 – The structure of propofol.....	31
Figure 3.2 – Schematic representation of microchip with its two sensor configurations. The parallel electrodes are highlighted on the right.	34
Figure 3.3 – Covalent immobilisation of vinyl groups onto SiO ₂ surface. a) activation of silanol groups, b) derivatisation of surface with vinyl-silane and c) free radical formation in polymer solution.	35
Figure 3.4 – Schematic of polymerisation using a grafted initiator. A) polymerisation and B) final sensor.	36
Figure 3.5 – Schematic of polymer deposition technique, a) pre-polymerisation mixture being deposited and b) deposited polymerisation mixture being polymerised by UV radiation.....	37
Figure 3.6 – Circuit diagrams of the impedance monitoring system and the simplified system assuming negligible capacitive effect at high frequencies. Reference resistance (r_{ref}), electrode resistance (r_{elec}), solution resistance (r_{sol}) and electrode capacitance (C_{elec}).	39
Figure 3.7 – Schematic of flow cell sensor.....	40
Figure 3.8 – Response of microchip sensor to varying concentrations of propofol (Red – MIP, Blue – NIP).	41
Figure 3.9 – Response of bare microchip sensor to varying concentrations of propofol.	42
Figure 3.10 – Impedance response of a bare microchip sensor to propofol (100 μ M). Propofol introduced at $t = 100$ s for 50 s and at 200 s for 100 s with no flow.....	42

Figure 3.11 – Impedance response of a molecularly imprinted microchip sensor (with 1% PVA) to propofol (100 μM). Propofol introduced at $t = 100$ s for 50 s and at 200 s for 100 s with no flow.....	43
Figure 3.12 – Nyquist plot and equivalent circuit of a Randles cell. R_s – solution resistance, R_t – charge transfer resistance and C_{dl} – double layer capacitance.....	45
Figure 3.13 – Impedance spectrum of deposited MIP (5 l) microchip electrodes with varied polymerisation times and distances. Polymerisation time; blue – 1 minute, red – 5 minutes and green – 10 minutes. Polymerisation distance; square – 1 cm, diamond – 3 cm and triangle – 5 cm.....	47
Figure 3.14 – Impedance spectrum of deposited MIP (5 nl volume of monomer mixture) microchip electrodes as shown in Figure 3.13 with varied y-axis scale. Polymerisation time; red – 5 minutes and green – 10 minutes. Polymerisation distance; diamond – 3 cm and triangle – 5 cm.....	48
Figure 3.15 – Nyquist plot of MIP (5 nl volume of monomer mixture) deposited microchip electrode, polymerised for 5 minutes at a distance of 1 cm.....	48
Figure 3.16 – Nyquist plot of bare and deposited MIP (5 nl volume of monomer mixture) microchip electrode in PBS (pH 7.5) and 100 μM propofol. Blue – MIP in PBS, orange – MIP in propofol, red – bare in PBS and green – bare in propofol.	49
Figure 3.17 – Nyquist plot of bare and deposited MIP (20 nl volume of monomer mixture) microchip electrode in PBS (pH 7.5) and 100 μM propofol. Blue – MIP in PBS, orange – MIP in propofol, red – bare in PBS and green – bare in propofol.	49
Figure 3.18 – Bode plot of bare and deposited MIP (5 nl volume of monomer mixture) microchip electrode in PBS (pH 7.5) and 100 μM propofol. Blue – MIP, red – bare, line – impedance and square – phase.....	50
Figure 3.19 – Bode plot of bare and deposited MIP (20 nl volume of monomer mixture) microchip electrode in PBS (pH 7.5) and 100 μM propofol. Blue – MIP, red – bare, line – impedance and square – phase.....	50
Figure 3.20 – Cyclic voltammetry (50 mVs^{-1}) of bare and deposited MIP (5 nl volume of monomer mixture) microchip electrode. Blue – bare in PBS, red – MIP in PBS and green – MIP in propofol.....	51
Figure 3.21 – Cyclic voltammetry (50 mVs^{-1}) of bare and deposited MIP (20 nl volume of monomer mixture) microchip electrode. Blue – bare in PBS, red – MIP in PBS and green – MIP in propofol.....	52
Figure 4.1 – Illustration of the complex metonidazole reduction.....	57
Figure 4.2 – A schematic of cephalosporin general structure (left) and cefoxitin (right).	58
Figure 4.3 – Illustration of gentamicin.....	59
Figure 4.4 – Model of metronidazole in highest binding conformation as calculated using Leapfrog (Sybyl), the monomer is DEAEM+. Hydrogen bonds (blue dashed line), carbon atoms (white), nitrogen atoms (blue), oxygen atoms (red), phosphorus atoms (orange) and hydrogen atoms (cyan).....	62

Figure 4.5 – Model of gentamicin in highest binding conformation as calculated using Leapfrog (Sybyl), the monomer is DEAEM+. Hydrogen bonds (blue dashed line), carbon atoms (white), nitrogen atoms (blue), oxygen atoms (red), phosphorus atoms (orange) and hydrogen atoms (cyan).	62
Figure 4.6 – Model of cefoxitin in highest binding conformation as calculated using Leapfrog (Sybyl), the monomer is EGMP-. Hydrogen bonds (blue dashed line), carbon atoms (white), nitrogen atoms (blue), oxygen atoms (red), phosphorus atoms (orange) and hydrogen atoms (cyan).	63
Figure 4.7 – Model of cefoxitin in a binding conformation as calculated using Leapfrog (Sybyl), the monomer is EGMP. Hydrogen bonds (blue dashed line), carbon atoms (white), nitrogen atoms (blue), oxygen atoms (red), phosphorus atoms (orange) and hydrogen atoms (cyan).	63
Figure 4.8 – Solubility of metronidazole, cefoxitin and gentamicin in DMF (blue) and acetonitrile (red) expressed as a percentage of total MIP mass.	64
Figure 4.9 – Volume of metronidazole (50 μ L) at 50% breakthrough of the SPE cartridge. Standard NIP mixture (blue) and NIP mixture with assumed extra functionality (red) as explained below.	68
Figure 4.10 – Percentage of uric acid (50 μ L) bound to the SPE cartridge. Standard NIP mixture (blue) and NIP mixture with assumed extra functionality (red).	69
Figure 4.11 – Percentage of ascorbic acid (50 μ L) bound to the SPE cartridge. Standard NIP mixture (blue) and NIP mixture with assumed extra functionality (red).	70
Figure 4.12 – Predicted monomer-template complex showing a binding ratio for metronidazole : EGMP of 1:2. Hydrogen bonds (blue dashed line), carbon atoms (white), nitrogen atoms (blue), oxygen atoms (red), phosphorus atoms (orange) and hydrogen atoms (cyan).	70
Figure 4.13 – Predicted monomer-template complex showing a binding ratio for metronidazole : itaconic acid of 1:2. Hydrogen bonds (blue dashed line), carbon atoms (white), nitrogen atoms (blue), oxygen atoms (red), phosphorus atoms (orange) and hydrogen atoms (cyan).	71
Figure 4.14 – Imprinting factor at 50% breakthrough. Monomer : template ratio; 1:2 (blue), 1:3 (green) and 1:4 (red). Predicted functional groups: 1 – X, 2 – X' and 3 – X'.	71
Figure 4.15 – Plot of forward scans from cyclic voltammograms (small plot) of metronidazole with increasing concentrations 0, 10, 25, 50 100 and 360 μ M (arrow going down) using platinum microchip electrodes. Arrow indicates increasing concentration.	78
Figure 4.16 – Amperometric (-750 mV) response to metronidazole (228 μ M) injections, also including noise from the injector.	79
Figure 4.17 – Amperometric (-300 mV) response to metronidazole (228 μ M) injections, also including noise from the injector.	79
Figure 4.18 – Cyclic voltammetry of metronidazole (100 μ M) in PBS (pH 7.5) with (red) and without (blue) degassing.	80

Figure 4.19 – Cyclic voltammetry of PBS (pH 7.5) with (red) and without (blue) degassing.	80
Figure 4.20 – Cyclic voltammetry of metronidazole (200 μM) in PBS (pH 7.5) with (red) and without (blue) degassing on carbon paste electrode.	81
Figure 4.21 – Cyclic voltammetry of PBS (pH 7.5) with (red) and without (blue) degassing on carbon paste electrode.	81
Figure 4.22 – Microscope images of microchip electrodes pre (a & b) and post (c & d) polymerisation (for 2 hours). Images b and d were taken using a darkfield filter.	82
Figure 4.23 – AFM imaged of thermally grafted polymer on microchip electrodes shown in Figure 4.22.	82
Figure 4.24 – Nyquist plot of bare microchip sensor (blue) and with immobilised SAM (red) and polymer grafted for 2 hours (green) in PBS (pH 7.5).	83
Figure 4.25 – Change in impedance observed for a NIP coated microchip electrodes to consecutive injections of metronidazole at concentrations of 1, 10, 25, 50 and 100 μM . At each concentration, the injection was repeated three times.	84
Figure 4.26 – Change in impedance observed for a MIP coated microchip electrodes to consecutive injections of metronidazole at concentrations of 1, 10, 25, 50 and 100 μM . At each concentration, the injection was repeated three times.	84
Figure 5.1 – Schematic of experimental setup for two electrode impedance monitoring.	98
Figure 5.2 – Contact angle of electrode surface at various stages throughout the polymer immobilisation.	98
Figure 5.3 – AFM images of A) topography and B) deflection of a bare gold electrode surface.	99
Figure 5.4 – AFM images of A) topography and B) deflection of a thiolated gold electrode surface.	100
Figure 5.5 – AFM images of A) topography and B) deflection of a NIP coated gold electrode surface.	100
Figure 5.6 – AFM of topography of scratched (1 μm x 1 μm) NIP coating and corresponding profile plots. Profile 1 – red, 2 – blue and 3 – green.	101
Figure 5.7 – Bode plot demonstrating the variation in impedance during various stages of the grafting polymerisation. Blue – bare gold, red – thiolated gold and green – grafted polymer.	101
Figure 5.8 – Bode plot demonstrating the variation in phase during various stages of the grafting polymerisation. Blue – bare gold, red – thiolated gold and green – grafted polymer.	102
Figure 5.9 – Example sensor response to alternative injections of creatinine and creatine (3 x 200 μL , 3 x 500 μL and 3 x 1000 μL) in 25 mM phosphate buffer with 100 mM NaCl at pH 7.5.	102
Figure 5.10 – Response of NIP sensor to changes in concentration of creatinine (blue) and creatine (red) from 100 μM to 2000 μM	103

Figure 5.11 – Response of MIP sensor to changes in concentration of creatinine (blue) and creatine (red) from 100 μ M to 2000 μ M.	104
Figure 5.12 – NIP (diamond) and metronidazole-MIP (square) capacitive changes to additions of metronidazole (blue) and imidazole (red).....	105
Figure 5.13 – Bode plot of thiol (Blue) and MIP (Red) coated electrodes (impedance – square, phase – diamond) created using the improved self assembly procedure.	108
Figure 5.14 – Example response to 100 μ M additions of creatinine to three-electrodes prepared using the original protocol with initial capacitances of 500 nF (blue), 293 nF (red) and 119 nF (green).	109
Figure 5.15 – Illustration of capacitive device with the selective layer modelled as a Randles cell.	110
Figure 5.16 – Illustration of capacitive device produced using a thiol insulating layer to anchor a thin polymer film. θ is the percentage of the surface (covered with polymer) which affects the capacitance. This is dependent on polymer coverage and porosity..	112
Figure 6.1 – Schematic of dithiocarbamate polymerisation.....	116
Figure 6.2 – Proposed NPEDMA electropolymerisation, based on the electropolymerisation of diphenylamine-4-sulphonic acid {Wen, 2002 #470}.....	119
Figure 6.3 – Experimental setup for iniferter attachment and polymer grafting.....	121
Figure 6.4 – Cyclic voltammetric scans of NPEDMA being electropolymerised (50 mV s ⁻¹). Consecutive cyclic scans 1 (blue), 2 (red), 3 (green) and 15 (purple). ...	123
Figure 6.5 – CV of MIP coated electrodes polymerised at a distance of 1 cm from light source for 5 minutes (blue), 10 minutes (green) and 30 minutes (red).....	124
Figure 6.6 – Bode plot of MIP (blue) polymerised for 10 minutes at a distance of 1 cm, NPEDMA (green) and bare (red) gold electrodes in PBS (pH 7.5).	124
Figure 6.7 – Nyquist plot of MIP (blue) polymerised for 10 minutes at a distance of 1 cm, NPEDMA (green) and bare (red) gold electrodes in PBS (pH 7.5).....	125
Figure 6.8 – CV of MIP coated electrodes polymerised for a period of 10 minutes at a distance of 3 cm (blue), 2 cm (green) and 1 cm (red).....	125
Figure 6.9 – CV of MIP coated electrodes polymerised at a distance of 3 cm for of period of 1 minute (blue), 3 minutes (green) and 10 minutes (red).....	126
Figure 6.10 – Capacitive step response of a NIP electrode, polymerised for 10 minutes at a distance of 3 cm to additions of creatinine (3 x 200 μ L, 3 x 500 μ L and 3 x 1000 μ L). The resulting calibration curve is shown in Figure 6.12.	128
Figure 6.11 – Capacitive step response of a MIP electrode, polymerised for 10 minutes at a distance of 1 cm to additions of propofol (3 x 200 μ L, 3 x 500 μ L and 3 x 1000 μ L). The resulting calibration curve is shown in Figure 6.13.....	129
Figure 6.12 – Calibration curves of capacitive NIP (red) and MIP (blue) electrodes in creatinine (square) and creatine (diamond). The NIP and MIP electrodes were polymerised for 10 minutes at a distance of 3 cm.	129

- Figure 6.13 – Calibration curves of capacitive NPEDMA (green), NIP (red) and MIP (blue) electrodes. The NIP and MIP electrodes were polymerised for 10 minutes at a distance of 1 cm. 130
- Figure 6.14 – Cyclic voltammogram performed in 50% PBS (pH 7.5) and 50% methanol (blue) and with 5 mM propofol, scans 1 (red), 5 (green), 10 (blue) and 15 (purple). 132
- Figure 6.15 – Chart showing the peak oxidation potential of propofol (5 mM) with background subtraction. The potential from the first (red and blue) and fifteen scan (yellow and green) is shown for different electrolytic conditions (HClO₄ or PBS) containing 50% methanol (red and yellow) or 50% acetonitrile (blue and green). 133
- Figure 6.16 – Chart showing the oxidation current of propofol (5 mM) at the peak oxidation current with background subtraction. The current from the first scan is shown for different electrolytic conditions (HClO₄ or PBS) containing either 50% methanol (yellow) or 50% acetonitrile (red). 133
- Figure 6.17 – Square wave voltammetry of propofol in 50% ACN and 50% PBS (pH 7.5). Arrow indicates increasing concentrations of propofol (0, 50, 100, 500, 1000, 5000 μM). 134
- Figure 6.18 – Square wave voltammetry of propofol in 50% ACN and 50% of 55 mM HClO₄ in deionised water. Arrows indicates increasing concentrations of propofol (0, 50, 100, 500, 1000, 5000 μM). 135
- Figure 6.19 – Calibration plot of peak response from SWV of propofol in PBS (blue) at pH 7.5 and HClO₄ (red) on bare gold electrodes. 135
- Figure 6.20 – Square wave voltammetry of gold electrode in 10 mM KFe(CN)₆ before (red) and after the oxidation of 1 mM propofol by cyclic voltammetry in 55 mM HClO₄ with varying amounts of acetonitrile (blue). The arrow indicates increasing concentrations of acetonitrile from 10 to 50 %. 136
- Figure 6.21 – Square wave voltammetry of gold electrode in 10 mM KFe(CN)₆ before (red) and after the oxidation of 1 mM propofol by cyclic voltammetry in PBS (pH 7.5) with varying amounts of acetonitrile (blue). The arrow indicates increasing concentrations of acetonitrile from 10 to 50 %. 137
- Figure 6.22 – Cyclic voltammetry (scan no. 1 of 15) of 1 mM propofol in 55 mM HClO₄ with 10% (blue), 20% (red), 30% (green), 40% (purple) and 50% (light blue) acetonitrile. 138
- Figure 6.23 – Cyclic voltammetry (scan no. 15) of 1 mM propofol in 55 mM HClO₄ with 10% (blue), 20% (red), 30% (green), 40% (purple) and 50% (light blue) acetonitrile. 138
- Figure 6.24 – Chart showing the peak oxidation potential of propofol (5 mM) with background subtraction. The potential from the first (red) and last scan (yellow) is shown for different electrolytic conditions (HClO₄ or PBS) containing 50% acetonitrile. 139
- Figure 6.25 – Chart showing the oxidation current of propofol (5 mM) at the peak oxidation current with background subtraction of a NPEDMA coated electrode. The

peak current from the first scan is shown for different electrolytic conditions (HClO ₄ or PBS) containing 50% acetonitrile.....	139
Figure 6.26 – Difference in currents between square wave voltammograms of bare gold electrode (blue) and NPEDMA coated electrode (red) with and without 1 mM propofol in PBS (PH 7.5) with 10% acetonitrile.	140
Figure 6.27 – Cyclic voltammetry of 5 mM propofol in 50% acetonitrile and 50% deionised water with 25 mM HClO ₄ . The first scan is shown in red.	141
Figure 6.28 – Schematic of experimental setup using a custom flow cell for the amperometric detection of propofol.	144
Figure 6.29 – Amperometric response the bare gold electrodes at 522 mV to propofol. Additions of 47.62, 43.29, 20.20, 9.77, 3.85, 1.91, 0.95 μM propofol were made.	144
Figure 6.30 – Amperometric response of NPEDMA coated electrodes at 522 mV to propofol. Additions of 1.25, 1.25, 2.48, 2.48, 4.90, 4.85, 11.93, 11.64, 22.46, 21.44, 40.06 μM propofol were made.	145
Figure 6.31 – Amperometric response of MIP coated electrodes to various additions of propofol with resulting concentrations of 1.25, 1.25, 2.48, 2.48, 4.90, 4.85, 11.93, 11.64, 22.46, 21.44, 40.06, 36.70 μM. The MIP layers were polymerised at a distance of 1 cm for 10 (blue), 5 (red) and 3 (green) minutes.	145
Figure 6.32 – Amperometric response of MIP coated electrodes, polymerised for 1 minute at a distance of 1 cm, to various additions of propofol resulting in a concentration of 1.25, 1.25, 2.48, 2.48, 4.90, 4.85, 11.93, 11.64, 22.46, 21.44, 40.06, 36.70 μM.	146
Figure 6.33 – Calibration plot of amperometric response of NIP (blue) and MIP (red) electrodes to injections of propofol in PBS (pH 7.5) with 10% acetonitrile. The polymers layer were prepared at a distance of 3 cm for 1 (square), 2 (diamond) and 3 (triangle) minutes. The arrow indicates increasing polymerisation times.	147
Figure 6.34 – Amperometric response of MIP (blue) and NIP (red) electrodes polymerised for 3 minutes to injections of propofol (5 μM, 10 μM, 25 μM, 50 μM and 100 μM).....	147
Figure 6.35 – Amperometric response of MIP (blue) and NIP (red) electrodes polymerised for 1 minute to injections of propofol (5 μM, 10 μM, 25 μM, 50 μM and 100 μM).....	148
Figure 6.36 – Calibration plot of amperometric response to NIP coated electrodes with a flow rate of 7 μLs ⁻¹ . Polymerised for 1 minute (blue) and 3 minutes (red) at a distance of 3 cm (square), 5 cm (diamond) and 10 cm (triangle).	148
Figure 6.37 – Calibration plot of amperometric response to MIP coated electrodes with a flow rate of 7 μLs ⁻¹ . Polymerised for 1 minute (green), 2 minutes (red) and 3 minutes (blue) at a distance of 3 cm (square), 5 cm (diamond) and 10 cm (triangle). The arrow shows increasing UV exposure.....	149
Figure 6.38 – Calibration plot of amperometric response of ascorbic acid injections at 7 μLs ⁻¹ on MIP (blue) and NIP (red) electrodes polymerised for 1 minute at a distance of 3 cm.....	150

Figure 6.39 – Calibration plot of amperometric response of ascorbic acid injections at $7 \mu\text{Ls}^{-1}$ on MIP (blue) and NIP (red) electrodes polymerised for 3 minutes at a distance of 3 cm..... 150

Notation

AC	Alternating current
AFM	Atomic force microscopy
AMPSA	2-acrylamido-2-methyl-1-propanesulphonic acid
ANN	Artificial neural networks
APTES	Aminopropyltriethoxysilane
ATES	Allyltriethoxysilane
CV	Cyclic voltammetry
DEAEM	Diethylamino ethylmethacrylate
DMF	Dimethylformamide
DPV	Differential pulse voltammetry
ECE	Electrochemical-chemical-electrochemical (reaction)
EGDMA	Ethleneglycol dimethacrylate
HCl	Hydrochloric acid
HClO ₄	Perchloric acid
HF	Hydrofluoric acid
IDE	Inter-digitated electrode
IgG	Immunoglobulins
ISFET	Ion-sensitive field effect transistor
MIP	Molecularly imprinted polymer
MS	Mass spectroscopy
NaOH	Sodium hydroxide
NIP	Non-imprinted polymer

NO	Nitric oxide
PBS	Phosphate buffer saline
PCO ₂	Partial pressure of carbon dioxide
PLS	Partial least squares
PO ₂	Partial pressure of oxygen
SAM	Self-assembled monolayer
SPE	Solid phase extraction
SWV	Square wave voltammetry
UV	Ultra violet

Chapter 1 - Introduction

“Science may set limits to knowledge, but should not set limits to imagination.”

Bertrand Russell (1872 - 1970)

The aim of this thesis is to investigate the possibility of developing a sensing device based on molecularly imprinted technology for the selective detection of clinically relevant analytes. The development of a real-time microchip-based sensing device produced by Sphere Medical (Cambridge, UK) served as the transducer platform for this investigation. The sensor chip is based on Sphere’s Proxima system and is primarily an electrochemical platform which can currently monitor glucose, pH, pO₂, pCO₂, K⁺, Ca²⁺, Na²⁺, haematocrit and lactate using potentiometric, amperometric or conductometric techniques.

Molecularly imprinted polymers (MIP) have selective properties for a chosen analyte which is present when the MIP is formed. The removal of the analyte after polymerisation results in a cross-linked matrix with cavities which have steric and functional selectivity for the particular analyte employed. By incorporating a MIP onto Sphere’s electrochemical sensor chip, the range of analytes which can be detected by the Proxima system could potentially be increased.

Thus, this thesis seeks to investigate: firstly, the development of MIPs for the selective detection of therapeutic substances; secondly, the immobilisation of MIPs onto transducer surfaces; thirdly, the detection of target analytes with MIP functionalised sensors. Finally, the thesis plans to propose a universal methodology which can act as a platform for the production of MIP-based devices.

The abovementioned aims are addressed in this thesis in the following manner: Firstly, a review of the current technology and devices being developed for monitoring clinical parameters was conducted and is outlined in Chapter 2. Secondly, an initial investigation into the conductive detection of propofol was performed, with the aim of developing knowledge and skills in MIP sensor development, the results of which

comprise Chapter 3. Thirdly, an antibiotic was selected and a computationally designed MIP for the selective detection of this antibiotic was produced and tested. Following this development the MIP was immobilised onto a sensor platform and the detection of the antibiotic was investigated: the outcomes of this testing is described in Chapter 4. In addition, an examination of previously published methodologies for the capacitive detection of creatinine-based MIP were investigated and optimised, the outcomes of which are recorded in Chapter 5. In Chapter 6, new innovative materials (Lakshmi et al., 2009a, Lakshmi et al., 2009b) were employed in the immobilisation and growth of a MIP for the detection of propofol. In the final chapter of this thesis, conclusions are drawn on the aforementioned investigations and possible further work is proposed.

Chapter 2 - Review of clinical sensing devices and their technology

“In science the credit goes to the man who convinces the world, not the man to whom the idea first occurs.” Sir Francis Darwin (1848 - 1925), *Eugenics Review*, April 1914

2.1 Introduction

This chapter aims to review clinical sensors, the difficulties which are currently faced in their development and the technologies being used to overcome these difficulties.

2.2 Sensors for clinical analysis

To assist healthcare professionals in effectively managing therapy and to optimise patient outcomes in a hospital, the monitoring of patients' clinical parameters is essential. Currently, chemical parameters and therapeutic drug concentrations are monitored via blood samples which are assessed in a dedicated laboratory (Hillberg et al., 2005), a procedure which is both time-consuming and logistically demanding. In addition, as the administration of therapeutic drugs is based on the average dose, taking into consideration the mass of the patient, this does not account for variations in a patients drug absorption, distribution, metabolism or elimination.

A bedside patient monitoring system capable of taking real time measurements of a patients' critical chemical parameters would be more ideal. Especially if this monitoring system was capable of automatically administrating the appropriate therapeutic substances in the required concentrations. The real time monitoring of therapeutic drugs is considered to be very important because if the concentration of the drug is not within the therapeutic window it could have no effect or may even cause harm to a patient.

In-vivo sensors are being developed to measure parameters within intra-cellular, tissue, intra vascular, surface skin and gastrointestinal environments (Rolfe, 1988). However,

there are still several challenges which hold back this technology. Two of these main challenges are; i) the stringent quality control required to ensure that any device produced is suitable for a clinical environment and ii) the biocompatibility of monitoring biological fluids, where, for example, the device must not be toxic, induce adverse side effects (i.e. inflammation) or suffer from severe biofouling.

The position of an implanted device on a patient has several inherent challenges which can have a large impact on the resulting performance of the sensor (Frost and Meyerhoff, 2002). For example, in intravascular devices if proteins in the blood adsorb on the surface of the device, this can lead to the adhesion and activation of platelets (Figure 2.1a) which are highly metabolic and can then alter the localised concentrations of administered drugs around the sensor. Localised concentrations can also be caused by the ‘wall effect’ (Figure 2.1b) due to the device touching the endothelial cells on a blood vessel’s wall. Platelet adhesion, the wall effect and constricted blood flow can occur in the case of vasoconstriction (Figure 2.1c) where the vessel contracts around the device, however this is usually due to inflammation. Inflammatory responses also occur with subcutaneously implanted devices, which leads to mass transport problems and then, consequently, the device provides wrong readings.

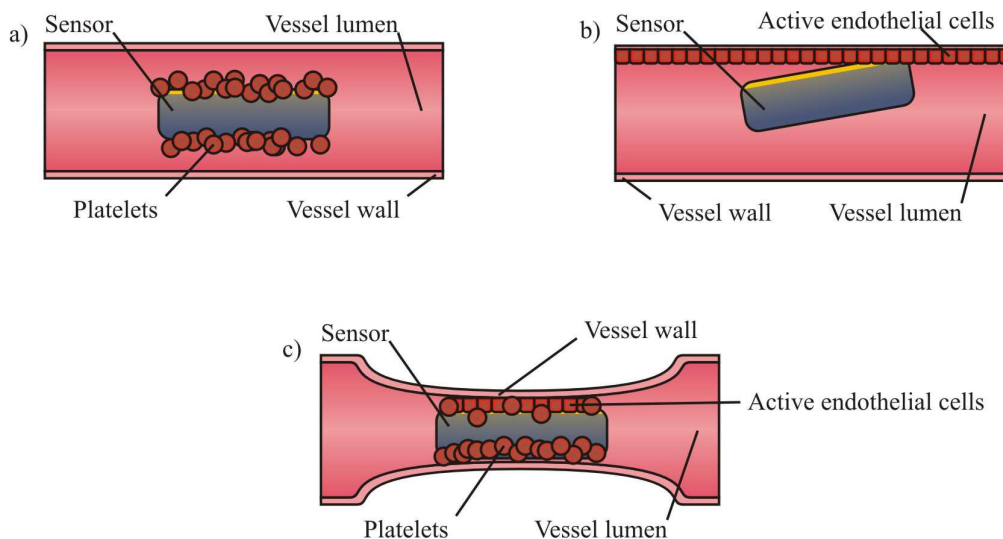


Figure 2.1 – Illustration of complications occurring from the positioning of implanted clinical devices, a) Platelet adhesion, b) the ‘wall effect’ and c) vasoconstriction. (Frost and Meyerhoff, 2002).

There are numerous strategies that have been investigated to reduce biofouling, several of which were reviewed by Wisniewski and Reichert (Wisniewski and Reichert, 2000). One of these strategies is the use of hydrogels like poly(hydroxyethyl methacrylate) (polyHEMA) and poly(ethylene glycol) (PEG) (Singh et al., 2007), where the hydrophilic nature of the material is used to reduce protein adsorption and, consequently, cell adhesion. Other strategies include the use of phosphorylcholine mimics, which mimic the outer lipid layer of cell membranes. This has been shown by Yang and co-workers to reduce biofouling for the detection of glucose in blood (Yang et al., 2000) and reduce the fouling of marine bacteria in the optical detection of oxygen, as illustrated by Navarro-Villoslada and co-workers (Navarro-Villoslada et al., 2001). The slow release of anti-fouling agents, such as nitric oxide (NO), has demonstrated a reduction in platelet aggregation and vasoconstriction (Zhang et al., 2002). Espadas-Torre and co-workers (Espadas-Torre et al., 1997) sandwiched a NO releasing polymer between two ion-selective membranes to measure H^+ and K^+ and Schoenfish and co-workers (Schoenfish et al., 2000) dip coated silicone tubing in NO releasing polymer used for the detection of pO_2 . Both of these devices showed a significant reduction in biofouling.

External devices also allow for more complex separation. For example, in in-vitro testing where biofouling complications can be overcome by separating the sample before analysis (Hillberg et al., 2005). External in-situ monitoring devices avoid the complications of vasoconstriction and also reduce platelet adhesion and the wall effect, as they are more accessible for cleaning, regeneration and calibration purposes. This can reduce the effects of biofouling which helps to ensure the sensitivity of the device and allow adjustment for possible drift.

Microdialysis catheters have been developed for separation and external in-situ detection. Examples of microdialysis can be seen in Cooney and co-workers' research where they utilised a membrane to separate CO_2 from a blood reservoir; the dialysate was then mixed with a reagent and used for the optical monitoring of this gas with an accuracy of 2 mmHg with a 2 minute response time (Cooney and Towe, 1997). Cooney and co-workers later combined this technology with a pH sensor in a dual concentric-flow microdialysis approach (Cooney and Towe, 2000). This measured pH and pCO_2 with accuracies of ± 0.01 pH units (from pH 7.02 – 7.87) and ± 1.5 mmHg (from 0-

80 mmHg), respectively. The design of a generic microdialysis device which incorporated electropolymerised membranes has been seen by Rhemrev and co-workers (Rhemrev-Boom et al., 2001), and the study of microdialysis for glucose detection in both healthy (Wientjes et al., 1998) and type 1 (Lutgers et al., 2000) diabetic subjects has been reported by Lutgers and Wientjes.

Once a selective sensor with an acceptable level of biofouling has been successfully produced, assurance needs to be provided for the device to be sterile, non-toxic, blood compatible and robust in order for it to conform to the required standards for operation in a clinical environment. One commercial example is the external in-situ blood gas and electrolyte monitor which was produced by VIA Medical (Skoog, 2000). This device incorporates conductivity detection for hematocrit, a Clark voltammetric sensor for pO₂ determination, and the other analytes are detected using potentiometry combined with ion-selective membranes (a summary of these analytes can be seen in Table 2.1). It operates by drawing blood over the sensors, monitoring the parameters at 37 °C and putting the blood back into the patient while calibrating with an isotonic solution.

Table 2.1 – Summary of VIA Medical’s blood gas and electrolyte monitoring systems analytes. Including the analyte range and sensitivity.(Skoog, 2000)

Analyte	Range	Sensitivity
pO ₂	20-699 mm Hg	1 mm Hg
pCO ₂	10-99 mm Hg	1 mm Hg
Na ⁺	80-190 mM	1 mM
K ⁺	0.2-9.9 mM	0.1 mM
	10-20 mM	1 mM
Ca ²⁺	0.2-4.25 mM	0.01 mM
pH	6.80-7.70	0.01
Hematocrit	12-70%	1%

Commercial examples of in-vivo testing can be seen with Diametrics Medical's Paratrend 7 (Myles et al., 1999) and Neurotrend (Henze et al., 2004). The Paratrend 7 and Neurotrend both measure pO_2 , pCO_2 and pH using optodes based on the fluorescence or light absorption of reactive dyes where membranes are utilised for selective recognition. The surrounding temperature is also measured using a thermocouple. The Paratrend 7 is an intravascular device designed to be used in a critical care environment when fast changes in blood gas levels are anticipated or for use over prolonged periods of time while attaining a large quantity of data on critically ill patients (Ganter et al., 2004). The Neurotrend is designed to take measurements within the cerebral tissue to assess the degree and progression of brain injuries.

The knowledge of a patient's clinical parameters could potentially significantly improve patient outcomes in a critical care environment. These clinical parameters can be feasibly attained in near real time by both in-vivo and in-situ devices. However, an in-situ device that is situated outside the patient allows for easier cleaning, calibration and replacement, therefore overcoming some of the inherent challenges, for example biofouling, that occur from measuring analytes in biological media like blood.

2.3 Targets

To improve critical care, the knowledge of concentrations and variations in a patient's critical parameters is vital as this will allow clinicians to administer the appropriate treatment when it is required. These critical parameters can be divided into three categories, blood gases, electrolytes and metabolites, examples of these parameters and their normal clinical concentrations can be seen in Table 2.2.

Table 2.2 – Normal range values for blood-gas and electrolyte measurements. a (Meyerhoff, 1993), b (Pfeiffer et al., 1997), c (Berger et al., 1997), d (Eggenstein et al., 1999) and e (Berberich et al., 2005).

	Analyte	Range
Blood gases	Oxygen partial pressure (PO ₂)	80 – 104 mmHg ^a
	Carbon dioxide partial pressure (PCO ₂)	33 – 48 mmHg ^a
	pH	7.31 – 7.45 ^a
Electrolytes	Sodium (Na ⁺)	135 – 155 mM L ^{-1 a}
	Potassium (K ⁺)	3.6 – 5.5 mM L ^{-1 a}
	Ionised calcium (iCa ²⁺)	1.14 – 1.31 mM L ^{-1 a}
Metabolites	Lactate	< 2.7 mM L ^{-1 b}
	Glucose	4 – 7 mM L ^{-1 c}
	Urea	1.7 – 8.3 mM L ^{-1 d}
	Creatinine	35 – 140 μM L ^{-1 e}

2.3.1 Blood gas

Blood gas monitoring is the measurement of O₂ and CO₂ partial pressures along with H⁺ concentrations (Lam and Atkinson, 2007) and is one of the most demanding analytical requests in a hospital's laboratory. The continual monitoring of blood gases is usually associated with situations when the clinician predicts a rapid or unexpected change in blood gas values (Ganter et al., 2004), for example during thoracic and cardiovascular surgery or during organ transplants. Other common applications include monitoring of blood gas values over a long period of time, for example when patients are suffering from respiratory disease, sepsis and severe trauma (Herrejon et al., 2006).

Sampling blood for in-vitro blood gas testing usually requires the puncturing of an arterial line which can be discomforting for a patient, especially if a large number of samples are required over a long period of time. Oximetry devices remove the need for arterial punctures they are a non-invasive technique for monitoring oxygen saturation

and pressure. Oximetry works by monitoring two different wavelengths which change in absorbance resulting from variations in the oxygenated and deoxygenated haemoglobin within the arterial line. Oximetry devices can measure arterial oxygen saturation within an acceptable sensitivity for medical applications. However, the difference between oxygen pressure measured using oximetry and the true value is not accurate enough for medical application (Herrejon et al., 2006).

Transcutaneous devices offer a possible alternative to monitor oxygen pressure at an acceptable sensitivity. Examples of transcutaneous devices are disposable carbon paste electrodes produced by Lam and co-workers (Lam and Atkinson, 2007) for monitoring the partial pressure of oxygen. They measured the oxygen by heating the skin to aid diffusion of the gases in the blood and then amperometrically reduced the oxygen. They investigated two different working electrodes, one based on KNO_3 and the other on Nafion, with sensitivities of 33 nA/mmHg and 25 nA/mmHg respectively. Iguchi and co-workers (Iguchi et al., 2005) constructed an oxygen sensor from non-permeable and gas-permeable membranes which encased KCl on Pt and Ag/AgCl electrodes. The device was designed to measure oxygen from the conjunctiva; hence it was very thin (width 3 mm, thickness 84 μm). It also eradicated skin rashes and skin burns which are caused by traditional transcutaneous devices due to the adhesion and heating of the device. It had a 45 second response time with a 0.01-8 mg/L sensitivity range and was considered stable enough for PO_2 measurements.

The Paratrend 7 (Ganter et al., 2004, Myles et al., 1999, Hwang et al., 2005) and Neurotrend (Henze et al., 2004, Codman., 2001) are commercial devices for measuring pH and the partial pressure of oxygen and carbon dioxide. They have been shown to provide data in excellent agreement with laboratory blood gas analysers and their mechanisms of operation are described in Section 2.2. However, they are in-situ devices therefore arterial puncturing is necessary to attain the blood sample.

2.3.2 Electrolytes

The vital electrolytes in blood that are considered to be useful for patient care are K^+ , Na^+ and Ca^{2+} . These electrolytes are often monitored for intensive care patients and patients undergoing cardiac surgery and renal dialysis (Gumbrecht et al., 1990). Traditionally, sensors for such electrolytes use selective glass membranes. However,

these devices are hard to miniaturise for use in arterial lines and arterial line catheters. Possible alternatives are silicon based potentiometric sensors, ISFETs and optodes, which have become increasingly popular in recent years.

The miniaturisation of silicon based ion-selective sensors has been hindered due to the lack of a decent reference electrode (Yoon et al., 2000). However, liquid-free reference electrodes, which are generally constructed using PVC membranes doped with electroactive components, have shown promise. Heng and co-workers (Heng and Hall, 2001) produced a photocured membrane on a Ag/AgCl electrode for the detection of Na^+ and K^+ . These sensors demonstrated potentiometric behaviour comparable to PVC based ion-selective membrane devices. Scheipers and co-workers (Scheipers et al., 2001) also produced a liquid-free silicon-based sensor which they used to simultaneously monitor K^+ , Na^+ and pH in human blood using three integrated sensors on one chip. The correlation between the sensor and a clinical electrolyte analyser demonstrated a linear regression of 0.9977 for the K^+ measurements.

ISFETs are an attractive platform for electrolyte detection and they lend themselves to the biosensor market as they can be easily miniaturised and mass produced (Lee et al., 2000). However, ISFETs tend to have problems with the poor stability of their reference electrode and drift. Gumbrecht and co-workers (Gumbrecht et al., 1990) created an ISFET sensor system that utilised an ISFET as the reference, this was achieved by using the calibration solution as a salt bridge. The system had a 2 minute calibration time, a 30 second response time and a drift of 0.05 mV/h for the first 200 hours. Also, it did not suffer from clotting problems due to the simple arrangement of the apparatus.

2.3.3 Metabolites

There are four main metabolites that are of clinical interest: these are lactate, glucose, urea and creatinine. Each of these metabolites can provide a clinician with initial information about the health of the patient and thus improve the quality of patient care and recovery. The mechanism of detecting these metabolites in a sensor format is generally achieved by using enzymes to produce a detectable compound which has a concentration related to the concentration of the metabolite. Examples of these enzymes and their reactions as used by Suzuki and co-workers are shown in Table 2.3.

Table 2.3 – Examples of enzymes, reactions and buffer solutions used in the production of metabolite sensors (Suzuki et al., 2001). Activity is quoted in enzyme units per cm².

Analyte	Enzyme	Activity (U cm ⁻²)	Reactions	Buffer solution
Glucose	Glucose oxidase	186	Glucose + O ₂ → gluconolactone + H ₂ O ₂	20 mM KH ₂ PO ₄ ⁻ NaOH (pH 6.5-8.0)
				20 mM Tris-HCl (pH 8.5-9.0)
Urea	Urease	24	Urea → 2NH ₃ + CO ₂	20 mM KH ₂ PO ₄ ⁻ NaOH (pH 5.5-8.0)
				20 mM Tris-HCl (pH 8.5-9.5)
Uric acid	Uricase	24	Uric acid + H ₂ O ₂ + O ₂ → allantoin + H ₂ O ₂ + CO ₂	20 mM KH ₂ PO ₄ ⁻ NaOH (pH 6.5-8.0)
				20 mM Borate-NaOH (pH 8.5-9.5)
Creatine	Creatinase	34	Creatine + H ₂ O → sarcosine + urea	20 mM KH ₂ PO ₄ ⁻ NaOH (pH 6.5-8.0)
	Sarcosine oxidase	52	Sarcosine + H ₂ O + O ₂ → glycine + HCHO + H ₂ O	20 mM Borate-NaOH (pH 8.5-9.5)
Creatinine	Creatininase	62	Creatinine + H ₂ O → creatine	20 mM KH ₂ PO ₄ ⁻ NaOH (pH 6.5-8.0)
	Creatinase	27	Creatine + H ₂ O → sarcosine + urea	20 mM Borate-NaOH (pH 8.5-9.5)
	Sarcosine oxidase	41	Sarcosine + H ₂ O + O ₂ → glycine + HCHO + H ₂ O ₂	

2.3.3.1 Lactate

Lactate concentrations can be monitored to provide information about anaerobic metabolism and indicate the hypoxemic situation of the respective tissue. An example of an amperometric lactate oxidase-based sensor, which had a linear response in a concentration range on 0.5 to 20 mM with a response time of less than 2 minutes has been described by Pfeiffer and co-authors (Pfeiffer et al., 1997). The sensor was reliable during in-vivo monitoring after Gamma-irradiation.

Double lumen catheters have been used for sampling in blood and subcutaneously by Meyerhoff (Meyerhoff, 1993) and Ellmerer (Ellmerer et al., 1998), respectively.

Meyerhoff's device had a linear range of 0 and 15 mM with a peak response of 2.2 minutes in blood, but it also had a 4 minute lag time. Hence, it only gave an estimation of blood lactate, which in turn can give an insight into lactate metabolism. Ellmerer's subcutaneous device demonstrated a good correlation when the test subject was at rest, however when measurements were taken during exercise, the correlation between the sensor and blood was very poor. This was explained by the measurements only showing the local concentrations to the device, hence there was no direct correlation with the lactate levels in blood.

A comparison of double lumen and heparin-coated catheters was conducted by Gfrerer and co-workers (Gfrerer et al., 1998) who tested their devices during exercise and had a linear response up to 25 mM with a 95% response in less than 30 seconds. The double lumen catheter had a correlation coefficient between 0.93 and 0.98 (standard deviation 1.47 mM) whereas the heparin-coated catheter had a correlation coefficient between 0.94 and 0.99 (standard deviation 0.88 mM). Thus, the heparin catheter performed better and the system was safer and easier to use as it avoids complications in handling heparin-saline solutions.

2.3.3.2 Glucose

There are significant developments of glucose sensors due to the growing commercial opportunities. As a result there have been many approaches proposed for glucose monitoring, for example implanted electrochemical devices, subcutaneous interstitial fluid microdialysis, capillary filtrate and the transdermal collection of glucose (Gerritsen et al., 1999). Subcutaneous devices allow good accessibility and are easily replaced, although they tend to suffer from significant drift. Monitoring the interstitial fluid also has the advantage of a lower protein concentration when compared to blood. Interstitial fluid also has a very similar composition to plasma for electrolytes and small solutes, hence accurate glucose concentration can be attained.

To improve on the presently available glucose monitoring system for diabetics, Kaimori and co-workers (Kaimori et al., 2006) produced a glucose sensor chip with the world's smallest sample volume (200 nL), thus making the lancing less painful. This reduction in sample volume was achieved by reducing the cavity thickness of the chip sensor to approximately 50 μm by using adhesive ink. However, the reduction in cavity

thickness requires a high production tolerance as a change in thickness of $4\mu\text{m}$ was equivalent to a 5% reduction in current. Despite this, the sensor demonstrated good performance with a correlation coefficient of 0.98 in blood glucose with a range of 60 to 493 mg dL^{-1} .

As the accuracy and durability of the enzyme glucose devices is well proven in in-vitro, most of the current development is to optimise a device for long term in-vivo operation. Woderer (Woderer et al., 2007) and co-workers tested a glucose device consisting of a sensor foil with a carbon paste glucose oxidase electrode and a Ag/AgCl reference electrode for amperometric monitoring. Their sensor had a high sensitivity ($0.35\text{ nA mg}^{-1}\text{ dL}^{-1}$) with a 60 second response time: it operated with a single calibration and showed a good correlation for normal and hypoglycaemic glucose levels. The hyperglycaemic measurements reflected the blood glucose apart from when the change in glucose level was very rapid.

2.3.3.3 Urea

The urea cycle is a vital metabolic cycle in humans as it neutralises toxic ammonium waste products. Thus, the monitoring of blood urea can be used as an indicator of renal function and liver disease. Currently, most of the urea monitoring devices measure NH_4^+ after an enzymatic reaction with urease (Miyahara et al., 1991). Moreover, monitoring in blood is complicated due to high ionic strength, strong buffering capacity and high protein concentrations.

The resulting production of NH_4^+ after the enzymatic reaction of urea with urease causes local pH changes around the active area of the sensor: these changes in pH are ideally detected using ISFET technology. Boubriak and co-workers (Boubriak et al., 1995) used a silicon chip ISFET with an ISFET reference to monitor changes in pH as a result of the presence of urea. The device had a response time of 1-3 minutes depending on membrane thickness and a linear response of up to 2 mM. However, the high protein content in the test serum decreased the response, but it was subsequently found that a twenty-five fold dilution of the serum produced more reliable measurements. There was still a high interference from alkali metals in the sample as it was found that 200 mM of NaCl caused a 50% fall in sensor output.

Potentiometry is another alternative method of detecting NH_4^+ and thus urea. Devices based on this approach rely on ion selective membranes to separate interfering substances from the sensor surface. However, Na^+ and K^+ are not separated in most NH_4^+ membranes, as seen with Eggenstien and co-workers' disposable double matrix membrane (Eggenstein et al., 1999). Vel Krawczyk and co-workers (Vel Krawczyk et al., 1994) addressed this problem by using an outer hydrophobic gas permeable membrane and a three-electrode setup during monitoring. With this setup urea concentrations from 0.05 to 2 mM were monitored with a correlation coefficient of 0.9996 and a sensitivity of 53.3 mV/decade.

2.3.3.4 Creatinine

In the evaluation of muscle disorders and renal dysfunction monitoring the level of creatinine has become increasingly important in the development of patient care as it is the product of creatine metabolism. The normal range of creatinine in blood is 35–140 μM ; however, if a patient is suffering from a muscle or a kidney disorder it can be as high as 1 mM (Berberich et al., 2005).

A low cost disposable ISFET based device for the detection of creatinine was produced by Sant and co-workers (Sant et al., 2004). The device was a pH-ISFET with a dip-coated enzymatic membrane deposited on the surface, where the reaction of creatinine deiminase with creatinine leads to creatinine's hydrolysis and the production of NH_3 . Variations in the NH_3 levels alter the local pH which is thus related to the creatinine concentration. A sensitivity of 30 mV/pCreatinine over a range of 10–100 μM was demonstrated.

An elaborate three-enzyme creatinine sensor converts creatinine to H_2O_2 which can then be amperometrically detected. However, these systems are considered to have decreased sensitivity due to interference of creatine and the complicated sequence of the three-enzymatic reactions. Berberich and co-workers (Berberich et al., 2005) developed a three-enzyme sensor by immobilising enzymes in polyurethane membranes; this immobilisation increased the enzyme half-life from 6 to 80 days. Unfortunately, these devices displayed a large loss of activity when the enzymes were immobilised on the sensor chip; this enzyme deactivation was attributed to silver ions from the reference electrode.

2.4 Detection Methods

There are various electrochemical techniques that can be used for the detection of analytes, all of which have advantages and disadvantages which depend on the setup of the electrochemical cell and the selective component within the device. The following section outlines the fundamental electrochemical techniques and gives examples of how they have been applied in the detection of therapeutic substances.

2.4.1 Potentiometry

Potentiometry is a well-established technique where the variations in potential between a working electrode (which is commonly ion-selective) and a reference electrode are monitored; a schematic of the equivalent electrochemical cell can be seen in Figure 2.2. Due to the rapid, low-cost and accurate analysis that these devices offer they have been widely used in many fields, such as clinical diagnostics, industrial process control and environmental monitoring.

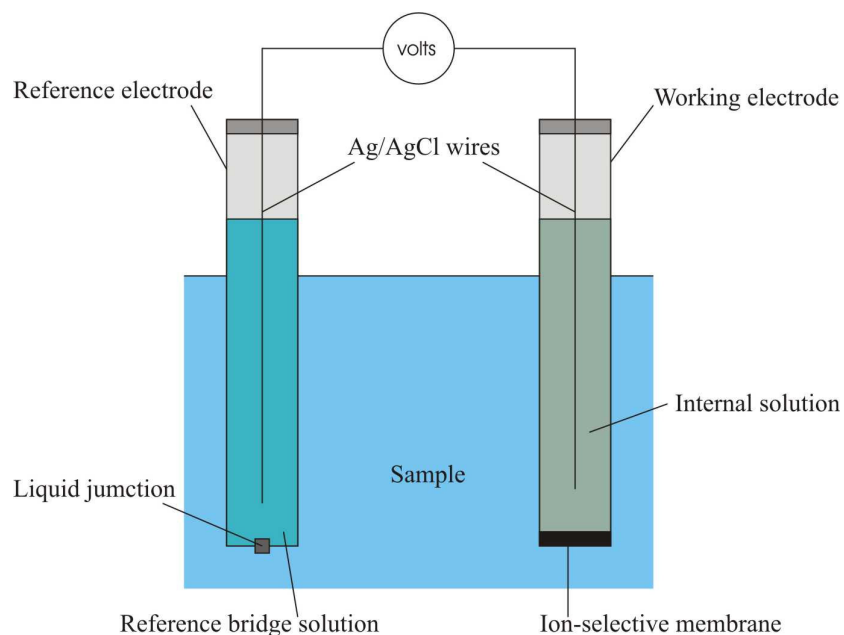


Figure 2.2 – Schematic of potentiometric electrochemical cell as illustrated (Wang, 2000).

The ion-selective electrodes are generally constructed using membrane technology where the membrane is capable of selectively binding ionic species. The membrane separates the internal solution of the working electrode, which contains the ion of

interest at a constant activity, and the sample solution. Selective binding of the ionic species causes an unequal distribution of the analyte across the membrane boundary and thus creates a potential gradient (Wang, 2000). As the reference potential is fixed and activity of the inner solution is constant, the cell potential monitored is proportional to the activity of the ionic species in the sample. The main source of error with this system are changes in the reference electrode junction potential, although this is usually resolved by using an intermediate salt bridge.

The most common example of this traditional approach is the pH electrode which is predominantly based on a glass membrane. This is due to the extremely high selectivity of the electrode for hydrogen ions, its broad response range, and its fast and stable response. However, recent developments in wafer technology for sensor fabrication (Schnakenberg et al., 1996) have increased the number of reported chip-based potentiometric devices which are low-cost and reproducible in batch production.

Potentiometric devices can be incorporated into solid state devices and due to their small size are ideal for sensor arrays. An example of such a device is the array developed by Gutierrez and co-workers (Gutierrez et al., 2007) for the monitoring of urea and alkaline ions (ammonium, potassium, sodium, hydrogen). The array consisted of twelve individual potentiometric sensors with 7 different membranes coatings. The data obtained from the array was analysed with artificial neural networks (ANN) and partial least squares (PLS). Their ammonium transducer lasted for 20 days and the ANN model was accurate with near unity slopes and a zero intercept. Other examples of array devices are electronic tongues, an example of which is the tongue created by Verrelli and co-workers (Verrelli et al., 2007) for identifying defects, fermentation markers and the storage conditions of wine. They used PLS to analyse their data and have demonstrated good stability and reproducibility of the device. A good correlation of the markers H_2S and SO_2 at low concentrations and acetic acid at high concentrations was also found.

2.4.2 Voltammetry

Cyclic voltammetry is a versatile and informative technique that can be used to obtain qualitative information concerning electrochemical reactions. It can expose information about the thermodynamics, kinetics of heterogeneous electron transfer, coupled

chemical reactions and adsorption processes (Wang, 2000). However, it is rarely used as a method of detection in a sensing device as other methods have greater advantages. Nevertheless, it is an invaluable tool for locating the redox potentials of electroactive species within a given media and thus helping to optimise and understand the principal reactions of a device.

The technique works by monitoring the current resulting from a potential scan that follows a triangular waveform. A peak in the monitored current is caused by the formation of a diffusion layer near the electrode surface, this diffusion layer expands with continual scanning. The current due to the redox reaction is directly proportional to the surface concentration of the redox reactant and is proportional to the square root of the scan rate.

A voltammetric technique which is useful for detection within a device is pulse voltammetry. This technique is similar to cyclic voltammetry but a step or square signal is superimposed on the normal linear voltammetric scan, which creates a pulse. The short pulse duration results in a thinner diffusion layer, hence the faradic current increases, and by monitoring the current shortly after the pulse the charging current is close to zero. All this contributes to an increased ratio between the faradic and non-faradic currents, thus sensitivity can be increased between 5 to 10 times when compared to normal voltammetry.

An example of the voltammetry was demonstrated by Huang and co-workers (Huang et al.) who used cyclic voltammetry to investigate the response of tyrosine at a modified glassy carbon electrode. The cyclic voltammetry study showed an oxidation peak at -640 mV with a linear response of between 100×10^{-9} to 50×10^{-6} mol/L, then using differential pulse voltammetry (DPV) gained a detection limit of 80×10^{-9} mol/L. Similar studies were performed by Shahrokhian and co-workers (Shahrokhian et al., 2005) who investigated Captopril using carbon paste electrodes with an incorporated cobalt mediator. In another work Ferancova and co-workers (Ferancova et al., 2001) incorporated cyclodextrins into carbon screen printed electrodes to detect tricyclic antidepressants.

2.4.3 Stripping Voltammetry

Stripping voltammetry essentially consists of two stages. In the first stage there is deposition of the analyte on the electrode surface; this can be seen as a pre-concentration. During the second stage, the pre-concentrated analyte is 'stripped' from the electrode surface causing the measurable change. There are several versions of stripping analysis depending on the nature of the aforementioned stages. These methods are summarised in Table 2.4.

The use of stripping analysis is extremely useful for the detection of trace metals as it can achieve favourable signal-to-noise ratios and pre-concentration factors of 100 to 1000. Detection limits when compared to voltammetric measurements can be lowered by an order of 2 to 3 in magnitude (Wang, 2000). For the stripping of organic compounds there are two strategies, either adsorptive or cathodic stripping, depending on whether the analyte of interest has surface-active properties or is capable of forming insoluble salts (see Table 2.4).

Stripping techniques have been used for the detection of several organic therapeutic compounds, for example glucose (Ly and Kim, 2006), Ceftriaxone (Ferreira et al., 1997), Benzodiazepines (Hernandez et al., 1988), Cephalothin (Al-ghamdi et al., 2004) and Prefloxacin (Beltagi, 2003). Ly and co-workers used stripping analysis for the detection of glucose in drinking water and urine with correlation coefficients of 0.9822 and 0.9996, respectively (Ly and Kim, 2006). The detection of the other aforementioned compounds was successfully achieved using stripping techniques in various buffer solutions. However, when measurements were conducted in biological fluids a pre-accumulation separation was required to remove interfering compounds which would have otherwise accumulate onto the electrode surface.

Table 2.4 – A summary of stripping analysis techniques (Wang, 2000).

Stripping Technique	Analyte	Accumulation	Stripping
Anodic Stripping Voltammetry	Metals	Cathodic deposition (for mercury electrode) $M^{n+} + ne^- + Hg \rightarrow M(Hg)$	Anodic scan (for mercury electrode) $M(Hg) \rightarrow M^{n+} + ne^- + Hg$
Potentiometric Stripping Analysis	Metals	Cathodic deposition (for mercury electrode) $M^{n+} + ne^- + Hg \rightarrow M(Hg)$	Oxidation (by oxidizing agent) $M(Hg) + oxidant \rightarrow M^{n+}$
Adsorptive Stripping Voltammetry and Potentiometry	Metals (Surface-active complex) Organic compounds (with surface active properties)	Formation and absorption of metal complex $M^{n+} + nL \rightarrow ML_n$ $ML_n \rightarrow ML_{n,ads}$	Cathodic scan $ML_{n,ads} + ne^- \rightarrow M^{n+} + nL$
Cathodic Stripping Voltammetry	Organic and inorganic compounds capable of forming insoluble salts	Anodic deposition (for mercury electrode) $A^{n-} + Hg \rightarrow HgA + ne^-$	Cathodic scan $HgA + ne^- \rightarrow A^{n-} + Hg$

2.4.4 Amperometry

Amperometry is the monitoring of a current produced from faradic reactions at an electrode surface, when the potential between the electrodes is constant. This constant potential is ideally the half-wave potential of the analyte being monitored. Thus electron transfer is energetically more favourable for the analyte, thus inducing an inherent selectivity. Also taking into consideration mass transport effects, the current produced is proportional to the concentration of the analyte.

An amperometric biosensor requires an appropriate electrode surface to reduce or oxidise an electroactive species that has been produced by an immobilised selective material (Harwood and Pouton, 1996). The operating potential of the device is not only dependent on the electroactive species, but also on the background current, interfering reactions, surface reproducibility, mechanical properties and cost (Wang, 1999). In order to gain the best compromise for the operating potential of a device a mediator is often used.

A mediator, for example Prussian Blue (Lowinsohn and Bertotti, 2007) or Toluidine Blue (Vostiar et al., 2002), can be electrochemically deposited on an electrode surface. Prussian Blue reduces the oxidation potential of hydrogen peroxide which is used for direct monitoring of glucose and L-Lactate. This reduction in potential makes the device less sensitive to oxygen fluctuations, reduces running costs and moves the operating potential away from the half-wave potential of several possible interfering compounds. Toluidine Blue has amperometric pH-sensitive properties which can be utilised in a biosensor with selective materials that cause changes in the local pH. A urea biosensor is an example of this, the enzymatic reaction of urea and urease produces NH_3 which causes a local change in pH.

2.4.5 Impedance

The properties of an electrochemical system can be attained and monitored by measuring a system's impedance. The impedance of a system is comprised of real (resistive) and imaginary (reactive) components. In most electrochemical systems inductance is assumed to be negligible hence the imaginary component consists purely of capacitance; this is illustrated in Figure 2.3.

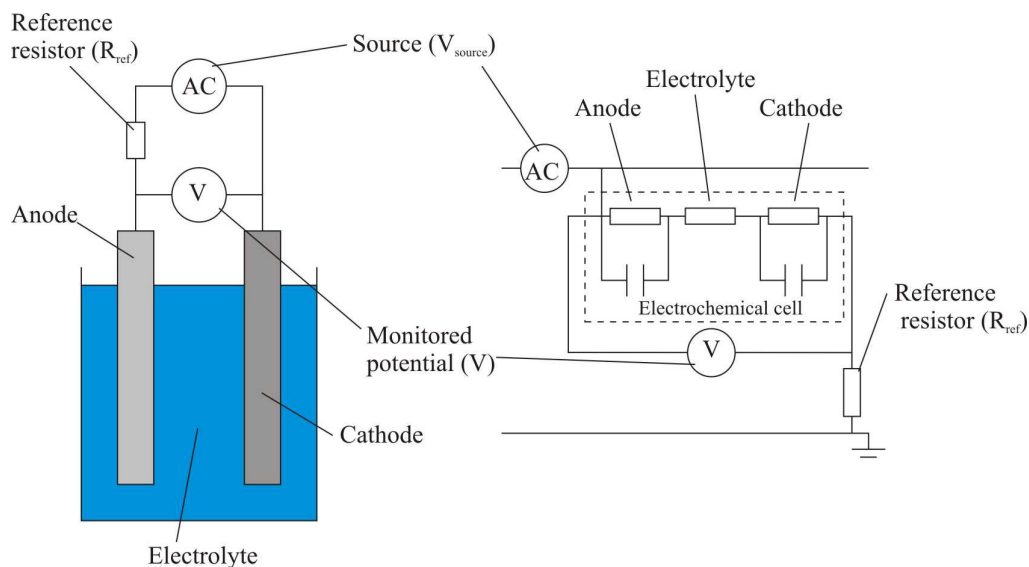


Figure 2.3 – Schematic of electrochemical system and its corresponding circuit.

By either monitoring the impedance while varying the frequency (electrochemical impedance spectroscopy) or by fixing the frequency and monitoring the impedance over time changes in both bulk and interfacial electrical properties and processes can be monitored.

Impedance spectroscopy has been used to measure glucose in PBS by Shervedani and co-workers (Shervedani et al., 2006). They immobilised glucose oxidase on a gold electrode surface using a 3-mercaptopropionic acid SAM and parabenzoquinone as an electron mediator. Increasing levels of glucose leads to a decrease in the faradic charge transfer resistance via the increased reduction of hydroquinone in the diffusion layer; this change in faradic resistance can be seen using impedance spectroscopy. Comparing this approach to an amperometric system reduces the required redox potential (600 to 280 mV) and provides more accurate results; however it was very time-consuming taking 15 minutes to measure a spectrum over a frequency range of 100 mHz to 10 KHz.

The concept of non-intrusive monitoring of blood glucose concentrations via impedance measurement was shown to be possible by Caduff and co-workers (Caduff et al., 2003). They developed a wristwatch-sized device with an open resonant circuit to take the impedance measurements. They concluded that as glucose did not affect the dielectric spectrum in the MHz range the concentration could not be measured directly. However

the electrolyte balance across the tissue membranes caused by variations in glucose could be monitored. These results followed the variations in blood glucose more closely than when using interstitial fluid devices to monitor the variation. Tura and co-worker (Tura et al., 2007) followed this by investigating impedance-based non-intrusive glucose monitoring confirming Caduff results. They showed that at a lower frequency (0.1 – 800 Hz) the impedance was directly affected by the glucose concentration and not reliant on a secondary effect for detection.

Impedance-based devices for monitoring urea have also been investigated: these work on the basis of urea hydrolysis by urease which causes a local change in pH. Sheppard and co-workers (Sheppard et al., 1996) modelled the spatial and temporal evolution of the hydrolysis products to predict the conductivity of such a urea sensor. This model was tested within a concentration range of 10 μ M to 5 mM and the data correlated well to the actual concentration. The change in pH due to urea hydrolysis was also utilised by Cortina and co-workers (Cortina et al., 2006) with degrading polymers which were immobilised on the sensor surface. The polymer degradation caused a measurable change in capacitance.

2.5 Transducers

The performance of any electrochemical investigation is strongly dependent on the working electrode. The choice of electrode material will influence the signal to noise ratio, reproducibility, redox behaviour, charge transfer kinetics and the potential window. In addition, the electrode geometry can strongly affect the diffusion of components to the electrode surface.

2.5.1 Material

The material that a working electrode is constructed of is essential for a good response and reproducible characteristics. One of the most reproducible electrode materials is mercury when used in a drop electrode, as the electrode surface is constantly renewed. This renewal means that the surface is not contaminated and the mercury is in a liquid state it is very smooth with an effective roughness factor of one. Other advantages of using mercury depend on the analyte; mercury has a high hydrogen overvoltage thus, a

large cathodic window, however the anodic range is somewhat limited due to the oxidation of mercury.

Nobel metals, when used as electrode materials, offer several advantages over mercury electrodes, for example they are less toxic. Since they are in a solid state they are more malleable and can be formed into a large variety of configurations which lend themselves to a wider variety of applications. Platinum and gold are some of the most commonly used noble metals. They exhibit good electron transfer and have a large anodic potential window; however, their low hydrogen overvoltage limits their cathodic potential window. In addition, their reproducibility is not as good as the mercury electrode due to the high background current produced by surface oxide and absorbed layers which strongly alter the electron transfer kinetics.

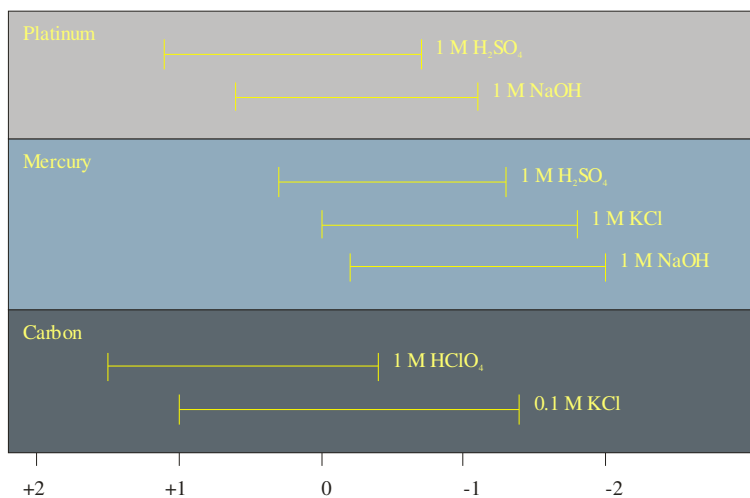


Figure 2.4 – Potential windows of platinum, mercury and carbon electrodes in various electrolytes. (Wang, 2006)

Possibly the most universal electrode material is graphite: this is due to its large potential window, low-cost and chemical inertness, which results in low background currents. However the appropriate preparation of the carbon is essential to ensure that the electrode performs well. This is due to the orientation of the graphite planes: edge orientated plans have a preference towards electron transfer and adsorption, as apposed to basal planes. This is readily demonstrated with carbon nanotubes (Banks and Compton, 2006).

2.5.2 Surface modification

Variations in the electrode surface play an essential role in determining the response of a system: for example, surface modification can influence the electron transfer, result in a preferential accumulation, reduce fouling and act as a selective membrane. These can make the electrode more sensitive and stable, with a higher selectivity. For the purposes of this review, surface modification by imprinted polymers and biologically selective components will be considered as recognition systems and reviewed in detail in Section 2.6.

Self assembled monolayers (SAM) are very versatile materials for modifying electrode surfaces. There are two main methods of self-assembly: i) the spontaneous chemical adsorption of alkanethiols on a noble metal surface and ii) the silanation of an activated surface. Both of these methods can leave an electrode surface with a varied functionality and hydrophobicity depending on the functionality of the end group. It also serves as an ideal anchor for growing polymer to further modify a surface.

As well as growing polymer from anchored SAM, other methods such as electropolymerisation and spin-coating can be used to immobilise polymer. Polymers have been investigated for their anti-fouling properties (Wisniewski and Reichert, 2000), generally due to their hydrophobic nature but they have also been used in vivo for releasing anti-fouling compounds, for example NO (Zhang et al., 2002). Polymers have also been used for immobilising biological recognition compounds and in the construction of molecularly imprinted polymers to increase the specificity of an electrode.

2.5.3 Geometry

The geometry of large electrodes does not significantly affect the response of an electrode. This is because the large surface area of the electrodes dominates the response and effects, such as diffusion and electron transfer, are more dependent on the system and on the electrodes material than on the geometry. However, as the electrode decreases in size geometrical effects become more significant.

Small electrodes do have several advantages, for example higher scan rates can be used in voltammetry due to the lowered double layer capacitance and the signal to

background noise ratio is improved due to the increased rate of mass transport. However, microelectrodes, where a dimension is less than 20 μm , can suffer from a high influence of radial diffusion (Heinze, 1993); this causes a large diffusion layer relative to the size of the electrode resulting in a sigmoidal voltammogram. This effect can be lowered by decrease the electrolysis time which in turn results in a reduction in the thickness of the diffusion layer.

2.6 Recognition systems

A sensor without a recognition element is limited when detecting a specific analyte as it is reliant on the interactions of the analyte with the transducers surface to distinguish itself from other compounds in the sample. In certain circumstances, for example if the analyte forms a complex with the electrode surface or has a distinctive redox potential, direct detection is possible, but within a complex matrix it becomes extremely difficult to distinguish the analyte of interest from background interference.

Due to the difficulties of direct detection, recognition elements in biosensors and chemical-sensors allow the selective detection of the chosen analyte. These recognition elements, in their simplest form, have a single property that causes a change which can be detected by a transducer. Most recognition elements fall into three categories; enzymes, immunosensors and molecular imprinted polymers.

2.6.1 Enzyme

Enzymes are catalytic proteins generally found in biological systems where they play a vital role in determining the metabolic pathway. Each enzyme has a very high specificity for its given substrates. However, their uses in biosensing applications are limited by their narrow operating conditions as they can be easily denatured by changes and extremes in temperature, chemical conditions (pH, salinity, etc) and organic solvents.

Possibly the most well known and commercially available enzyme based sensor is the glucose sensor, which in its simplest form operates on the oxidation of glucose by glucose oxidase (Harwood and Pouton, 1996). Other common applications on the gas sensing of ammonia and CO_2 are when the enzymatic products of deaminating and decarboxylating enzymes are used to measure the concentration of NH_4^+ and CO_2 ,

respectively (Dobay et al., 1999). Enzymatic sensors can be used to detect many metabolites such as urea, creatinine and uric acid. The finding and synthesising of a specific enzyme for a chosen analyte which has good electron transfer, stability and biocompatibility is both extremely difficult and expensive to achieve.

To enhance the enzymes' life time and their resistance to environmental and chemical changes during the operation of enzyme-based devices the enzymes are often immobilised or entrapped (Kobos, 1987), usually directly onto a transducer or in a membrane. Mediators are also used when enzymes are incorporated within electrochemical sensors to reduce the operating potential and increase electron transfer.

2.6.2 Immunosensors

Immunosensors are devices that use immunological reactions as the selective element of the device. Antibodies are immunological proteins that are used to identify alien entities within bodily fluids. The recognition properties of antibodies are defined by the hypervariable part which selectively binds to the epitope of an antigen through a highly specific interaction process, referred to as an induced fit. However as antibodies are proteins, like enzymes, they can only operate under restricted conditions as they are easily denatured.

Immunosensors have several advantages over immunoassays, these advantages include simplification, reduced diagnostic costs, miniaturisation and automation (Wu et al., 2007). Their general principle of operation is based on two methodologies referred to as the sandwich and competitive binding systems (Figure 2.5). There are also other types of immunosensors, such as electroactive labels, metal nanoparticle tracers and label-free capacitive, impedance and amperometric measurements (Wang, 2006).

In the sandwich system (Figure 2.5a), antigens capable of binding two antibodies are utilised. These antigens will bind to the immobilised antibody on the transducer and the labelled secondary antibodies will bind to the immobilised antigen (Wu et al., 2007). In the competitive binding system (Figure 2.5b) the antigen competes with a labelled antigen for the immobilised antibodies binding site. Thus the measured quantity of the labelled antigen remaining after washing is 'negatively proportional' to the concentration of the competing antigen.

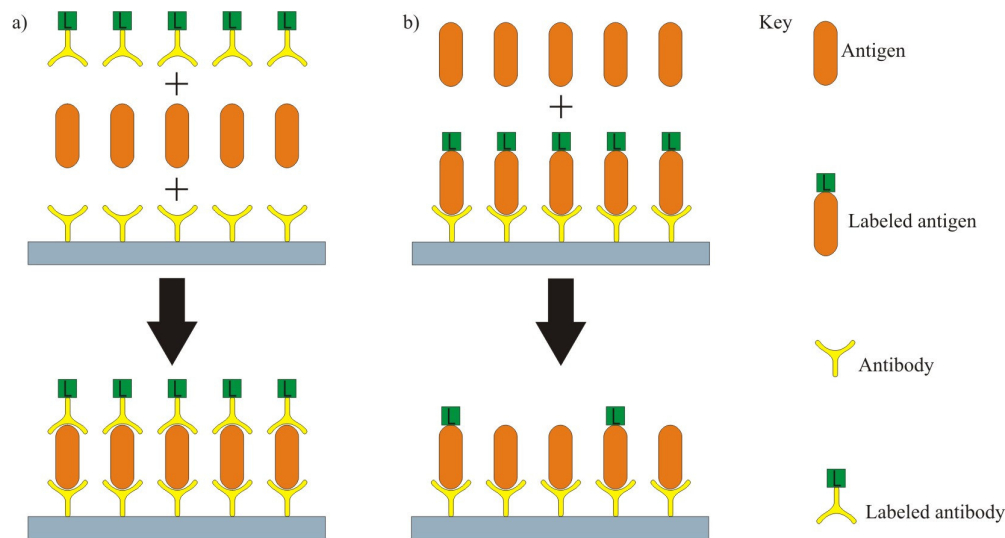


Figure 2.5 – Two immunosensor strategies; a) sandwich technique and b) competitive technique

Most immunosensors can be categorised depending on the transducer used in the device: one typically distinguishes between optical (optoelectronic), electrochemical and mass-based, for example piezoelectric, transducers. Optoelectronic immunosensors tend to have a higher sensitivity than piezoelectric and electrochemical immunosensors (Kim et al., 2004). However their selectivity can be compromised by colouring substances and they are not as reproducible as piezoelectric and electrochemical devices.

Amperometric immunosensors tend to be the most popular as they have a high sensitivity. For example, they have been used for detecting *E. coli* (Abdel-Hamid et al., 1998) using a sandwich approach on carbon rods within a range of 200 to 7000 cells/mL, lactate (Kelly et al., 1998) between 0.005 to 0.12 Units, cocaine (Suleiman and Xu, 1998) by mounting membrane on an oxygen sensor within a range of 0.1 to 10 μM and rabbit IgG (Darain et al., 2003) by using a competitive assay within a range of 0.5 to 2 $\mu\text{g/mL}$. Other electrochemical methods include potentiometric detection, which has been used to detect human IgG (Brown and Meyerhoff, 1991) and rabbit IgG (Sole et al., 1998), conductivity used for detecting human IgG and herbicide (Hianik et al., 1999) and capacitance used for detecting transferrin (Hu et al., 2002).

2.6.3 Molecularly imprinted polymers

Due to the instability and the limitations of biologically derived receptors synthetic alternatives have been investigated. These alternatives involve the design and production of synthetic receptors; however this method has proven extremely difficult for larger or more complex molecules (Haupt and Mosbach, 2000). Another alternative is to use molecularly imprinted polymers (MIP) which are constructed with the aid of supramolecular self-assembly to achieve molecular recognition mimicking that of the antibodies.

The formation of MIP can be illustrated in three stages (Figure 2.6): firstly, the pre-organisation of chosen functional monomers around a target analyte, also known as the template, secondly, the fixing of the monomers around the template in the form of a complex followed by polymerisation with a crosslinker to maintain the orientation of the complex, and finally, the removal of the analyte after polymerisation by washing the resultant MIP which has specific binding sites for the template molecule.

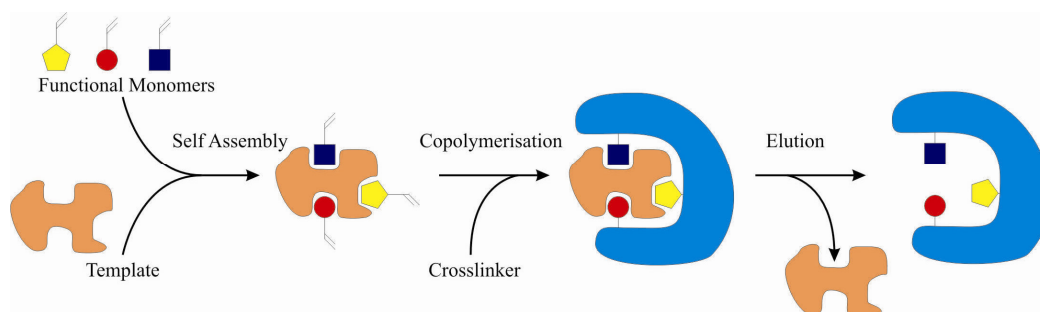


Figure 2.6 – Illustration of the preparation of molecular imprinted polymers.

Currently, the mechanisms governing MIP recognition are not thoroughly understood, for instance a MIP imprinted with tamoxifen has been shown to have a greater affinity for propranolol despite the differences in molecular structure (Mahony et al., 2005). This lack of understanding sometimes results in the poor performance of MIP in practical applications. However, the recent development of computational approaches to molecular modelling in the design of high performance MIPs offers a possible solution (Subrahmanyam et al., 2001). These approaches are based on the hypothesis that a strong monomer-template complex in solution during polymerisation will be preserved, yielding a specific polymer. The advantages of mechanical and chemical

stability, robustness, price and compatibility with mass production (Li et al., 2005) makes MIPs a very competitive alternative to biological derived devices.

MIPs have been used for the detection of a large range of clinically relevant compounds in various ways (Piletsky et al., 2006). For example, Kriz and co-workers used MIP within a competitive binding assay to detect morphine from 0.1 to 10 μgL^{-1} (Kriz and Mosbach, 1995). Piletsky and co-workers monitored the conductivity of imprinted membranes for L-phenylalanine, atrazine and sialic acid (Piletsky et al., 1998) and also grafted MIP onto micro-plates for the detection of epinephrine with target applications for drug screening (Piletsky et al., 2000). Voltammetric techniques incorporating MIPs have also been used for detecting adenine (Spurlock et al., 1996), cholesterol (Piletsky et al., 1999) and clenbuterol (Andrea et al., 2001). Custom dyes have been synthesised and incorporated into MIP for the detection of adenosine (Turkewitsch et al., 1998) and fructose (Wang et al., 1999). In addition, Thin polymer layers have been grafted for the capacitive detection of creatinine (Panasyuk-Delaney et al., 2002) and glucose (Cheng et al., 2001).

2.6.4 Conclusions on clinical sensing technology

Patient care can be enhanced by providing health care professionals with monitoring systems to observe the essential clinical parameters of their patients. These monitoring systems require sensing devices with specificity for analytes of interest and responses which effect the analyte concentrations accordingly. The range of critical parameters that a clinician may wish to monitor is vast, although there is usually a priority depending on the treatment and condition of the patient. Several methodologies have been investigated to monitor these parameters with varying success. However, with such a large range of targets finding and developing technologies for monitoring these analytes remains a significant and unresolved challenge.

There are various ways to utilise electrochemical techniques to detect the presence and concentration of an analyte. The technique chosen is dependent on the redox properties of the analyte and/or the availability of selective materials, for example membranes, enzymes and grafted polymers. The consequence of this is that a wide range of possible solutions can be considered for the detection of an analyte using electrochemical techniques. It can be seen that choosing the right transducer for a device depends on the

analyte being investigated and the surface modifications required. For most applications the use of solid state electrodes is preferred and the effects of electrode materials and geometry need to be considered as this could strongly affect the response.

The analysis of a single compound in a complex matrix, for example blood or plasma, is difficult due to the interference of the other components; thus a recognition element is essential for these systems. Although enzymes and antibodies have extremely selective recognition they have several limitations which can possibly be overcome by using molecular imprinting.

From this review the possibility of creating a MIP-based electrochemical device to detect a chosen clinical analyte seems feasible.

Chapter 3 - Conductometric detection of propofol using molecular imprinting

“Insanity: doing the same thing over and over again and expecting different results.”
Albert Einstein (1879 - 1955)

3.1 Introduction

An initial introduction into molecularly imprinted polymer-based sensors for use in clinical analysis was conducted to investigate the possibility of an impedance based device for the detection of propofol. The intention of this investigation was to look at the feasibility of such a sensor while allowing valuable experience and knowledge to be gained about the production of MIP sensors and various analytical techniques used in clinical environments.

3.1.1 A review of propofol and its detection

Propofol is an anesthetic agent used worldwide in both medical and veterinary practices. It was initially developed as an ‘outpatient’ anesthetic (Smith et al., 1994), however due to its fast action (30-50 s) and recovery (4-6 minutes) with few side effects, it has become more widely used as an intravenous sedative in intensive care units.

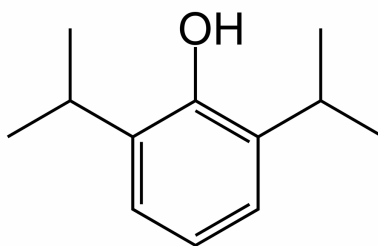


Figure 3.1 – The structure of propofol.

A variety of methods have been investigated for the detection of propofol; these generally employ a sample preparation, then HPLC separation with UV, fluorimetric or

electrochemical detection. Plummer and co-workers (Plummer, 1987) found the most sensitive technique by combining liquid-to-liquid extraction with HPLC fluorescence detection to obtain a detection limit of 2 ng mL^{-1} . Plummer also expressed a preference for using whole blood during the analysis, as propofol's lipophilicity leads to extensive propofol-blood binding (Bajpai et al., 2004). Solid phase extraction (SPE) has also been used to separate propofol from plasma (Bajpai et al., 2004) or serum (Eubel et al., 1990) which is advantageous as it is less time-consuming and can achieve a good recovery. Using this technique, Bajpai and co-workers used hydrophobic-lipophilic cartridges with recoveries of greater than 95% and attained a detection limit of 10 ng mL^{-1} (Bajpai et al., 2004).

The electrochemical detection of propofol has been achieved using both SPE (Benoni et al., 1990) and liquid-to-liquid extraction (Eubel et al., 1990, Dowrie et al., 1996), followed by HPLC detection. The latter allowed detection limits of 10 ng mL^{-1} from a $250 \mu\text{L}$ sample of plasma or serum and 5 g mL^{-1} from a $1000 \mu\text{L}$ sample. An investigation and optimisation into the detection of purchased propofol on glossy carbon electrodes showed that increasing the pH above the pK_a (11.65), so that the propofol becomes deprotonated, shifts the potential to a more negative value (Pissinis and Marioli, 2007). This reduces the background current and increases the sensitivity of detection.

3.2 Investigations into the use of molecularly imprinted polymers for the detection of propofol

Prior to this research, Cranfield University performed research on behalf of Sphere Medical aimed at the development of MIPs for the detection of propofol. In a first phase of the work computational design of a polymer composition was implemented and corresponding polymers were synthesised and tested for their affinity to propofol using solid phase extraction and UV spectroscopy. The best polymers were made using diethylamino ethylmethacrylate as a functional monomer.

The results from this initial investigation showed that the MIP synthesised had properties which were in good correlation with the results obtained from the computational design and the best MIP was produced using the composition shown in Table 3.1.

Table 3.1 – Propofol polymerisation mixture.

	Substance	Mass (mg)	Role
NIP	Diethylamino ethylmethacrylate (DEAEM)	525	Monomer
	Ethleneglycol dimethacrylate (EGDMA)	3262	Crosslinker
	Acentonitrile	3925	Porogen
MIP (as above but with template)	Propofol	125	Template

In the following work the aforementioned polymer was immobilised onto an electrochemical sensor and the detection of propofol, using impedance methods, was investigated.

3.2.1 Impedance monitoring and strategies for MIP immobilisation

Due to difficulties experienced in previous investigations by Cranfield University and Sphere Medical in the detection of propofol via its oxidation, an investigation into the detection of propofol by monitoring variations in impedance was undertaken.

The following is the summary of this investigation which illustrates the immobilisation of the computationally designed MIP and its response to propofol.

3.2.2 Sensors

The microchip used is a silicon based substrate of approximately 6 mm x 4 mm that currently has up to six sensors integrated on its surface. The sensors used in this work consisted of two parallel electrodes (highlighted on the right in Figure 3.2). The test solutions were delivered to the microchip via a flow cell (Figure 3.7). The other sensors used for the initial investigation were gold interdigitated microsensor electrodes supplied by Abtech Scientific (Virginia, US).

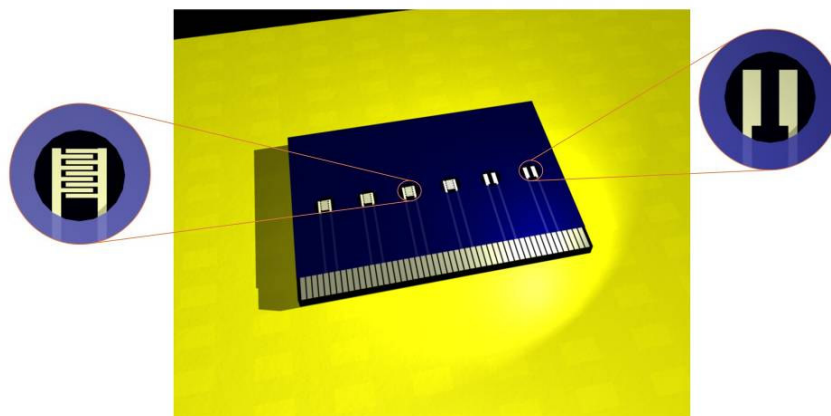


Figure 3.2 – Schematic representation of microchip with its two sensor configurations. The parallel electrodes are highlighted on the right.

3.2.3 Polymer immobilisation

A different process was used for the polymer immobilisation between the different sensor platforms. The first process used for immobilising the polymer onto the Abtech electrodes was by photografting, using the polymer onto the transducer's surface through a suitable covalently attached photo-initiator. The second process for the microchip sensor employed the deposition of a discrete amount of pre-polymerisation mixture, containing a photo-initiator, followed by an in-situ polymerisation.

3.2.3.1 Photografting on Abtech electrodes

In order to adhere a polymer film to the sensor's surface, vinyl groups were anchored to the substrate and during the photo-polymerisation these groups became bound to the polymer. Therefore the polymer was anchored to the sensor substrate. This procedure can be sub-divided into two parts, where (i) the substrate is derivatised via the creation of a vinyl monolayer and (ii) the substrate is immersed in the pre-polymerisation mixture and subsequently the polymerisation was initiated by UV irradiation. This is the procedure used to immobilise the polymers on the Abtech sensors.

(i) Creating vinyl monolayer

The sensor surface was first cleaned to remove any foreign particles by ultrasonically cleaning the silicon chips in acetone for 10 minutes. The chips were then removed, blown dry

with nitrogen and stored in a Petri dish. Secondly the silanol groups were activated in order to produce abundance of free hydroxyls (Figure 3.3a) (Williams and Blanch, 1994). This was achieved by immersing the chips in 30% acetic acid in hydrogen peroxide (30%) at room temperature for 40 minutes and then thoroughly rinsing the chip with deionised water.

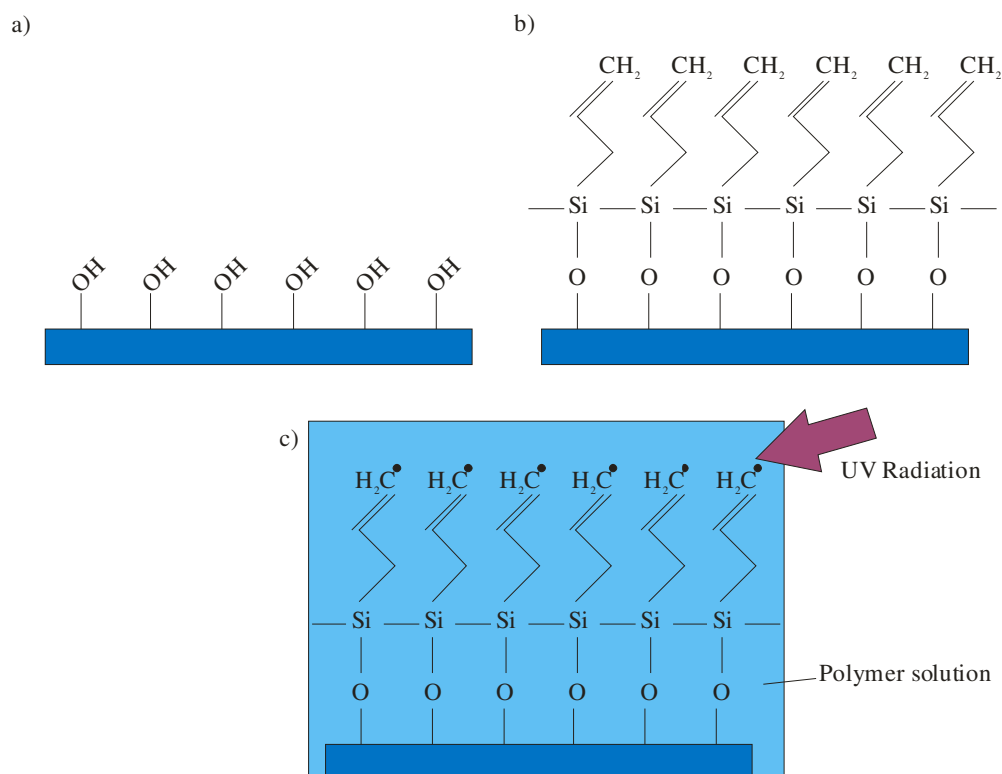


Figure 3.3 – Covalent immobilisation of vinyl groups onto SiO_2 surface. a) activation of silanol groups, b) derivatisation of surface with vinyl-silane and c) free radical formation in polymer solution.

The hydroxyls on the surface can be chemically derivatised via covalent coupling with allyltriethoxysilane (ATES) which results in vinyls as the reactive surface group (Figure 3.3b). By submersing the chips in 2% ATES in toluene for three hours this derivatisation was accomplished. The chips were then rinsed with acetone and blown dry in nitrogen to remove any unbound material.

(ii) Polymerisation procedure

The polymer mixture (Table 2.5) was degassed with nitrogen for 10 minutes to remove dissolved oxygen (as it is a free-radical scavenger). 2 μL of the polymer mixture was

deposited on the sensor and covered with a glass slide, which had been coated in dichlorodimethylsilane to prevent the slide from adhering to the polymer (Figure 3.4a). Finally, the sensor was exposed to UV radiation through a low-pass UV filter (< 350nm). The chip was then rinsed in methanol and dried in nitrogen.

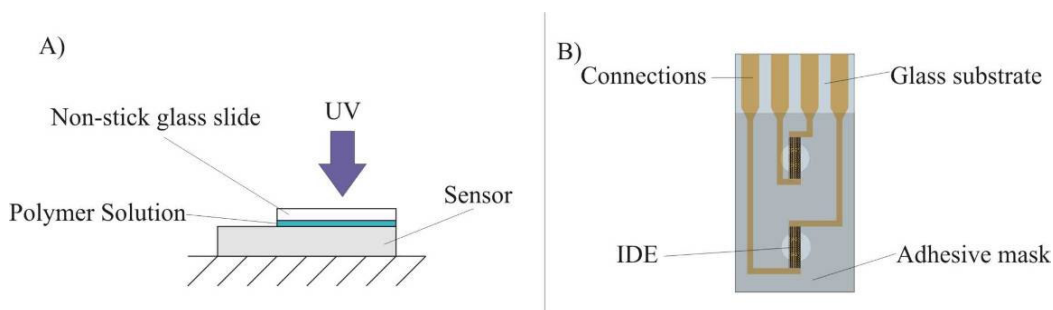


Figure 3.4 – Schematic of polymerisation using a grafted initiator. A) polymerisation and B) final sensor.

The connections to the IDE sensors are masked off using UV cured adhesive with the aid of a silicon template to produce the final sensor (Figure 3.4b).

Table 3.2 – Composition of grafting polymerisation mixture.

	Substance	Mass (mg)	Role
NIP composition	Diethylamino ethylmethacrylate	525	Monomer
	Oligourethane Acrylate : TriCethylene dimethacrylate, (15 : 85)	3262	Crosslinker
	DMF	3925	Porogen
	2-2-dimethoxy-2-phenylacetopenon	77	Initiator
MIP (as above but with template)	Propofol	125	Template

3.2.3.2 Deposition onto microchip sensor

The immobilisation of polymer using photopolymerisation is a quick and effective way to produce polymer films. The microchip sensors have wells surrounding the electrodes which allow easy deposition of the polymerisation fluid; the well was originally

designed for depositing membranes. The procedure is as follows: the deposition mixture stated in Table 3.3 was dispensed onto the sensor electrodes with varied volumes of 5 nL and 20 nL using a nano-syringe (Figure 3.5a) and the polymerisation was initiated by UV (Cermox xenon, PerkinElmer) radiation (Figure 3.5b). Parameters such as UV intensity, distance from the UV source to the sensor surface, UV exposure time and volume deposited could also be varied to attain a polymer film with optimum thickness.

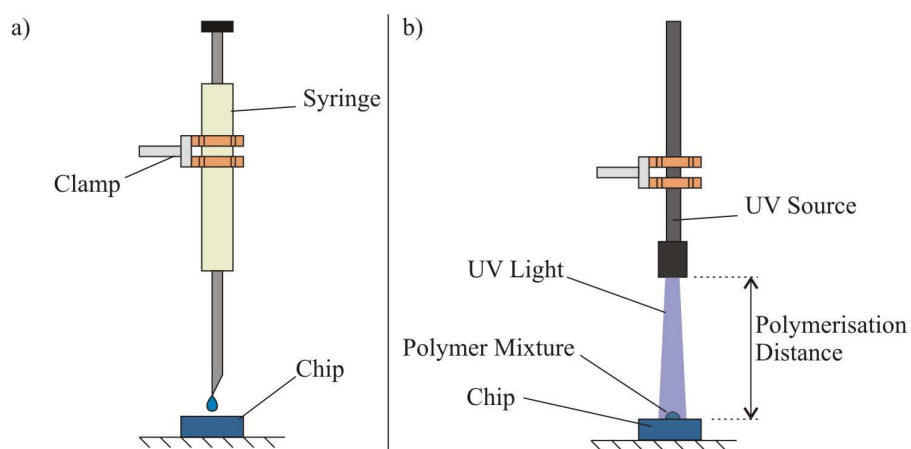


Figure 3.5 – Schematic of polymer deposition technique, a) pre-polymerisation mixture being deposited and b) deposited polymerisation mixture being polymerised by UV radiation.

After the polymerisation, the chips were rinsed in a stream of methanol to remove any polymeric material which had not strongly bound to the surface.

It is suggested in the literature (Le Noir et al., 2007, Liyong Zhang, 2002) that the addition of PVA to a MIP can increase its porosity once it has been washed out. Since the increase in porosity can be beneficial to the availability of binding sites, PVA was added to the MIP mixture in 1% and 5% by mass, to observe if it had any effect on the sensor response.

Table 3.3 – Protocol for deposition of NIP and MIP mixtures.

	Substance	Mass (mg)	Role
NIP	Diethylamino ethylmethacrylate	525	Monomer
	Ethleneglycol dimethacrylate	3262	Cross-linker
	Acentonitrile	3925	Porogen
	2-2-dimethoxy-2-phenylacetopenon	77	Initiator
MIP (as above but with template)	Propofol	125	Template

3.2.4 Impedance monitoring

The impedance of the sensors was monitored using a lock-in-amp (Stanford Instruments, RS830) to measure the magnitude and phase difference of the potential across a reference resistor. These measurements were then used to calculate the current in the system and, in turn, calculate the impedance in the sensor.

In order to simplify the impedance system, a high frequency (5 kHz) was used to monitor the sensors' impedance. This technique reduces the effects of the double layer capacitance to insignificant levels as can be seen in Equation 3.1, where X_c is the reactance due to a capacitive effect, c , at a frequency of f hertz.

$$X_c = \frac{1}{2\pi f c} \quad \text{Equation 3.1}$$

Figure 3.6 demonstrates the sensor modelled using a Randle cell and the simplified model of the circuit at high frequencies when the capacitance is negligible. This demonstrates that the sensor is equivalent to a series resistor.

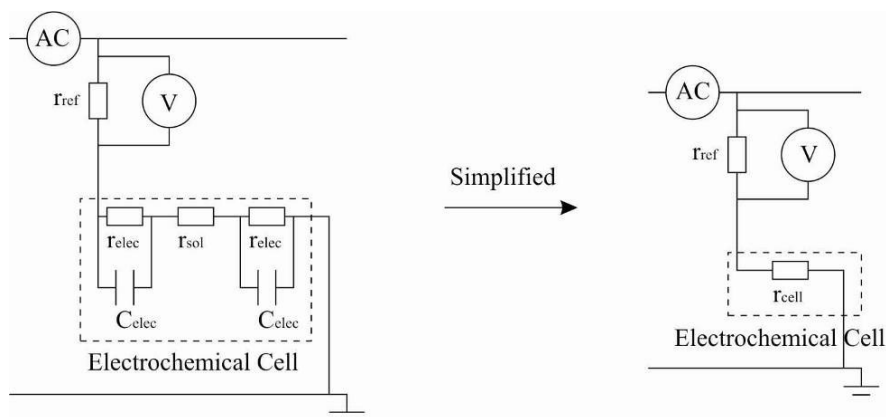


Figure 3.6 – Circuit diagrams of the impedance monitoring system and the simplified system assuming negligible capacitive effect at high frequencies. Reference resistance (r_{ref}), electrode resistance (r_{elec}), solution resistance (r_{sol}) and electrode capacitance (C_{elec}).

Following Ohm's, law the impedance can be expressed as;

$$r_{cell} = \frac{V_{sou}}{V_{ref}} r_{ref} - r_{ref} \quad \text{Equation 3.2}$$

where, r_{cell} is the sensor resistance, r_{ref} is the reference resistance, V_{sou} is the source potential and V_{ref} is the potential across the reference resistor.

3.2.5 Investigatory procedures

3.2.5.1 Procedure for testing the Abtech sensors

The conductivity measurements for the Abtech sensors were conducted by submerging the sensor into a test solution and using the lock-in amplifier to measure the potential difference across a reference resistor as explained in Section 3.2.4. Each sensor was washed in 10 mM HCl and 10 mM NaOH with deionised water before and after each wash to prevent salt formation, and then dried in a stream of nitrogen. To test the sensor it was immersed in the test solutions with varying concentrations of propofol. After each test, the chip was washed using the above procedure and once again dried in a stream of nitrogen. The concentration of the test solution was then changed to the next concentration and the above process was repeated until all concentrations were tested.

3.2.5.2 Procedure for testing the flow cell microchip sensors

It was foreseen that during the operation of the final sensor, the test fluid would be pumped over the microchip sensor and tests were conducted when the fluid was stationary. To simulate this, the test solution in the experiments was pumped through the flow cell (Figure 3.7) and tests were taken as the solution was flowing and stationary.

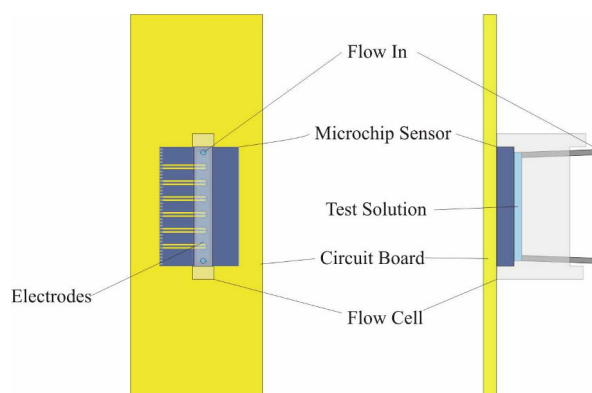


Figure 3.7 – Schematic of flow cell sensor.

The above was achieved by pumping PBS over the sensor for 100 seconds to attain a baseline, then the test solution was introduced into the system for 50 seconds at a constant flow rate and this was then flushed out again with PBS for 50 seconds. The test solution was once again introduced into the system but this time the pump was turned off for 100 seconds until the pump was restarted and the flow cell was flushed out with PBS.

To clean the sensors before and after use and to remove any propofol after injection, 0.1 M HCl in deionised water with 20% methanol and then 0.1 M NaOH in deionised water with 20% methanol were flushed over the sensor with deionised water used in between the aforementioned injections to prevent salt formation.

3.3 Results of impedance monitoring for immobilised MIP

3.3.1 Investigation of Abtech sensors with photografted MIP films

As an initial investigation into the possibility of detecting propofol using a conductometric sensor, the response of a sensor with molecularly imprinted (MIP) and

non-imprinted (NIP) polymers were compared (Figure 3.8). The NIP sensor had a lower overall resistance than the MIP sensor and both sensors demonstrated an exponential decrease in resistance, as the concentration of propofol increased. The change in resistance of the MIP sensor was approximately twice as large as the NIP sensor's resistance.

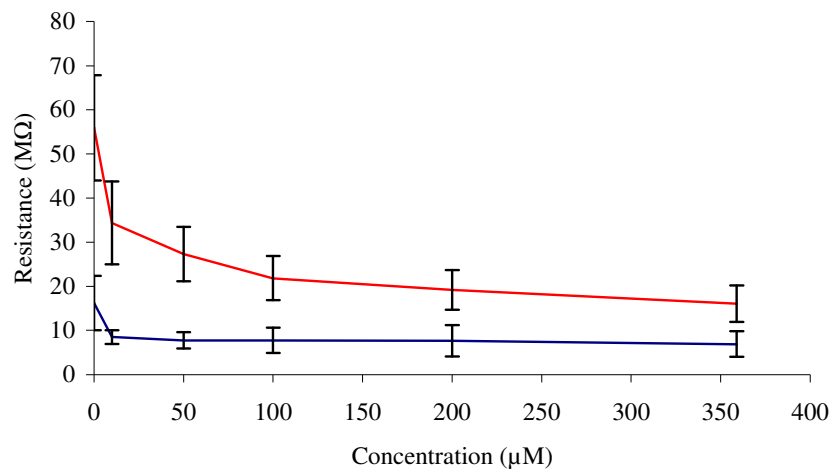


Figure 3.8 – Response of microchip sensor to varying concentrations of propofol (Red – MIP, Blue – NIP).

A bare sensor (Figure 3.9) with no immobilised polymer, had a slight increase in resistance as the propofol concentrations increased. This could be explained by the possible adsorption of propofol to the electrode surface thereby decreasing the electron transfer. However, this increase was minimal and no change was larger than the standard deviation.

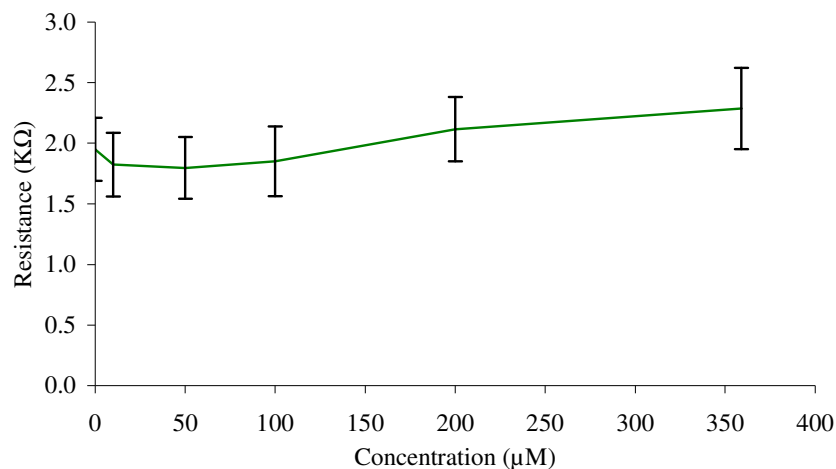


Figure 3.9 – Response of bare microchip sensor to varying concentrations of propofol.

3.3.2 Initial investigation of deposited MIP films on microchip sensors

As an initial investigation into the impedance response of the immobilised MIP layers using the deposition technique, several microchip sensors were prepared with a polymerisation distance of 3 cm and a polymerisation time of 3 minutes. These were tested, simulating the foreseen operating procedure of the final device by spiking the solutions with 100 μM of propofol.

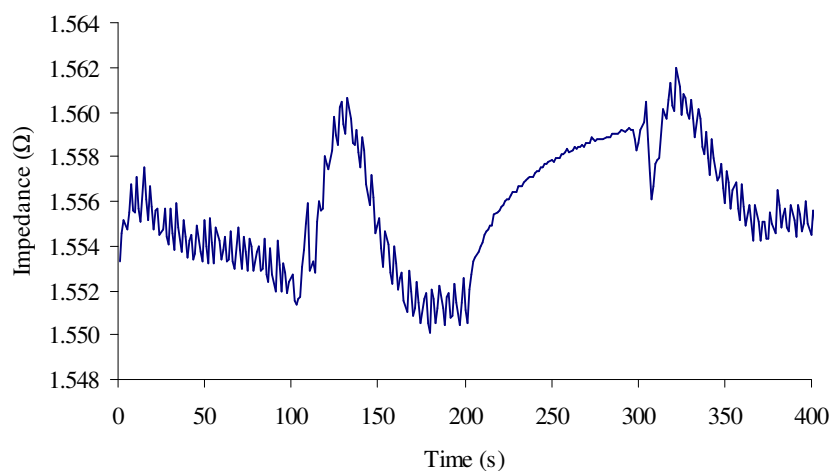


Figure 3.10 – Impedance response of a bare microchip sensor to propofol (100 μM). Propofol introduced at $t = 100$ s for 50 s and at 200 s for 100 s with no flow.

An example of the response of a bare microchip electrode can be seen in Figure 3.10. The peak response from the baseline achieved with 100 μM of propofol in stationary flow was approximately 7.7 m Ω . The same test was conducted on a microchip with a MIP layer, however this did not give any variation in the response.

The response of a microchip with an immobilised MIP layer containing 1% PVA can be seen in Figure 3.11. The peak response of this sensor was negligible when 100 μM of propofol was injected and it had a response of 8.3 m Ω in stationary flow. The trend of the 5% PVA MIP was the same as the 1% PVA MIP, however the magnitude of the change was 6.0 m Ω .

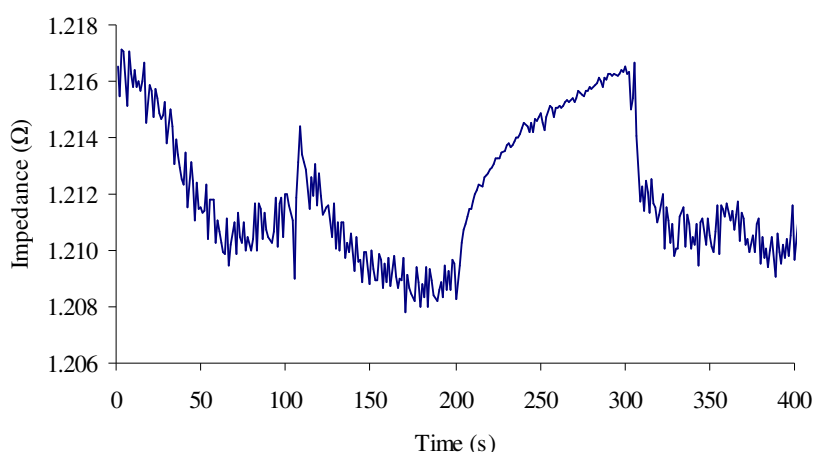


Figure 3.11 – Impedance response of a molecularly imprinted microchip sensor (with 1% PVA) to propofol (100 μM). Propofol introduced at $t = 100$ s for 50 s and at 200 s for 100 s with no flow.

3.3.3 Discussion of impedance monitoring using MIP-coated electrodes

3.3.3.1 Photografted MIP on Abtech electrodes

The variation in the impedance between the bare and polymer-coated Abtech sensors can be explained by the decrease in electron transfer, due to the non-conducting polymer layers immobilised onto the surface.

Both the immobilised NIP and MIP electrodes share a similar trend in their responses to various concentrations of propofol. The observed trend is an exponential decrease in resistance as the propofol concentration increases. A possible explanation for this is

that the binding of the propofol to the polymer causes the polymer to swell (Mahony et al., 2005) leading to an increase in the size of the polymer pores. Thus, making it easier for the ionic species in the buffer to reach the electrode surface.

The steeper gradient at low concentrations for the MIP microsensor suggests that it has a higher sensitivity and a larger range to propofol than the NIP. Also, at higher concentrations, the variation in the NIP becomes less apparent. This is probably due to the saturation of the NIP polymer with propofol, hence the polymer could not swell anymore.

3.3.4 Deposited MIP on microchip electrodes

In the flow cell microchip sensor, the bare sensor showed a response (increase in the impedance of the system) to the presence of propofol when the flow of propofol was both moving and stationary. The sensors responded to 100 μM concentrations of propofol demonstrating that the propofol solution has a lower impedance than the PBS solution.

The response of all the microchip sensors, with the immobilised polymer, had similar reactions to that of the bare microchip sensor's. Therefore the immobilised polymer had no or little effect on the sensor response.

3.3.5 Conclusion of impedance monitored MIP

The results from the Abtech microsensor with the photografted polymer shows promise, as there was a significant difference between the NIP and MIP responses. However, the deposited imprinted polymer films on the microchip sensors show little difference. Thus, the immobilised polymer formed using the deposition technique needs to be investigated.

3.4 Investigation of MIP immobilisation procedure on microchip device

The aim of this section is to explore some of the possible areas that will require further understanding to enable a selective response from the microchip sensor with a deposited MIP coating. The previous investigations using this procedure to produce a sensor did not produce a working sensor.

The areas of interest are in identifying the presence and quality of the polymer layer, the frequency at which any capacitive effects become negligible and, finally, the effect of varying the polymerisation parameters.

3.4.1 Analysis techniques for investigating immobilised MIP

3.4.1.1 Impedance analysis

Impedance analysis is a useful technique in investigating both interfacial and bulk electrical properties and processes in an electrochemical system. By monitoring the impedance of an electrochemical system changes in both capacitance and resistance can be seen. As the reactance of a system is related to the applied frequency of the source potential (Equation 3.1), model systems can be fitted to an acquired frequency spectrum. The simplest model is the Randles cell (Figure 3.12) which consists of three main components; the solution resistance (R_s), charge transfer resistance (R_t) and the double layer capacitance (C_{dl}). These result in a semi-circular response on a Nyquist plot.

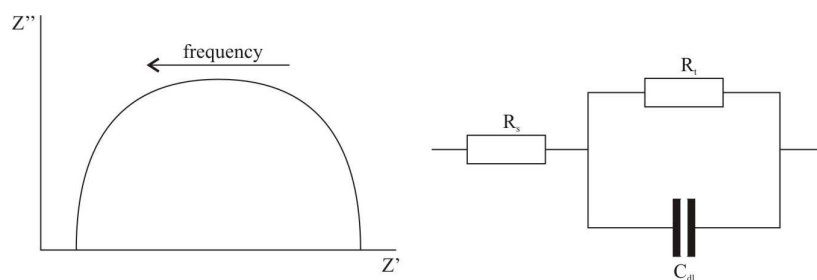


Figure 3.12 – Nyquist plot and equivalent circuit of a Randles cell. R_s – solution resistance, R_t – charge transfer resistance and C_{dl} – double layer capacitance.

All impedance analysis was conducted using an ACM AutoACpsp Impedance Analyser. The impedance was measured between a frequency of 1 to 10000 Hz with a 32 mV signal amplitude, 0 V offset and an automatic reference resistance.

3.4.1.2 Cyclic voltammetry

All voltammograms were attained using an AutoLab PSTAT10 (Netherlands) between -600 mV to 1200 mV at a scan rate of 200 mVs^{-1} in $5 \text{ mM K}_4\text{Fe}(\text{CN})_6^{4-}$ plus $5 \text{ mM K}_3\text{Fe}(\text{CN})_6^{3-}$ in deionised water (from now on referred to as $\text{KFe}(\text{CN})_6$).

3.4.1.3 Investigatory procedures

All of the following procedures were conducted on the microchip electrodes (Section 3.2.2) with various polymer coating immobilised by using the deposition technique explained in Section 0.

3.4.1.4 Procedure for investigating the changes from varying the polymerisation parameters

The two main polymerisation parameters are i) the polymerisation time which defines the time of exposure to the UV radiation and ii) the polymerisation distance which alters the intensity of the UV exposure. The polymerisation distance is illustrated in Figure 3.5. The impedance spectra of several polymerised electrodes were measured. The polymerisation distances varied between 1 – 5 cm and the polymerisation time varied between 1 – 10 minutes.

3.4.1.5 Procedure for investigating frequency at which to monitor deposited polymer layers

Each sensor underwent cyclic voltammetry (CV) and impedance analysis in PBS (pH 7.5) before and after polymerisation. The various test solutions were delivered to the flow cell (Figure 3.7) at 3 mLs^{-1} and left to settle for 1 minute before any measurements were taken.

Before and after each test the sensors were cleaned using 0.1 M HCl in deionised water with 20% methanol and then 0.1 M NaOH in deionised water with 20% methanol. Deionised water was flushed through the system before and after each of the aforementioned steps to reduce the possibility of salt formation. After cleaning, the test solution was pumped into the flow cell at 3 mLs^{-1} and then the device was left for 1 minute to settle before commencing with the measurement.

By comparing the CVs and impedance spectra before and after polymerisation, variations in the electrochemical properties of the electrodes, for example, charge transfer resistance, diffusion flux and cell impedance can be investigated. All of these comparisons will shed light on the polymer that was immobilised on the microchip electrodes. Also an optimal frequency for impedance monitoring can be acquired when the capacitive effects are lowest.

3.4.2 Results of measurements using MIP-coated microchip device

An example of the results obtained from sensor microchips coated with polymers prepared with various polymerisation times and distances can be seen in Figure 3.13 and Figure 3.14. There appears to be no correlation between the polymerisation time and distance and the impedance spectrum of the sensor. 70% of the sensors produced demonstrated a purely capacitive response. This shown by the inversely decreasing impedance with increasing frequency fitting the trend of Equation 3.1.

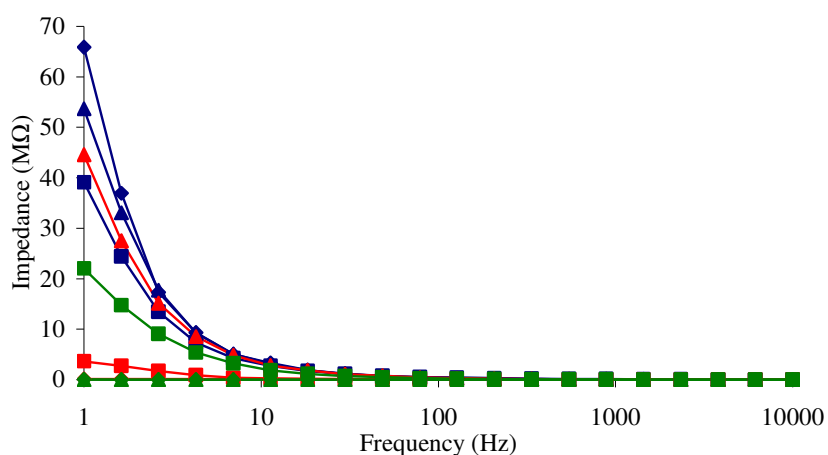


Figure 3.13 – Impedance spectrum of deposited MIP (5 l) microchip electrodes with varied polymerisation times and distances. Polymerisation time; blue – 1 minute, red – 5 minutes and green – 10 minutes. Polymerisation distance; square – 1 cm, diamond – 3 cm and triangle – 5 cm.

Some of the sensors had a trend typical of a Randles cell, these sensors have much lower impedances and can be seen in more detail in Figure 3.14 with a corresponding Nyquist plot of the 5 minute 3 cm polymerisation in Figure 3.15. However, there was no correlation between the polymerisation parameters and the trend of the impedance spectrums.

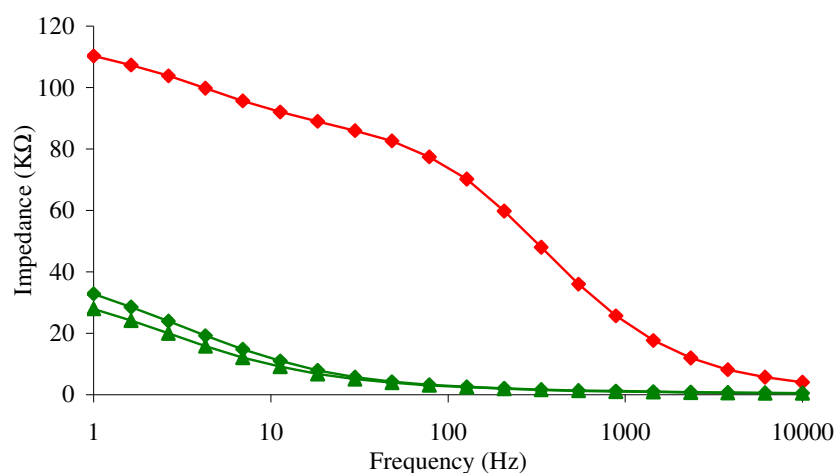


Figure 3.14 – Impedance spectrum of deposited MIP (5 nl volume of monomer mixture) microchip electrodes as shown in Figure 3.13 with varied y-axis scale. Polymerisation time; red – 5 minutes and green – 10 minutes. Polymerisation distance; diamond – 3 cm and triangle – 5 cm.

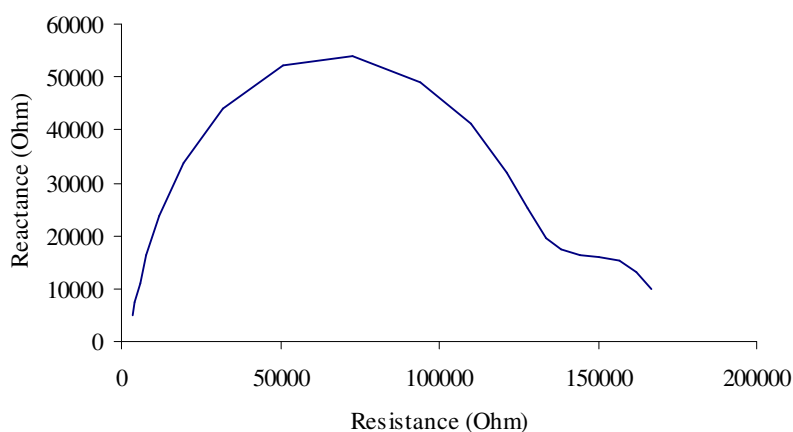


Figure 3.15 – Nyquist plot of MIP (5 nl volume of monomer mixture) deposited microchip electrode, polymerised for 5 minutes at a distance of 1 cm.

The bare microchip sensors that had a typical Randles cell behaviour, this is a semi-circular response which can be seen in the Nyquist plots (Figure 3.16 and Figure 3.17), were further investigated with the deposition of MIP.

The deposition of the MIP layer increases the charge transfer resistance and accordingly the 20 nL deposited MIP gave a greater increase in the resistance than the 5 nL MIP.

No difference in the impedance spectrums could be seen with the addition of 100 μM of propofol to the electrolyte on both the bare and MIP sensors.

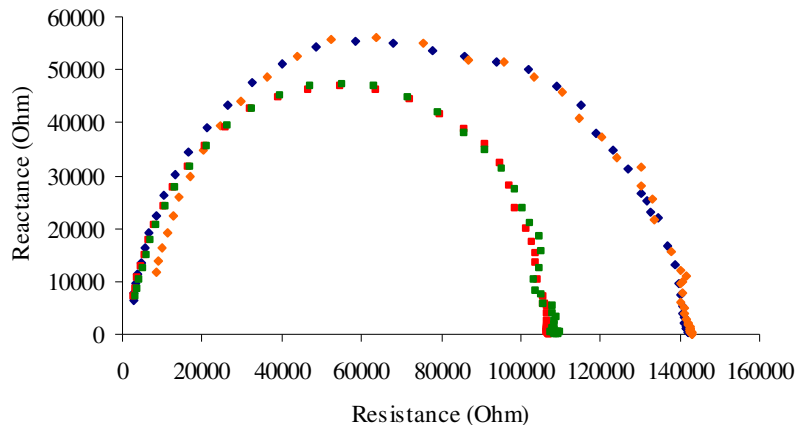


Figure 3.16 – Nyquist plot of bare and deposited MIP (5 nl volume of monomer mixture) microchip electrode in PBS (pH 7.5) and 100 μM propofol. Blue – MIP in PBS, orange – MIP in propofol, red – bare in PBS and green – bare in propofol.

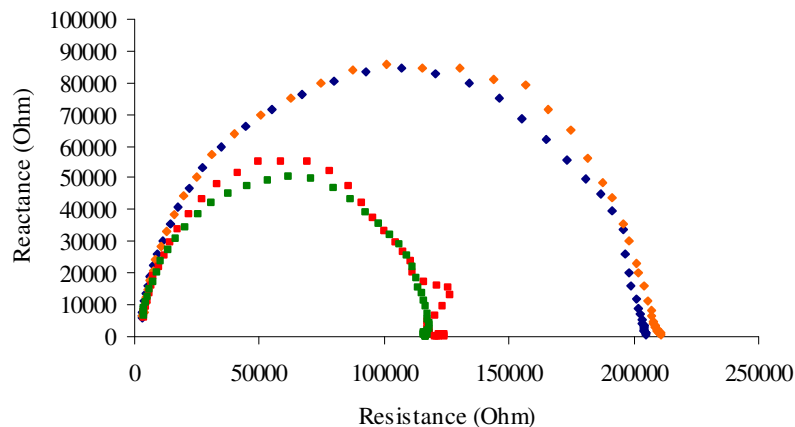


Figure 3.17 – Nyquist plot of bare and deposited MIP (20 nl volume of monomer mixture) microchip electrode in PBS (pH 7.5) and 100 μM propofol. Blue – MIP in PBS, orange – MIP in propofol, red – bare in PBS and green – bare in propofol.

Bode plots (Figure 3.18 and Figure 3.19) of the bare and deposited MIP layers, with deposited volumes of 5 nL and 20 nL, show that the impedance is mainly resistive (the phase tends towards 0°) below 100 Hz, capacitive (the phase tends towards 90°) at 5000 Hz and consisting equally of resistive and capacitive components at 1000 Hz.

The change in impedance in the Bode plots iterates that of the Nyquist plots, for example the difference in impedance between 1 and 200 Hz, is the difference in charge transfer resistance between the bare and MIP electrodes.

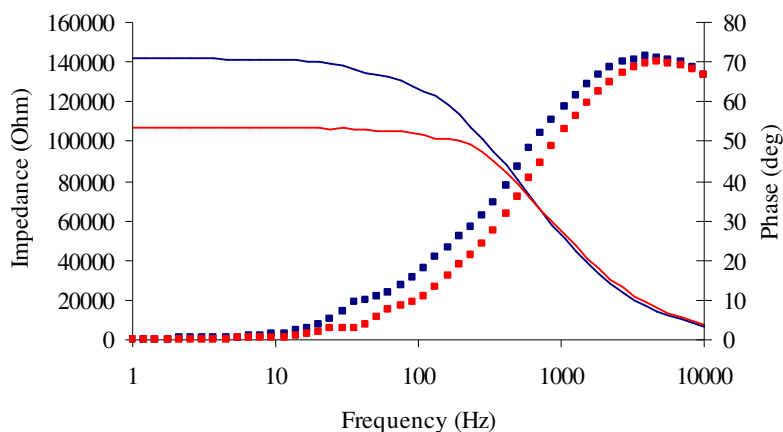


Figure 3.18 – Bode plot of bare and deposited MIP (5 nl volume of monomer mixture) microchip electrode in PBS (pH 7.5) and 100 μ M propofol. Blue – MIP, red – bare, line – impedance and square – phase.

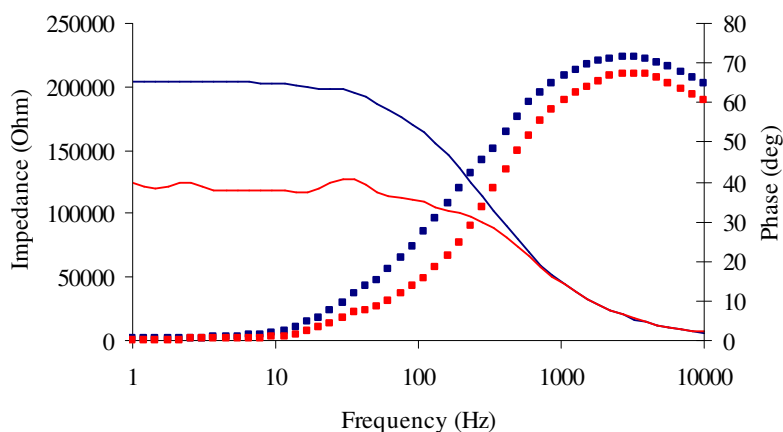


Figure 3.19 – Bode plot of bare and deposited MIP (20 nl volume of monomer mixture) microchip electrode in PBS (pH 7.5) and 100 μ M propofol. Blue – MIP, red – bare, line – impedance and square – phase.

Cyclic voltammograms (Figure 3.20) of the bare and 5 nL deposited MIP sensor in $\text{KFe}(\text{CN})_6$ show an increase in the redox peaks with the addition of the MIP, thus contradicting the conclusion from the impedance spectroscopy that there is an increase

in the charge transfer resistance. There is also no difference in the voltammogram when propofol is introduced to the test solution.

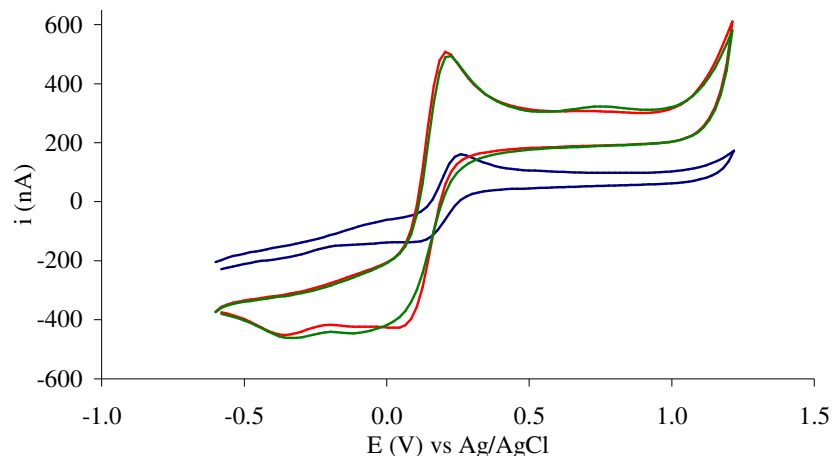


Figure 3.20 – Cyclic voltammetry (50 mVs^{-1}) of bare and deposited MIP (5 nl volume of monomer mixture) microchip electrode. Blue – bare in PBS, red – MIP in PBS and green – MIP in propofol.

The cyclic voltammograms (Figure 3.21) of the bare electrode used for the 20 nL deposition had a considerably higher redox peak than the electrodes used for the 5 nL deposition and the addition of the MIP caused a slight decrease in the current. The addition of propofol to the 20 nL deposited MIP caused a decrease in the current of the sensor, however this was only seen on one sensor.

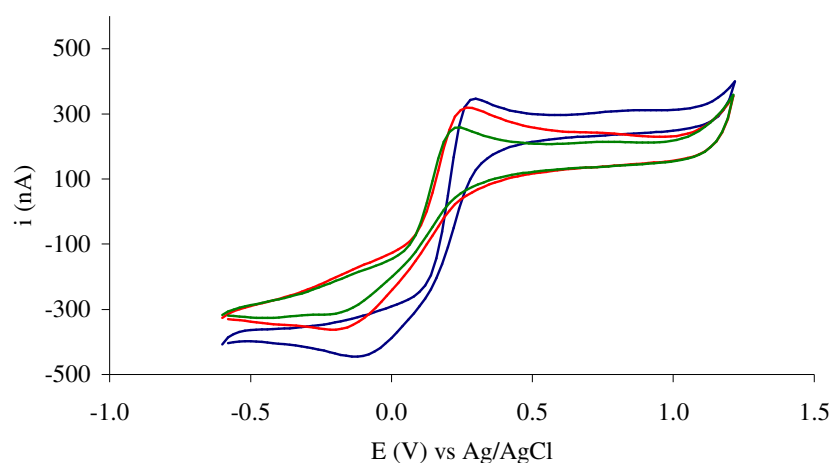


Figure 3.21 – Cyclic voltammetry (50 mVs^{-1}) of bare and deposited MIP (20 nl volume of monomer mixture) microchip electrode. Blue – bare in PBS, red – MIP in PBS and green – MIP in propofol.

3.4.3 Discussion of MIP immobilisation of microchip devices

Approximately 70% of the microchips tested demonstrated a purely capacitive response and as this response was also observed with the bare electrodes, it is proposed that this is not due to the deposited MIP passivating the electrode. From one batch of microchips the mean maximum impedance (at 1 Hz) was $53 \text{ M}\Omega$ with a standard deviation of $72 \text{ M}\Omega$ ($n = 24$). Thus, the vast majority of the microchip sensors tested were unsuitable for the application. A defect causing a purely capacitive response could be due to a flawed electrical connection or remaining resist on the electrode surface.

The microchips which did not exhibit a purely capacitive response fitted the trend of a Randles cell with a characteristic semi-circular Nyquist plot. For these sensors the deposition of MIP layer resulted in an increase in the charge transfer resistance, which suggests that the MIP decreases the conductivity of the sensor. This was expected as the MIP consists of a highly cross-linked polymer which does not contain any known conductive compounds. In addition, the increase in impedance with deposited volume suggests that the thickness of the MIP layer increases with larger volumes deposited.

No change in the response of the sensors with the addition of propofol could be seen with either the bare or MIP electrodes.

3.4.4 Conclusion of MIP immobilised on microchip device

Due to the inconsistencies with the microchip devices it is difficult to draw conclusions from this investigation regarding the detection of propofol. However, the necessity for a reliable and reproducible device that is capable of undergoing the polymerisation conditions has proved to be a significant challenge that must be overcome.

3.5 Conclusions on the conductometric detection of propofol

By taking the previously developed MIP composition and immobilising it onto a commercial sensor platform, the detection of propofol using impedance monitoring shows promise. Also, the simplicity of the impedance monitoring, as it does not require the oxidation or reduction of the target analyte, could resolve problems previously experienced by Sphere Medical and Cranfield University.

However, the microchip sensor platform in development at Sphere Medical was unreliable in its performance and lacked reproducibility when it did perform. This unfortunately renders most of results speculative at best. Therefore, the problems created by the microchip platform must be resolved before any further studies can be performed with them.

Chapter 4 - Developing a molecularly imprinted polymer for the detection of antibiotics

“I have not failed. I've just found 10,000 ways that won't work.” (*attributed*) Thomas A. Edison (1847 - 1931)

4.1 Introduction

The following investigation shows the selection of an antibiotic as a template for the development of molecularly imprinted polymers. This included the computational design of a MIP by the selection of functional monomers which are able to bind strongly to the antibiotic. These designed MIP are then synthesised and experimentally tested to find an initial optimal pre-polymerisation mixture. This initial mixture was immobilised onto Sphere Medical's microchip electrodes and polymerised to form a MIP layer. Subsequently, the possibility for electrochemical detection of the chosen antibiotic was then investigated.

4.2 Selection of antibiotic for development in MIP based sensor

Several antibiotics were proposed for use in a MIP based sensor by a panel of medical professionals based on the need for their detection and monitoring in an intensive care environment. Out of these antibiotics one was selected as the best candidate for the sensor. This selection was based on factors, such as the design and production of the molecular imprinted polymer (MIP) that will be immobilised on Sphere Medical's electrochemical microchip platform to allow selective detection. The following explains the justification for the antibiotic selection.

4.2.1 Review of MIP design

Initial methodologies at better understanding the assembly of MIPs were based on thermodynamic modelling (Nicholls, 1998). These studies focused on the energetic properties of the template-monomer complex. From this modelling five key points were

derived: I) the more monomers required to form the complex, the less stable the complex will be, II) the fewer conformations the template can undertake, the better the definition of the recognition sites, III) the stronger the complex interaction, the more stable the pre-polymerisation complexes are, IV) the hydrophilic and hydrophobic interactions between the template and monomers can further influence the stability of the complex and V) the equilibrium between template and monomer in forming the complexes will determine the number and heterogeneity of the binding sites.

Other approaches to MIP design involve the use of combinatorial techniques in the hunt for the best possible MIP. These combinatorial approaches have been semi-automated and are capable of producing and screening libraries of imprinted polymers (Batra and Shea, 2003). Not only can they be used to vary the type and concentration of templates and monomers but also the porogens and cross-linkers can be varied. However, the most valued benefit of using a combinatorial approach is being able to find unexpected template-monomer combinations that could not be predicted based on current models and understanding. Another approach is using chemometrics to take existing experimental data to help predict possible optimised solutions. Davies and co-workers (Davies et al., 2004) found this methodology to be useful, especially in optimising template : monomer : cross-linker ratios, and they also predicted that if used in combination with a combinatorial method, it could prove very effective.

Despite the fundamental understanding that a thermodynamic approach gives and the possibility of discovering an ideal MIP that the combinatorial approach offers, neither of these approaches really 'design' a MIP. However, this can be achieved by computationally modelling of the template-monomer complex to evaluate the best MIP components.

One of the first methodologies developed for the computational design of MIP was proposed by Piletsky and co-workers (Piletsky et al., 2001, Subrahmanyam et al., 2001, Chianella et al., 2006). Their approach was to screen a library of monomers against a target template and calculate a binding score representing the strength of the complex formed. This resulted in a ranking of the strongest binding monomers. Using one or more of the strongest binding monomers, at a time the template was modelled, in a solution of the monomer, an annealing process was simulated using a dynamics

package. This predicted the possible template-monomer complex that could form in the pre-polymerisation solution. This computational methodology forms the foundation of further MIP design (Wu and Li, 2004, Dong et al., 2005, Liu et al., 2007), with other software and similar models being implemented to assess the strength of template-monomer complexes. The most recent advances include the selection and modelling of porogen (Yao et al., 2008) and cross-linker (Wei et al., 2006) at the same time as the template-monomer complex.

Another promising approach is the use of NMR to study the pre-polymerised template-monomer complexes. O'Mahony and co-workers (O'Mahony et al., 2005, O'Mahony et al., 2006) used this technique and concluded that I) hydrophobic binding leads to higher binding affinities, II) the templates shape, size and functionality influence MIP performance, III) the interaction between the monomer and porogen can have a considerable effect of the MIP performance and IV) more stable complexes give better selectivity. These points further iterating the conclusions from the thermodynamic analysis.

Finally, the most successful approach to modelling seems to stem from combining computational modelling with NMR analysis (Salvador et al., 2007, Farrington and Regan, 2007). In particular, an iterative process where the computational models of the pre-polymerisation complexes can be validated using the NMR and the data from the NMR can be used to refine the computational models, resulted in successfully designed MIP.

4.2.2 Overview of the proposed antibiotics

The following is a review of three antibiotics initially proposed for this study, specifically considering their electrochemical detection and the properties required for MIP production.

4.2.2.1 Metronidazole

Metronidazole is a one of many 5-nitroimidazole drugs that have antibiotic properties. Their biological action is caused by derivatives, formed by its reduction, which oxidise DNA, resulting in the DNA becoming damaged (Oliveira Brett et al., 1997b). This action leads to in metronidazole and its metabolites being suspected to be carcinogens

and mutagens (Mohamed et al., 2008). Due to the biological action requiring the reduction of metronidazole, several studies (Oliveira Brett et al., 1997a, Ozkan et al., 1998, Lu et al., 2004, Mandal, 2004, La-Scala et al., 1999) have been conducted into its complex electrochemistry which involves 6 electrons reducing the nitro group (R-NO₂) to an amine derivative (R-NH₂) via a hydroxylamine (R-NHOH), see Figure 4.1.

The electrochemical detection of metronidazole has been successfully investigated on several transducer platforms. However, the most used platform is a glassy carbon electrode with a limit of detection of 20 μM (Zhi et al., 1998), which with an intensive surface activation (Ozkan et al., 1998) was increased to 2 μM and was further improved to 10 nM by adding an accumulation stage (Wang et al., 1993). By modifying a glassy carbon surface with carbon nanotubes (Lu et al., 2004) the detection limit has been further improved to 9 nM.

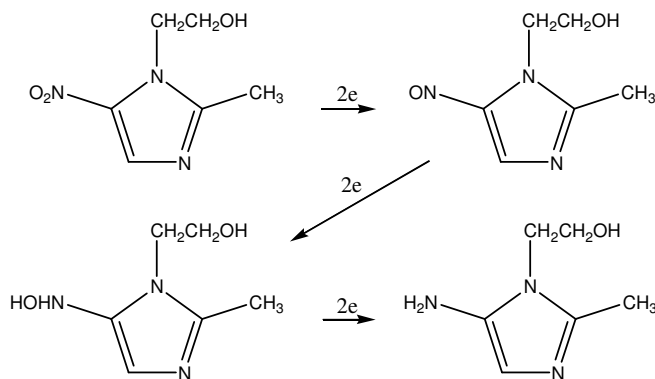


Figure 4.1 – Illustration of the complex metonidazole reduction.

Investigations into a selective component for the detection of metronidazole include using a metalloporphyrin incorporated into a carbon paste electrode as a recognition element (Gong et al., 2003). This had a limit of detection of 58 nM using amperometric detection with a satisfactory rejection of interfering compounds. Other selective detection (Mohamed et al., 2008) involved a MIP created by MIP Technologies using a template that was an analogue of 5-nitroimidazoles. The detection of several 5-nitroimidazoles, including metronidazole, in egg powder was investigated using solid phase extraction (SPE) with mass spectroscopy (MS) detection. This methodology was accurate, sensitive and reproducible to comply with the EU criteria.

4.2.2.2 Cefoxitin

Cefoxitin is a member of the cephalosporin family of antibiotics. Cephalosporin antibiotics are a sub group of β -lactam antibiotics as they contain a β -lactam nucleus (Figure 4.2).

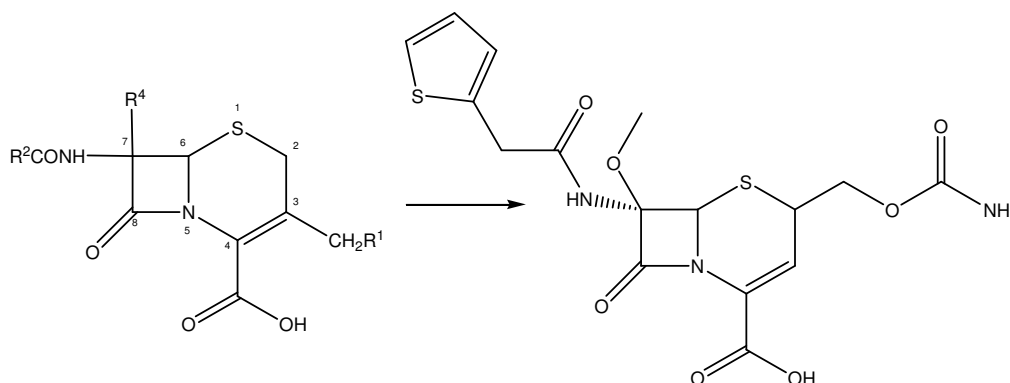


Figure 4.2 – A schematic of cephalosporin general structure (left) and cefoxitin (right).

Cephalosporins are highly soluble in water, hence they are generally supplied as sodium salts. Direct detection and the detection of cephalosporins degradation products have been carried out using microbiological, colorimetric, chromatographic, spectroscopic, fluorimetric, enzymatic and electrochemical means (Ogorevc et al., 1991). The cephalosporin family of antibiotics is deemed to be electroactive, due to the double bond reduction of the cepham nucleus at high potentials (approximately -1 V) (Ogorevc and Gomiscek, 1991).

Cephalosporins have been categorised by Zuman and co-workers (Zuman et al., 2000) depending on their electrochemistry. Cefoxitin was categorised as “cephalosporins with a reducible group in the side-chain on C-7 and a good leaving group in the side-chain on C-3” (see Figure 4.2). It is postulated in the paper that the leaving group of this category of cephalosporins is cleaved, resulting in a vinyl and, finally, a methyl group. For cefoxitin a pH dependence of the current response has been observed, this indicates an acid-base equilibrium (Kapetanovic et al., 1992).

4.2.2.3 Gentamicin

Gentamicin (Figure 4.3) is an aminoglycosidic antibiotic with a very narrow therapeutic window (Adams et al., 1998). Therefore, continual monitoring is required to ensure effective administration of the drug. There have been several methods proposed for the detection of gentamicin, most of these involving a pre-separation stage utilising ion exchange chromatography (Manyanga et al., 2008). However, the detection of gentamicin is not straightforward as it lacks UV absorbing chromophores (Kaine and Wolnik, 1994). Several methods have been proposed for the detection of gentamicin but pulse amperometric detection has proven to be the most suitable and is proposed by the European Pharmacopoeia for pharmaceutical quality control (Ghinami et al., 2007).

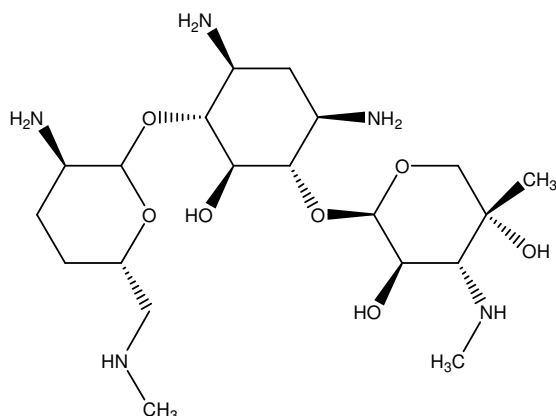


Figure 4.3 – Illustration of gentamicin.

There have also been several other non-chromatographic electrochemical detection methods for gentamicin. One of these methods used a competitive immunoassay for the detection of gentamicin in whole milk (Van Es et al., 2001). Where hydrogen peroxide was electrochemically detected upon the competitive binding of a gentamicin-glucose oxidase complex, thus the concentration was ‘negatively’ proportional to the response. Another method used potentiometry (Kulapina et al., 2004) where a custom ion-selective electrode was produced by immobilising gentamicin-tetraphenylborate onto a PVC membrane. The electrode demonstrated a good linear response to gentamicin with insignificant interference from inorganic cations.

No MIP with selective properties for gentamicin is currently known.

4.3 Antibiotic selection

The antibiotic drug was selected based on its suitability for detection and MIP production. This is divided into two different aspects: firstly, the ability of the antibiotic to bind to monomers resulting in the pre-polymerisation monomer-template complex. Secondly, the solubility of the antibiotics in a low polarity solvent is desirable because this results in less competition during the formation of the monomer-template complex.

4.3.1 Methodologies for antibiotic selection

4.3.1.1 *Computational analysis of antibiotic-monomer binding*

To assess the functionality and reduce the number of possible monomers to be assessed in the synthesis of a MIP, the binding strength between the antibiotics and a library of monomers was computationally assessed. This was achieved using the Leapfrog algorithm (SybylTM 7.3, Tripos Inc.) to iterate through many possible antibiotic-monomer binding configurations and allocating a binding score; the higher the binding score the stronger the complex. The monomers were selected from a library of well-known, commercially available, monomers which have been used extensively in previous MIP developments.

4.3.1.2 *Antibiotic solubility testing*

To test the solubility of the antibiotics, a known mass of the antibiotic was added to a known mass of solvent and the solubility was visually assessed. To help the antibiotic dissolve, both mechanical stirring and heating, to a maximum of 50°C, was applied where appropriate. A general rule for the mass of porogen/solvent and template are 50% and 1% of the total mass, respectively, for a MIP. However, as there needs to be room for optimisation and an allowance for the monomer to be dissolved in the solution, a ratio of 2:50 was deemed the minimum requirement for the solubility testing.

4.3.1.2.1 Crown ethers for increasing cefoxitin solubility

Crown ethers are heterocyclic compounds that have a high affinity for certain cations depending of the size of the cation and the size of the crown ether's 'cavity'. Due to the ring of oxygen atoms, crown ethers act like a Lewis base with extremely strong binding to the cation, which neutralises the cations charge. The non-polar cation complex is

thus soluble in non-polar solvents and, to maintain neutrality, the anion should be soluble.

By using 15-crown-5 to neutralise the sodium ion supplied in the cefoxitin salt, cefoxitin should therefore become more soluble in less polar solvents.

4.3.2 Results of antibiotic selection

4.3.2.1 Computational binding analysis of template-monomer binding

The computational binding analysis (Table 4.1) shows that gentamicin has the highest mean binding score when compared to the other two antibiotics, with cefoxitin being second. The strongest monomer binding scores for gentamicin and cefoxitin are for charged monomers. This behaviour is to be expected as both antibiotics have either polar or charged chemical groups, respectively.

Table 4.1 – Table of top five computationally calculated monomers with the strongest binding for metronidazole, gentamicin and cefoxitin. Value in brackets is the binding score (Kcal/mol). (DEAEM – 2-diethylaminoethyl methacrylate, EGMP – ethylene glycol methacrylate phosphate, VP – vinylpyridine, AMPSA – 2-acrylamido-2-methyl-1-propanesulphonic acid).

Monomer binding to:	Metronidazole	Gentamicin	Cerfoxitin
<i>Highest binding score</i>	DEAEM+ (-58)	DEAEM+ (-263)	EGMP- (-53)
	Bisacrylamide (-33)	4-VP+ (-77)	AMPSA (-40)
	EGMP (-31)	EGMP (-76)	Itaconic acid (-36)
	Acrylamide (-29)	2-VP+ (-59)	EGMP (-36)
<i>Lowest binding score</i>	Itaconic acid (-24)	Itaconic acid (-51)	Itaconic acid- (-35)

The binding of DEAEM+ to metronidazole and gentamicin is illustrated in Figure 4.4 and Figure 4.5 respectively. For metronidazole and gentamicin, the hydrogen bonding (blue dashed line) is both between the extra proton on the protonated DEAEM and the amino group, which is probably due to the negative charge of the lone pair of electrons.

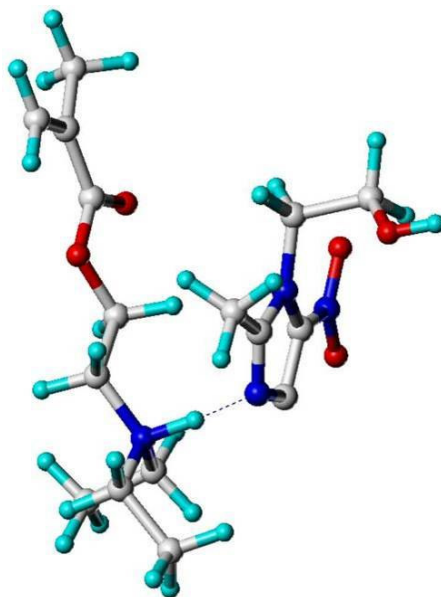


Figure 4.4 – Model of metronidazole in highest binding conformation as calculated using Leapfrog (Sybyl), the monomer is DEAEM+. Hydrogen bonds (blue dashed line), carbon atoms (white), nitrogen atoms (blue), oxygen atoms (red), phosphorus atoms (orange) and hydrogen atoms (cyan).

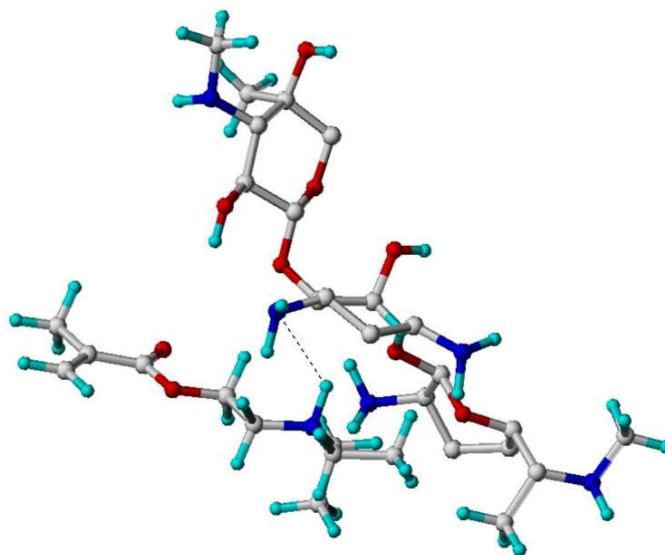


Figure 4.5 – Model of gentamicin in highest binding conformation as calculated using Leapfrog (Sybyl), the monomer is DEAEM+. Hydrogen bonds (blue dashed line), carbon atoms (white), nitrogen atoms (blue), oxygen atoms (red), phosphorus atoms (orange) and hydrogen atoms (cyan).

The strongest binding for cefoxitin was found to be on the hydrogen atoms of the terminal amino group of the EGMP- monomer (Figure 4.6) forming a complex with the

deprotonated oxygen atoms surrounding the phosphorous atom. This should be compared to the EGMP cefoxitin complex (Figure 4.7), where only one of the hydrogen's of the terminal amino group belonging to cefoxitin forms the complex with the neutral EGMP monomer.

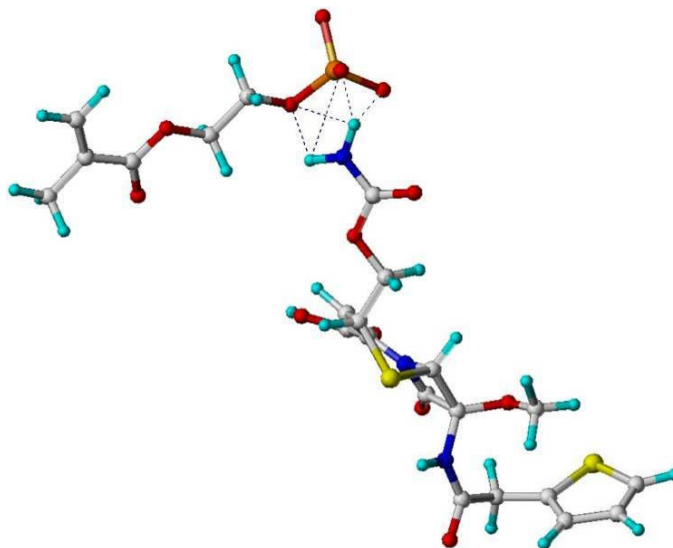


Figure 4.6 – Model of cefoxitin in highest binding conformation as calculated using Leapfrog (Sybyl), the monomer is EGMP-. Hydrogen bonds (blue dashed line), carbon atoms (white), nitrogen atoms (blue), oxygen atoms (red), phosphorus atoms (orange) and hydrogen atoms (cyan).

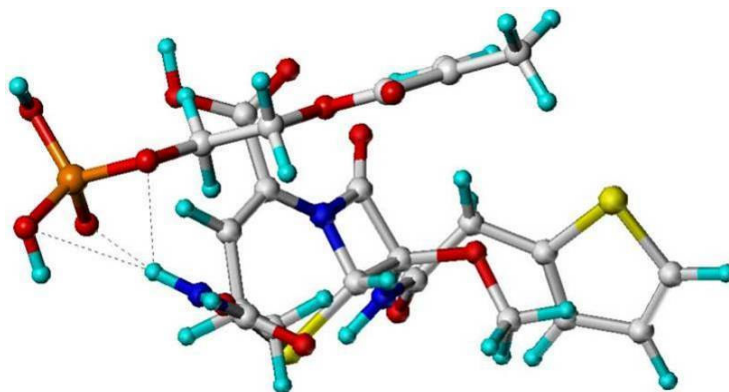


Figure 4.7 – Model of cefoxitin in a binding conformation as calculated using Leapfrog (Sybyl), the monomer is EGMP. Hydrogen bonds (blue dashed line), carbon atoms (white), nitrogen atoms (blue), oxygen atoms (red), phosphorus atoms (orange) and hydrogen atoms (cyan).

4.3.2.2 Antibiotic solubility

Gentamicin was insoluble in both DMF and acetonitrile, despite heating and long periods of sonication. Metronidazole and cefoxitin both dissolve in the desired quantities in DMF, although cefoxitin required the assistance of crown ether to achieve this. None of the antibiotics met the 2:50 ratio set for MIP production in acetonitrile (Figure 4.8), although metronidazole was not far from this goal and could possibly be used for making a MIP.

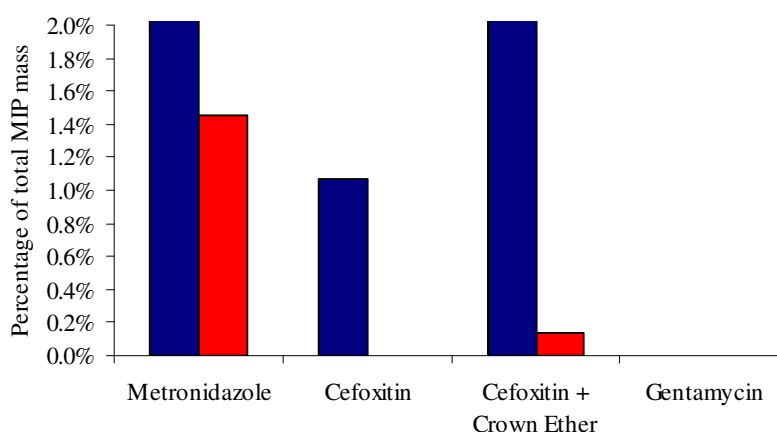


Figure 4.8 – Solubility of metronidazole, cefoxitin and gentamicin in DMF (blue) and acetonitrile (red) expressed as a percentage of total MIP mass.

4.3.3 Discussion of antibiotic and monomer selection

From the modelling of the antibiotics, gentamicin has the strongest binding to the monomers by nearly a factor of five. This is probably due to the large number of functional groups within the compound. However, these groups also cause a large quantity of distributed charge around the compound, which would explain why it would not dissolve in DMF or acetonitrile. Even attempts to extract the gentamicin to its freebase, with aqueous-organic liquid-to-liquid extraction, failed as the gentamicin did not dissolve in the immiscible solvent. The large number of functional groups could also cause significant non-specific binding of gentamicin to a polymer.

Cefoxitin demonstrated fairly strong binding to the monomers in the database and, like gentamicin, it demonstrated strong binding to charged monomers. This is expected as it

is a charged molecule itself. This was also reflected in the solubility of cefoxitin in both DMF and acetonitrile as it was only slightly soluble in DMF. The use of crown ether to form a complex with the sodium ions of the cefoxitin salt improved its solubility in DMF considerably and enabled a little cefoxitin to be dissolved in acetonitrile, but not enough to be useful for MIP production.

The binding strength of the monomers to metronidazole was very similar to cefoxitin. However, the preferred monomers for complex formation with metronidazole were neutrally charged. This is different to the other antibiotics but which was expected due to the neutral nature of metronidazole. Unlike the other antibiotics, metronidazole was highly soluble in DMF and is considered to be soluble enough in acetonitrile for MIP production.

4.3.4 Conclusion of antibiotic selection

Two key areas were highlighted for the production of a MIP, I) the ability for forming an antibiotic-monomer complex and II) the solubility of the antibiotic in low polarity solvents. From the investigations undertaken metronidazole was chosen as the best candidate for further investigation. It has a high solubility in acetonitrile and DMF, its ability to form a pre-polymerisation complex is acceptable and the numerous electrochemical studies within the literature show great promise for its detection on Sphere Medical's microchip sensor.

4.4 Computational design and testing of MIP with selective properties for metronidazole

In order to assess the monomer-antibiotic interaction experimentally, a non-imprinted polymer (NIP) was synthesised based on the strong binding monomers from the initial computational modelling (Section 4.3.1.1). Also, the monomer-template complex was computationally modelled to predict a possible monomer-template ratio which should be used to synthesise the MIP and to compare its performance with respect to a corresponding NIP.

4.4.1 Investigatory techniques

All consumables were supplied by Sigma-Aldrich unless stated otherwise.

4.4.1.1 Bulk polymer testing

The experimental testing of the bulk polymer was conducted using standard solid phase extraction (SPE) techniques with UV spectroscopy to measure the extracted solutions. The specific polymerisation solutions are stated in Table 4.2 and Table 4.3.

4.4.1.1.1 Polymer mixture

The polymerisation mixtures (Table 4.2) are based on general MIP quantities by mass with the quantity of monomer adjusted in each mixture so that all the mixtures have the same monomer concentration. Different monomers can be considered to have a greater number of functional groups than others, thus it is more likely for them to bind to the template than monomers with less functionality. The monomers with extra functionality are considered to be EGMP, bisacrylamide and itaconic acid. To fairly assess the binding of these monomers to the template, it was assumed that these monomers have twice the functionality, thus they could have two possible binding sites. So, the polymer was tested with half the standard quantity of monomer for comparison to the monomers with a proposed functionality of one.

Table 4.2 – Table of NIP compositions for highest binding monomers from computational analysis (monomer : cross-linker, 1:4.2). Initiator – 2-2-dimethoxy-2-phenylacetone, cross-linker – EGDMA, porogen – DMF.

Mass (g)	EGMP		Acrylamide	Bisacrylamide		Itaconic acid		DEAEM
Proposed functionality	1	2	1	1	2	1	2	1
Initiator	0.1	0.1	0.1	0.1	0.1	0.1	0.1	0.1
Cross-linker	4	4	4	4	4	4	4	4
Monomer	1	0.5	0.3	0.7	0.4	0.6	0.3	0.9
Porogen	4.9	5.4	5.6	5.2	5.5	5.3	5.6	5.0
Monomer : cross-linker	4.2	8.5	4.2	4.2	8.5	4.2	8.5	4.2

4.4.1.1.2 Polymer preparation

The polymerisation solutions were prepared in small glass vials and degassed with nitrogen for 10 minutes. They were then sealed and placed in a UV chamber (Hönle

100, Hönle UV, UK) for 20 minutes to polymerise. Following this, the vials were placed in an oil bath at 80°C for 18 hours to finish the polymerisation. The solid polymer was then ground using a milling machine (Ultra Centrifugal Mill ZM 200, Retsch, DE) and wet sieved in methanol. Particles between 63 to 106 µM were collected for the SPE.

4.4.1.1.3 Solid phase extraction

The SPE cartridges were packed with 100 mg of polymer and the binding experiments were carried out using a vacuum manifold. All cartridges were washed using 250 mM HCl with 50% methanol, then deionised water and finally 100 mM NaOH with 50% methanol followed again by deionised water. The cartridges were then preconditioned using phosphate buffer saline (PBS) (pH 7.5) and UV spectrometry was used to test for any interfering substances. This cleaning procedure was repeated a minimum of three times or until no interfering substances could be seen by UV.

4.4.1.1.4 Binding capacity

To test the binding capacity, 1 mL of metronidazole (50 µM in PBS, pH 7.5) was repeatedly passed through the cartridge and the UV absorbance of metronidazole was measured at 320 nm. This was repeated until the measured absorbance was over 50% of the maximum absorbance, i.e. the solution was greater than 25 µM; this is defined as the 50% breakthrough point and was calculated by linear interpolation for the comparison of polymer performance. The comparison between the NIP and MIP is expressed in term of an imprinting factor; this being the division of MIP / NIP. Thus it represents the capacity factor of the MIPs with respect to the NIPs.

4.4.1.2 Computational annealing

To predict the ratio of monomer-template complex a dynamics package is used within Sybyl to simulate an annealing process. The template is surrounded by a solvated monomer and an annealing process is achieved by stepping the temperature from 600 K to 300 K in 100 K steps. At the end of the process the position and interaction of the monomers with the template is assessed and a picture of the pre-polymerisation complex is obtained.

4.4.2 Result of MIP design and testing

4.4.2.1 Experimental analysis of metronidazole temple-monomer binding

The top five monomers that demonstrated strongest binding to metronidazole were experimentally tested using a SPE extraction technique, the results of which can be seen in Figure 4.9.

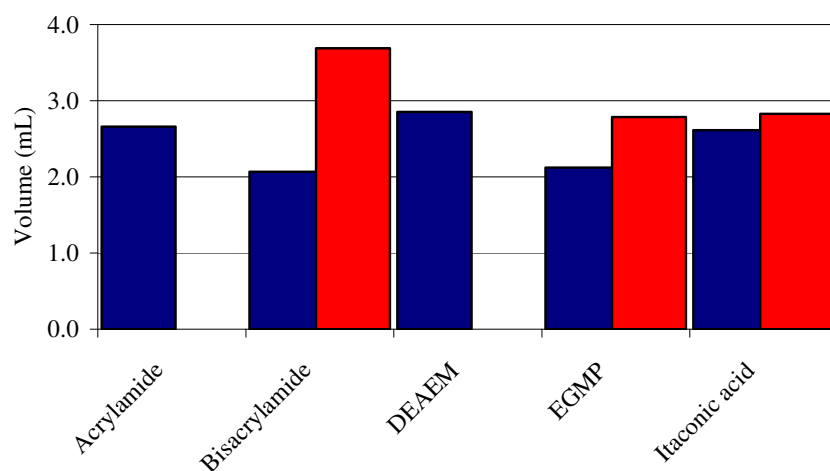


Figure 4.9 – Volume of metronidazole (50 µL) at 50% breakthrough of the SPE cartridge. Standard NIP mixture (blue) and NIP mixture with assumed extra functionality (red) as explained below.

The 50% breakthrough of the NIP shows that DEAEEM has the highest binding capacity to metronidazole. This is consistent with the computational modelling. However, in comparison to the other NIPs it was not significantly greater. The bisacrylamide and EGMP NIP and the acrylamide and itaconic acid NIP have similar breakthrough volumes. This is also consistent with the model. However, itaconic acid and acrylamide have greater breakthrough volumes than bisacrylamide and EGMP. This is not predicted the modelling.

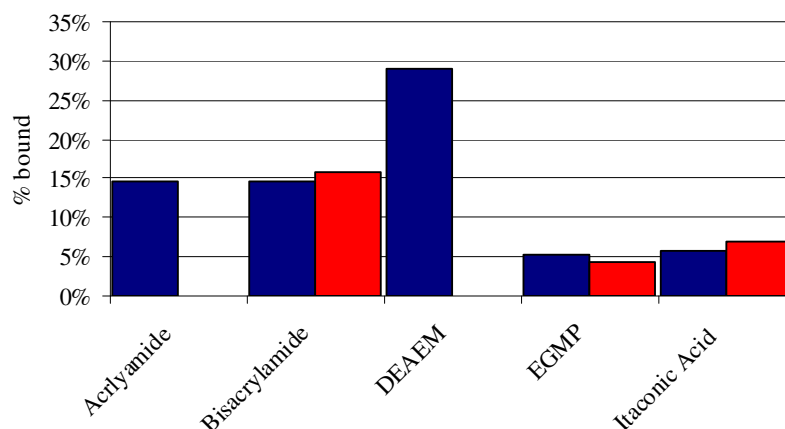


Figure 4.10 – Percentage of uric acid (50 μ L) bound to the SPE cartridge. Standard NIP mixture (blue) and NIP mixture with assumed extra functionality (red).

The reduction in monomer concentration, as a result of assuming a functionality of 2, caused an increase in the binding capacity in all the three cases. It particularly had a large increase in the binding capacity for bisacrylamide, increasing the capacity by a factor of 1.6.

It is foreseen that the antibiotic will be detected using electrochemical techniques in a biological fluid. Two of the worst electrochemically interfering compounds are ascorbic and uric acid, hence both of these materials were tested to see how they bind to the NIP (Figure 4.10 and Figure 4.11). Ascorbic acid binds to all of the NIPs. However, both EGMP and itaconic acid seem to reject ascorbic acid better than the other NIPs. Excluding DEAEEM, the binding of uric acid to the NIP was far less, with EGMP and itaconic acid giving very good rejection.

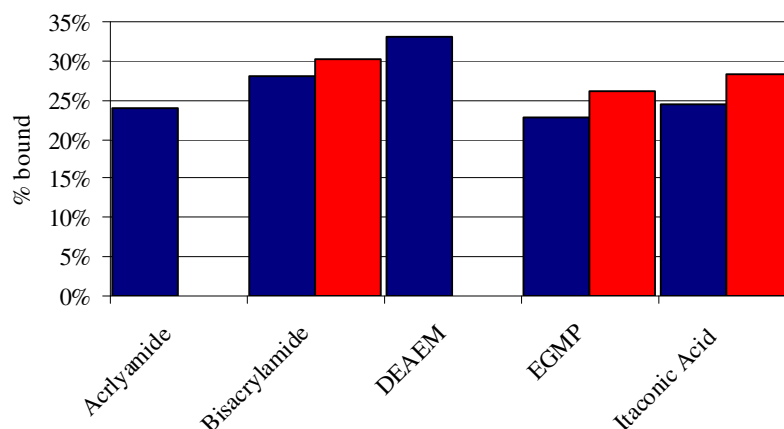


Figure 4.11 – Percentage of ascorbic acid (50 µL) bound to the SPE cartridge. Standard NIP mixture (blue) and NIP mixture with assumed extra functionality (red).

4.4.2.2 Computational modelling of monomer-template complex

The predicted monomer-template complex using either EGMP or itaconic acid monomers with a metronidazole template are shown in Figure 4.12 and Figure 4.13, respectively. Both complexes show that two monomers can bind to the metronidazole template to form the complex. In both cases the bonds were formed between the polar hydroxyl group and the double bonded nitrogen within the aromatic ring of the metronidazole template.

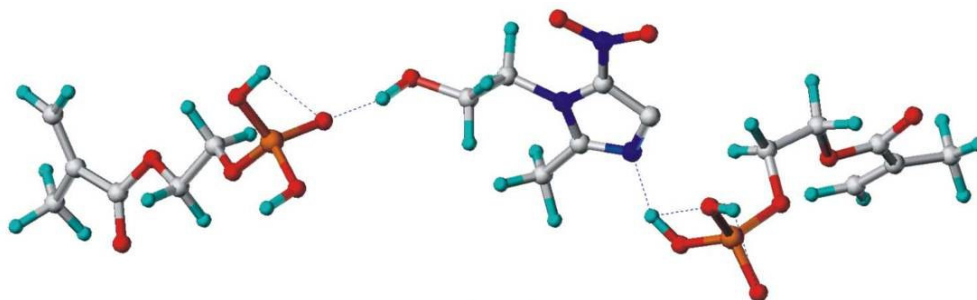


Figure 4.12 – Predicted monomer-template complex showing a binding ratio for metronidazole : EGMP of 1:2. Hydrogen bonds (blue dashed line), carbon atoms (white), nitrogen atoms (blue), oxygen atoms (red), phosphorus atoms (orange) and hydrogen atoms (cyan).

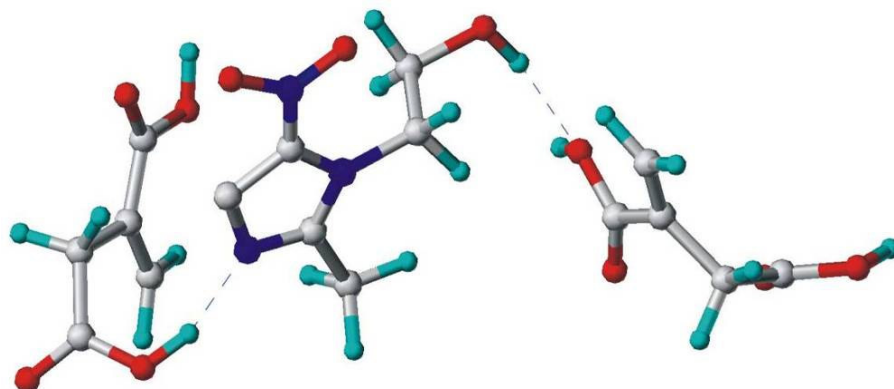


Figure 4.13 – Predicted monomer-template complex showing a binding ratio for metronidazole : itaconic acid of 1:2. Hydrogen bonds (blue dashed line), carbon atoms (white), nitrogen atoms (blue), oxygen atoms (red), phosphorus atoms (orange) and hydrogen atoms (cyan).

4.4.2.3 Experimental analysis of MIP for the selective binding of metronidazole

The composition of the MIP synthesised using EGMP and itaconic acid to selectively bind metronidazole can be seen in Table 4.3. The synthesised MIP, assuming normal functionality, gave a slightly higher binding capacity but nothing that could be considered as a vast improvement compared to the NIP. However, the synthesised MIP, assuming twice the functionality, hence half the monomer content, gave a significantly higher binding capacity and resulted in a imprinting factor around 1.4.

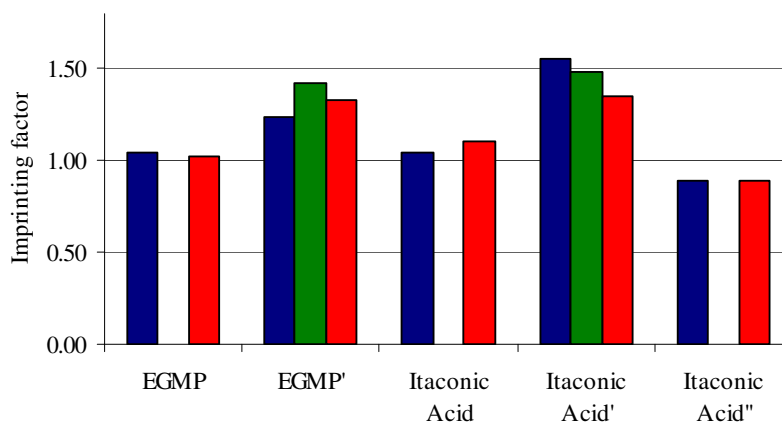


Figure 4.14 – Imprinting factor at 50% breakthrough. Monomer : template ratio; 1:2 (blue), 1:3 (green) and 1:4 (red). Predicted functional groups: 1 – X, 2 – X' and 3 – X''.

These better MIPs were also investigated with a monomer : template ratio of 1:3 to attain a better understanding of how this ratio affects the trend in imprinting factor (Figure 4.14). For EGMP a monomer : template ratio of 1:3 gave the highest imprinting factor, which suggests that the optimal ratio is around 1:3. However, for itaconic acid there was a decrease in imprinting with an increasing ratio, this suggesting that a ratio of 1:2 is more optimal.

To see if there was a trend with modelling greater monomer functionality, itaconic acid was modelled with having a functionality of 3. However, this led to a decrease in binding capacity.

Table 4.3 – Table of MIP compositions based on EGMP and itaconic acid monomers for the selective binding of metronidazole. Initiator – AIBN, cross-linker – EGDMA, porogen – DMF.

	EGMP					Itaconic Acid						
Proposed functionality	1	1	2	2	2	1	1	2	2	2	3	3
Template : monomer	1:2	1:4	1:2	1:3	1:4	1:2	1:4	1:2	1:3	1:4	1:2	1:4
	<i>Mass (g)</i>					<i>Mass (g)</i>						
Initiator	0.1	0.1	0.1	0.1	0.1	0.1	0.1	0.1	0.1	0.1	0.1	0.1
Cross-linker	4	4	4	4	4	4	4	4	4	4	4	4
Monomer	1	1	0.5	0.5	0.5	0.62	0.62	0.62	0.31	0.31	0.21	0.21
Template	0.41	0.2	0.41	0.27	0.2	0.41	0.2	0.41	0.27	0.2	0.41	0.2
Porogen	4.9	4.9	5.4	5.4	5.4	5.28	5.28	5.59	5.59	5.59	5.59	5.59
Template : Monomer : Cross-linker	1:2:8.5	1:4:17	2:2:17	1:1.5:12.7	1:2:17	1:2:8.5	1:4:17	2:2:17	1:1.5:12.7	1:2:17	1:0.7:8.5	1:1.3:17

4.4.3 Discussion of MIP design and testing

Following the successful solubility testing, the top monomers from the modelling were synthesised and experimentally tested. DEAEM was found to be the highest binding monomer which is consistent with the modelling. The other monomers had similar break-through capacities, which is consistent with the small range of binding energies seen in the computational investigation. However, the order of binding strength between the experimental and computation investigation varied.

The computational modelling of the monomer-template complex showed that the binding of two monomers to metronidazole was very similar. Both bound with a 1:2 ratio and to the same constituents within the metronidazole structure.

The MIP was initially synthesised with a template : monomer ratio of 1:2 as this was predicted from the modelling. Most of the MIP tested performed with a similar binding capacity to that of the NIP, apart from those produced with an assumed functionality of 2, which demonstrated a superior imprinting factor. The MIP with a functionality of 2 effectively has a lower template to monomer ratio. Their increase in performance could be due to a reduction in non-specific binding which previously masked the selective response of the MIP with higher template to monomer ratios.

4.4.4 Conclusion

The successful design and testing of MIP has shown that by the screening of monomers, computational modelling of the monomer-template complex and experimental MIP testing, a MIP with an increased binding capacity for metronidazole can be synthesised. This MIP uses itaconic acid as its functional monomer with a template : monomer : cross-linker ratio of 2:2:17. Although, this may not be an optimal MIP composition for the detection of metronidazole on a transducer. However, this is a good starting point for MIP immobilisation experiments allowing for more efficient optimisation and testing to proceed in a more realistic environment.

4.5 Investigation into the detection of metronidazole using immobilised MIP

The previous section has demonstrated the development of a bulk MIP with an increased binding capacity for metronidazole. The following section shows the immobilisation of this MIP to Sphere Medical's transducer surface and investigations into both amperometric and conductometric detection. This forms the foundation for further MIP optimisation in a more realistic system and environment based on the device's final application.

4.5.1 Methodologies for the immobilisation and detection of metronidazole

All consumables were supplied by Sigma-Aldrich unless stated otherwise.

4.5.1.1 Electrochemical detection of metronidazole

Both cyclic voltammetry and amperometric investigations were conducted using Sphere Medical's amperometric electrodes. This consisted of a three-electrode cell with a platinum working electrode, a platinum counter electrode and an external Ag/AgCl wire reference electrode. The measurements were conducted using a microAutoLabII (Eco Chemie, Netherlands) potentiostat.

Unless stated otherwise all cyclic voltammetry was performed with a scan rate of 50 mVs^{-1} in PBS (pH 7.5).

4.5.1.2 Thermal grafting of metronidazole specific polymer

4.5.1.2.1 Pre-polymerisation electrode cleaning

The microchip electrodes supplied from the foundry are coated in a protective metal layer. This is etched away using dilute HF which is washed with copious amounts of deionised water and dried in a stream of nitrogen. This etching procedure also cleans the electrode prior to the immobilisation of the silane monolayer.

4.5.1.2.2 Thermal grafting of metronidazole

The polymer was anchored to the surface using a silane monolayer with a covalently attached initiator. The electrode surfaces were activated following the procedure from

Section 3.2.3. Following this a SAM of aminopropyl triethoxysilane (APTES) was assembled on the surface by leaving the activated electrodes in a 2% solution in toluene for 3 hours. This resulted in reactive amines which allowed the 4,4'-azobis(cyanovaleric acid) initiator to be coupled on the electrode surface for 18 hours using the flowing coupling solution for 18 hours: 20 mM 4,4'-azobis(cyanovaleric acid), 28 mM 1-Hydroxybenzotriazole and 17 mM N-(3-Dimethylaminopropyl)-N'-ethylcarbodiimide dissolved in DMF.

The polymer was then grafted by immersing the initiator functionalised surfaces in the polymer solution (Table 4.4) which had been degassed for 10 minutes in a stream of nitrogen. It was then placed on a hot plate at 80°C for 30, 60, 120 and 240 minutes. After the polymerisation, the sensor was then rinsed in methanol and dried in a stream of nitrogen.

Table 4.4 – Composition of grafting polymerisation mixture (template : monomer : cross-linker, 2:2:17).

	Substance	Mass (g)
NIP	Itaconic acid	0.62
	EGDMA	4
	DMF	5.59
MIP (as NIP plus template)	Metronidazole	0.41

4.5.1.2.3 Immobilised polymer cleaning

Before testing the sensors with the immobilised polymer, they were cleaned with successive washing of 250 mM HCl with 50% methanol followed by deionised water and finally 100 mM NaOH with 50% methanol followed again by deionised water. This procedure was repeated three times.

4.5.1.3 Impedance analysis and monitoring of microchip electrodes

4.5.1.3.1 Impedance spectroscopy of electrodes

The impedance analysis was conducted using the procedure from Section 3.4.1.1 over a frequency range of 1 Hz to 10000 Hz.

4.5.1.3.2 Impedance monitoring of microchip sensors

The impedance monitoring was conducted using the procedure from Section 3.2.4.

4.5.1.4 AFM analysis of polymer coated microchip electrodes

The atomic force microscopy (AFM) analysis was conducted using a PicoScan AFM (Molecular Imaging, USA) in contact mode with Pointprobe® CONTR probes (NanoWorld).

An AFM in contact mode works by scanning a fine probe protruding from a silicon nitride cantilever over an area of interest. As the probe moves over the surface both lateral and torque forces are exerted on the probe. These cause the cantilever to bend and twist. The conformational changes in the cantilever are monitored by reflecting a laser off the back of the cantilever onto an optical detector. The detector's signal is fed into a feedback control system to maintain a constant force between the tip and the surface. The information from this feedback system is used to generate an image of the surface topography and the probe's deflection as it moves across the surface.

4.5.2 Results of the immobilisation and detection of metronidazole

4.5.2.1 Electrochemical detection of metronidazole

To detect metronidazole using electrochemical means, the potentials at which it is either reduced or oxidised need to be established. Using this potential will maximise the sensitivity and selectively by increasing the magnitude of the response, and by ignoring other compounds that may react at other potentials. To establish this potential, a cyclic voltammogram was performed on a bare platinum microchip electrode in different concentrations of metronidazole (Figure 4.15). It can be seen from this data that there are redox peaks at -740 mV and at -300 mV which increase and decrease with increasing concentration of metronidazole, respectively.

The amperometric detection of metronidazole (228 μM) can be seen in Figure 4.16 and Figure 4.17 at potentials of -750 mV and -300 mV respectively. At a potential of -750 mV there is a response to the presence of metronidazole. However, the amplitude of this response is very small (50 nA) for a 228 μM injection. At the -300 mV there is a negative step change (25 nA). Both of these responses concur with the cyclic voltammograms.

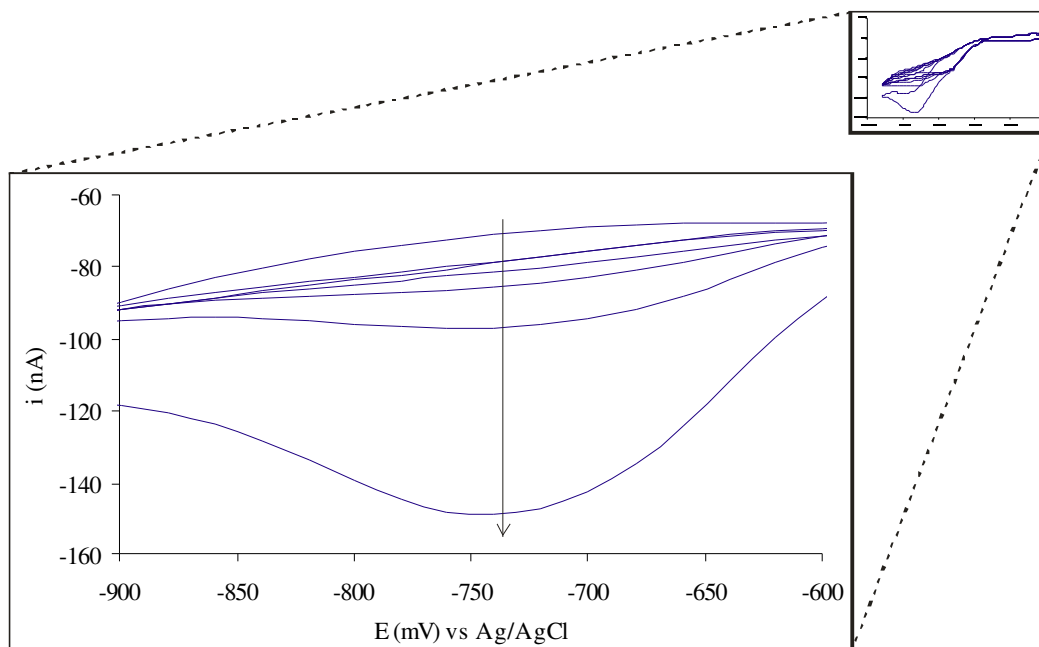


Figure 4.15 – Plot of forward scans from cyclic voltammograms (small plot) of metronidazole with increasing concentrations 0, 10, 25, 50, 100 and 360 μM (arrow going down) using platinum microchip electrodes. Arrow indicates increasing concentration.

Interferences are marked in Figure 4.16 and Figure 4.17 which occur when the injection loop is being filled and when the injector is switch from 'load' to 'inject'.

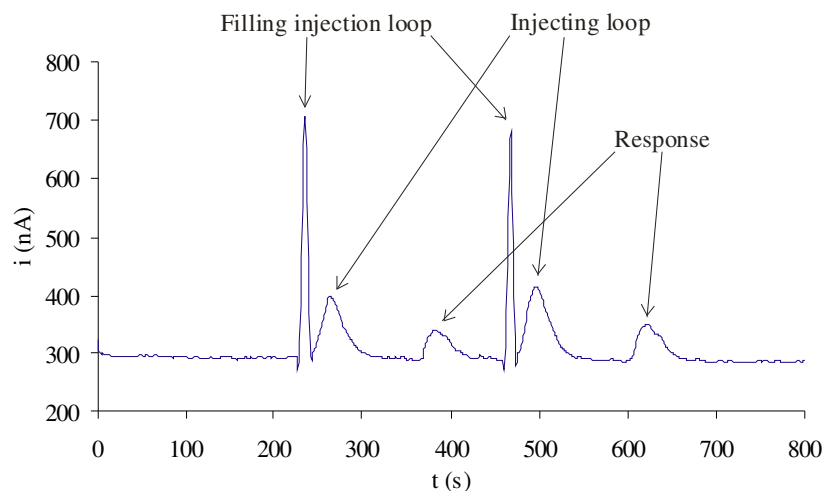


Figure 4.16 – Amperometric (-750 mV) response to metronidazole (228 μ M) injections, also including noise from the injector.

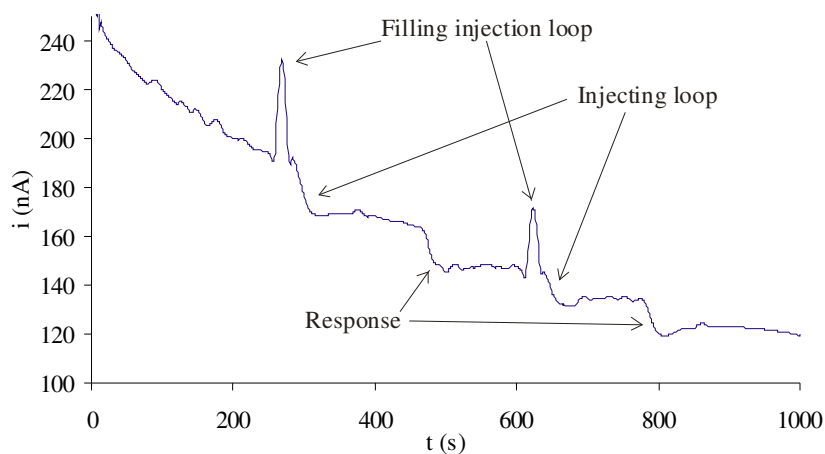


Figure 4.17 – Amperometric (-300 mV) response to metronidazole (228 μ M) injections, also including noise from the injector.

Further testing of metronidazole's electrochemistry (Figure 4.18) and that of the supporting electrolyte (Figure 4.19) in both normal and degassed states on the microchip electrodes showed that across the potential range from -150 to -900 mV, the degassing affected the resulting current. There is a large peak in the PBS solution at -300 mV and -750 mV with the significance of each peak being lowered with the presence of metronidazole.

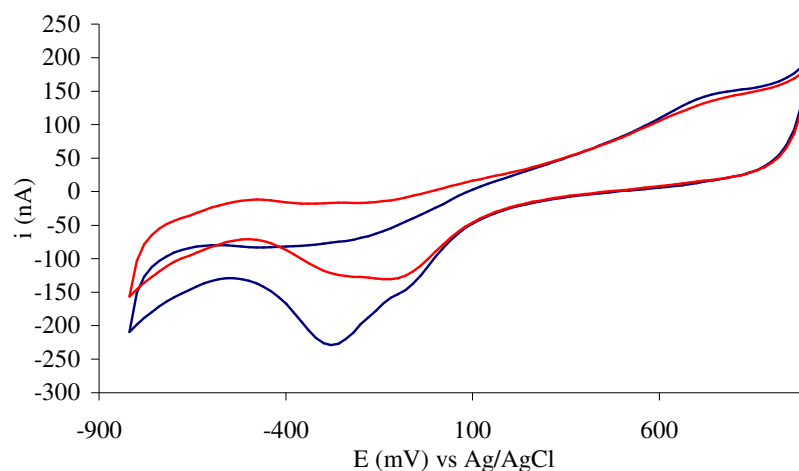


Figure 4.18 – Cyclic voltammetry of metronidazole (100 μ M) in PBS (pH 7.5) with (red) and without (blue) degassing.

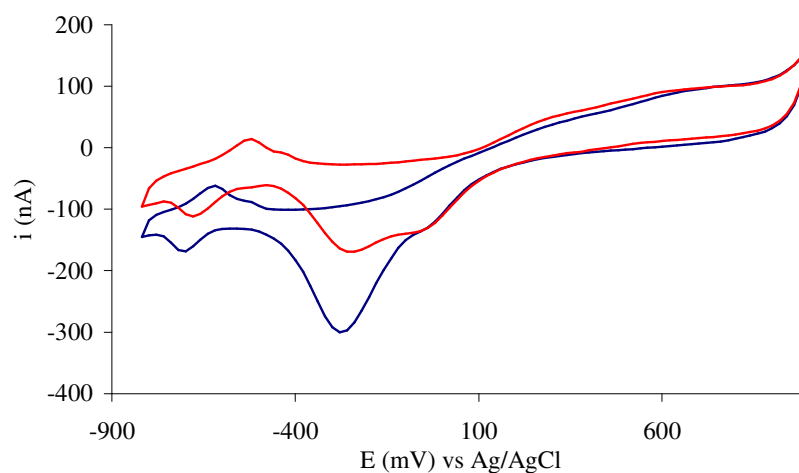


Figure 4.19 – Cyclic voltammetry of PBS (pH 7.5) with (red) and without (blue) degassing.

The electrochemistry of metronidazole was also investigated on carbon paste electrodes, as carbon electrodes have been successfully used in the literature (Oliveira Brett et al., 1997a, Ozkan et al., 1998, Oliveira Brett et al., 1997b, Gong et al., 2003, Lu et al., 2004, Bartlett et al., 2005) for investigations into metronidazole. It can be seen (Figure 4.21) that the degassing of the supporting electrolyte (PBS) greatly reduces the resulting current from -500 to -1000 mV and that the presence of metonidazole (Figure 4.20) shows a distinct peak at -750 mV, which is more pronounced without degassing.

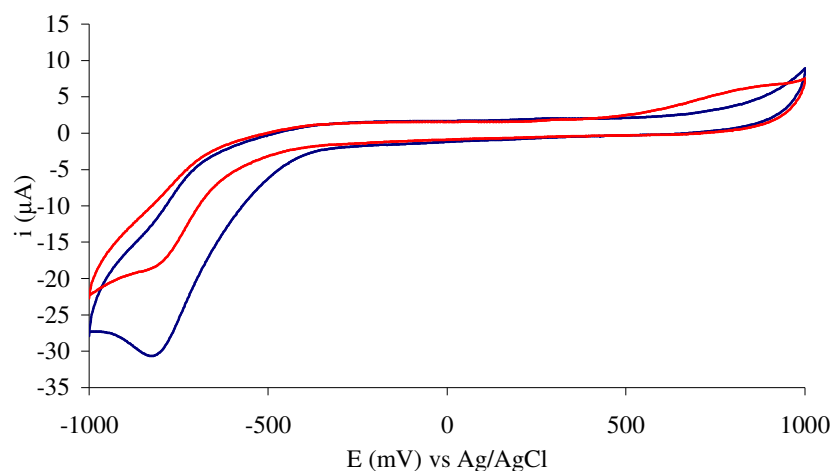


Figure 4.20 – Cyclic voltammetry of metronidazole (200 μM) in PBS (pH 7.5) with (red) and without (blue) degassing on carbon paste electrode.

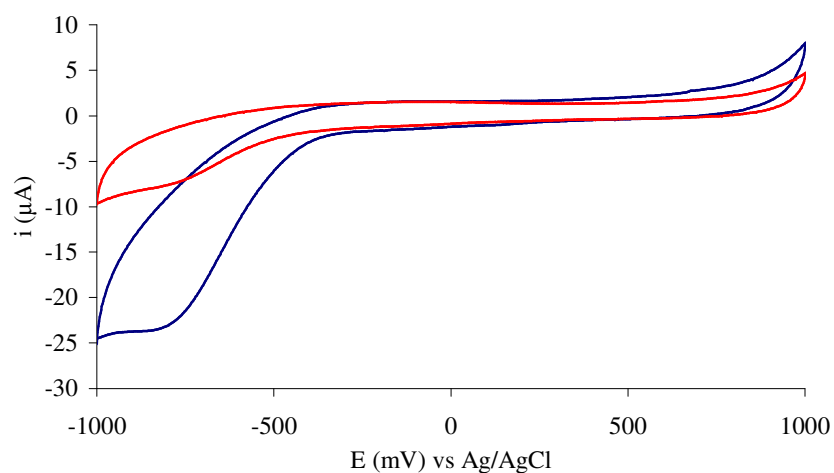


Figure 4.21 – Cyclic voltammetry of PBS (pH 7.5) with (red) and without (blue) degassing on carbon paste electrode.

4.5.2.2 Immobilisation of polymer and impedance monitoring

4.5.2.2.1 Thermal immobilisation procedure

Polymer thermally grafted for two hours can be seen in Figure 4.22. The polymer is immobilised specifically on the electrode surfaces as can be seen by the yellow and brown diffracted colours on the electrodes in the darkfield image (Figure 4.22d) compared to the black bare electrodes in Figure 4.22b. The topography of the

polymerised electrodes (Figure 4.23) shows a fairly smooth surface with varying grain size.

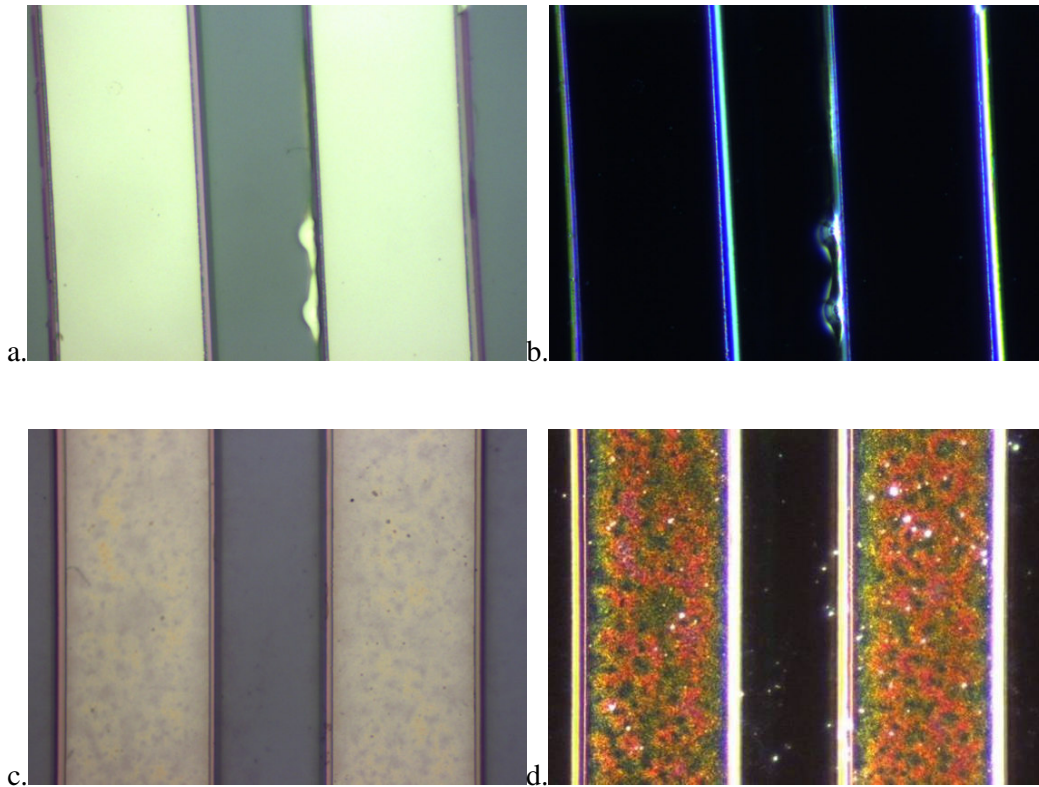


Figure 4.22 – Microscope images of microchip electrodes pre (a & b) and post (c & d) polymerisation (for 2 hours). Images b and d were taken using a darkfield filter.

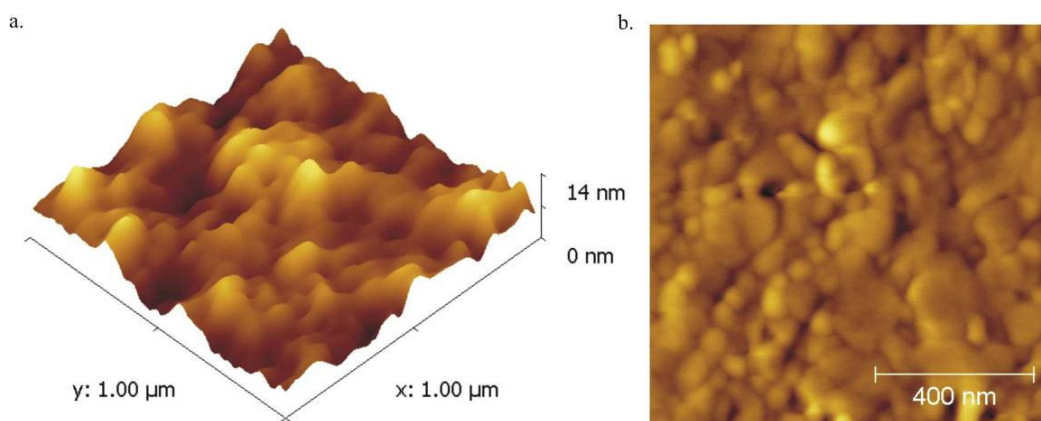


Figure 4.23 – AFM imaged of thermally grafted polymer on microchip electrodes shown in Figure 4.22.

Impedance spectra taken after each stage of the grafting procedure can be seen in Figure 4.24. The immobilisation of the self-assembled monolayer (SAM) increases the impedance and phase of the device; this further increases by a factor of four with the addition of the polymer, resulting in a device with an extremely high charge transfer resistance.

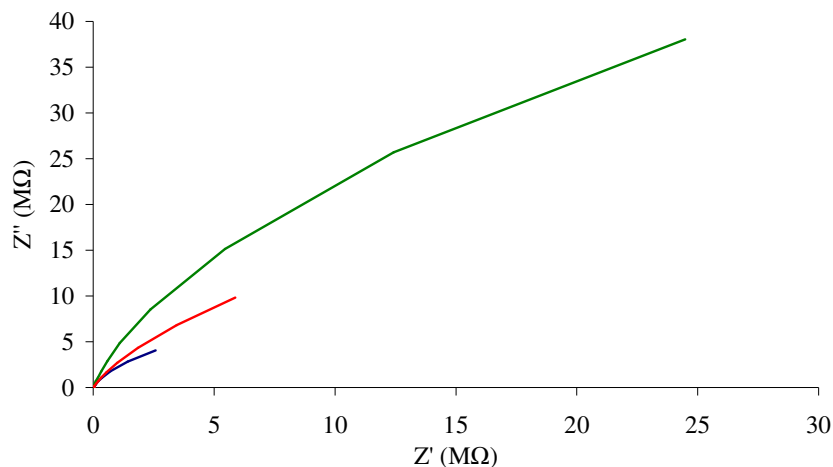


Figure 4.24 – Nyquist plot of bare microchip sensor (blue) and with immobilised SAM (red) and polymer grafted for 2 hours (green) in PBS (pH 7.5).

4.5.2.2.2 Impedance detection

The MIPs were thermally grafted using polymerisation times of 30, 60, 120 and 240 minutes; the only electrode to respond was the MIP polymerised for 30 minutes. The impedance of both NIP (Figure 4.25) and MIP (Figure 4.26) electrodes polymerised for 30 minutes were then tested by injecting various concentrations of metronidazole through a flow cell.

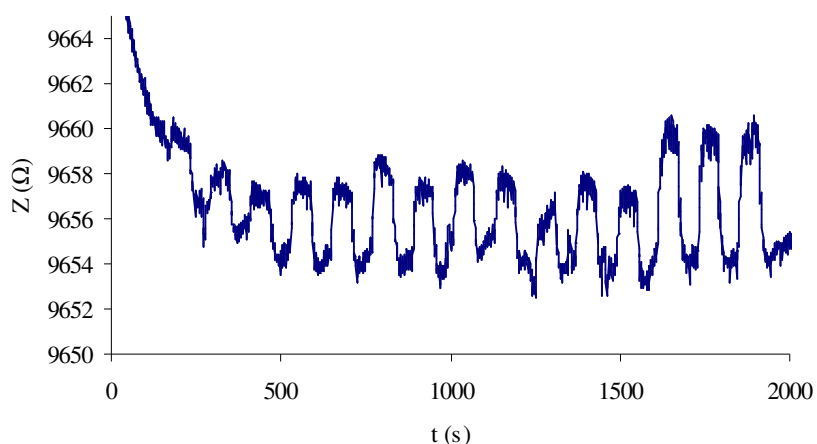


Figure 4.25 – Change in impedance observed for a NIP coated microchip electrodes to consecutive injections of metronidazole at concentrations of 1, 10, 25, 50 and 100 μM . At each concentration, the injection was repeated three times.

The magnitude of the change in impedance for both the MIP and NIP were very similar. There is a visible change in impedance between 1 μM and 100 μM , however the difference between 10, 25 and 50 μM is indistinguishable. This is further hindered by the low sensitivity of the electrodes.

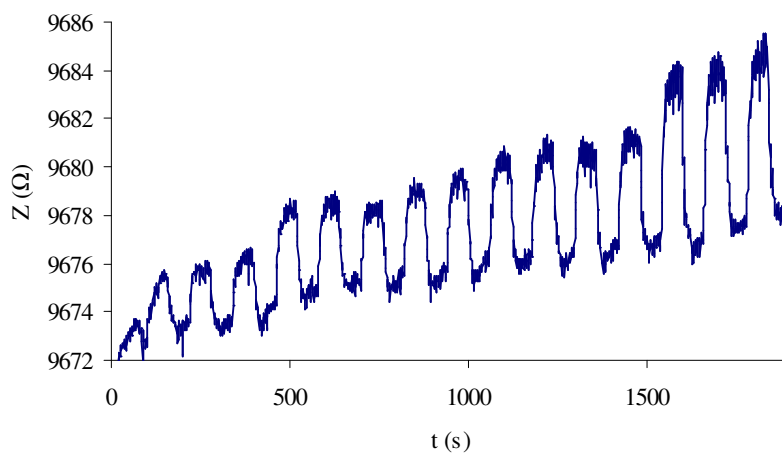


Figure 4.26 – Change in impedance observed for a MIP coated microchip electrodes to consecutive injections of metronidazole at concentrations of 1, 10, 25, 50 and 100 μM . At each concentration, the injection was repeated three times.

4.5.3 Discussion

The initial electrochemical investigation into metronidazole resulted in two oxidation potentials at -750 mV and -300 mV, which is consistent with the literature (La-Scalea et al., 1999). However the amperometric detection of metronidazole resulted in a very poor sensitivity. Moreover, the signal was affected when the injector was being used. The noise due to the injector being changed to 'inject' the sample was similar to the response to metronidazole, for example at -750 mV there was a peak response and at -300 mV there was a step change for both the injection and the response. Thus, the process that occurred due to the sample being injected could be the same as the response to metronidazole implying that the response to metronidazole is not due to its direct reduction.

The further testing of the electrochemistry of metronidazole and the supporting electrolyte show that flushing the solution with nitrogen has a large influence on the resulting current at large negative potentials and that oxidation peaks exist at -750 and -300 mV in the supporting electrolyte. This suggests that the reactions at large negative potentials are due to the reduction of dissolved oxygen, hence, other reactions are interfering with the detection of metronidazole.

The use of carbon electrodes to investigate the electrochemistry of the supporting electrolyte show that the peak at -300 mV disappears and the peak at -750 mV is less significant and becomes insignificant when the solution is flushed with nitrogen. Hence, the peak at -750 mV is probably due to the reduction of oxygen at the electrode surface and is thus dependent on the oxygen concentration in the solution. The peak at -300 mV, which is not visible on the carbon electrodes, is probably due to the reduction of platinum oxide.

As an attempt to improve the response of metronidazole, other buffers (citrate, britton-robinson and tris) were tried. However, as the observed peak at -300 mV is a property of the platinum electrodes, the different buffers did not make any difference.

In addition, it was postulated that the step response seen at -300 mV could be due to the absorption of metronidazole on the electrodes surface; which could be used to pre-concentrate metronidazole for stripping analysis. An Adsorption step was attempted, but no improved response was observed.

The detection of metronidazole by its direct electrochemical reduction on the platinum microchip electrodes seems highly improbable, thus the concentration of metronidazole was monitored by measuring changes in impedance of the polymer which was thermally grafted onto the microchip electrodes. The polymer was anchored to the electrodes surface using the silane SAM and were covalently attached to the initiator previously used in Section 3.2.3.1. However, the UV polymerisation of the polymer solutions containing metronidazole did not polymerise. As a thermally-initiated polymerisation did work, this would suggest that metronidazole is absorbing the UV radiation rather than inhibiting the polymerisation.

Initial thermal polymerisations of 2 hours resulted in a visible polymer layer on the surface of the electrodes. However, no response or changes could be seen with these electrodes to injections of metronidazole; presumably because the polymer's coating was too thick. To reduce the thickness and provide more control over the polymerisation, the polymerisation mixture was dissolved to 10% of its original concentration and microchips were polymerised for 0, 30, 60, 120 and 240 minutes. However, these sensors all gave very similar responses to injections of metronidazole suggesting that the coverage of the MIP on the surface was insufficient.

Electrodes which had a polymer grafted for 30 minutes without dilution did respond to injections of metronidazole. However, their lack of sensitivity meant that distinguishing between consecutive concentrations of 1, 10, 25, 50 and 100 μM was difficult. Also, there was no visible difference between changes in impedance between the NIP and the MIP electrodes.

4.5.4 Conclusion of metronidazole detection and MIP grafting

Although a concentration dependent change in current can be seen, it is not a direct result of metronidazole's reduction, as the reduction is interfered or masked by the platinum electrodes' electrochemistry. Thus impedance monitoring was investigated as an alternative.

The procedure for thermally grafting the polymer for impedance monitoring was very successful as the immobilised polymer showed good coverage of the electrodes. However, the polymer was initially too thick to gain any response. By reducing the polymerisation times, less polymer was grafted and a response to the injection of

metronidazole could be detected. However, distinguishing between the various injected concentrations was difficult.

4.6 Chapter conclusion

This chapter shows the systematic selection of a target antibiotic for detection in a MIP-based electrochemical device, the computational design and testing of the MIP and finally the immobilisation of the designed MIP and the testing of the device.

The selection of the appropriate antibiotic was based on the functionality and solubility of the antibiotic for use in MIP synthesis and its electrochemical activity based on a review of the literature. Although all the antibiotics under consideration had electroactive properties, they were not all suitable for MIP production, mainly due to their insolubility in organic solvents.

The computational design and testing of the MIP proved successful as a MIP was produced with an increased binding capacity for metronidazole. This MIP was not optimised for use in an electrochemical device as the grafting procedure may produce a polymer with differing properties and once the MIP is immobilised screening of various MIP compositions will be far easier and efficient.

The electrochemical detection of metronidazole proved unreliable due to interference at larger reduction potentials. However, the detection of metronidazole using impedance monitoring was possible. The grafting of the MIP resulted in visible polymer specifically immobilised on the platinum electrodes, which proved to be a very reliable procedure, although the sensitivity of these devices was not sufficiently high to produce a reliable and usable sensor.

Chapter 5 - Exploration into the capacitive detection of therapeutic compounds using molecularly imprinting technology

“The important thing in science is not so much to obtain new facts as to discover new ways of thinking about them.” Sir William Bragg, British physicist (1862 - 1942)

5.1 Introduction

It has been seen in the previous chapters that the ability of detecting an analyte by a Faradic process is dependent on many factors, including the electrodes' potential window and electron transfer, and the pH of the supporting electrolyte, ion concentration and composition. In addition the preferred conditions of operation of the sensing device, such as the use of platinum electrodes and a biological electrolyte (blood, plasma, serum, PBS), put limitations on the detection using a Faradic process. Therefore, a non-Faradic process was considered.

5.2 Review of capacitive sensors

Initial capacitive devices (Knichel et al., 1995) used redox probes (usually $\text{Fe}(\text{CN})_6^{4-/3-}$) where the Faradic processes of the redox probe was hindered by the selective binding of an antibody to a surface bound epitope. Thus, upon binding a decrease in capacitance was observed. It was later shown by Rickert and co-workers (Rickert et al., 1996) that the most reproducible results from a capacitive immunosensor based device were attained without a redox probe and by building the device in layers. For example, these layers can be constructed by assembling a thiol monolayer and then by immobilising a selective biological component.

The capacitive detection of surfactants was achieved by binding them to a hydrophobic methyl-terminated thiol monolayer in an aqueous environment (Krause et al., 1996). This resulted in a decrease in the capacitance in a similar fashion to the aforementioned immunosensor based devices. It was found that the quality of the insulating monolayer

was essential in the operation of the corresponding device. Defects in the monolayer would be 'filled' by absorbed surfactant, this led to strong changes in the local dielectric constant, therefore producing a large decrease in capacitance. However, these changes in capacitance were uncontrollable and could cause problems with the operation of the device.

Mirsky and co-workers investigated several short and long chain monolayers for antibody immobilisation (Mirsky et al., 1997) and found that short chain monolayers were unstable as they desorbed from the surface, resulting in capacitive drift and low sensitivity. They also investigated the desorption of long-chain thiols in various solvents (aqueous, methanol, ethanol, DMF, chloroform) (Riepl et al., 1999a). Most of the thiols tested did not desorb in aqueous, methanol and ethanol environments, however, desorption was observed in both DMF and chloroform, and acidic terminated thiols desorb in aqueous environments. The amount of desorption was accredited to the solubility of the thiol in the surrounding solution. In addition, Riepl and co-workers investigated controlled deposition of thiols, based on applied surface potentials (Riepl et al., 1999b). They have shown that thiol gold binding involves the oxidation of sulphur, thus it could be a potential controlled redox process. They also demonstrated that thiols bound to an electrode surface held at -1400 mV are held by physical forces and at the most stable potential (+300 mV) in basic solution absorption does not occur.

These capacitive devices have been used for monitoring the decrease in monolayer coverage at a fixed surface pressure (Mirsky et al., 1996, Mirsky et al., 1998). This method has been used for the detection of phospholipase A₂ immobilised to the thiol monolayer. The product from the interaction between the phospholipase and the phospholipids, results in a soluble compound which desorbs into the bulk solution, which in turn results in an increase in the capacitance of the device.

One of the first capacitive MIP sensor (Panasyuk et al., 1999) used a mercaptophenol monolayer as an anchor for the addition of an electropolymerised MIP layer. However, neither the mercaptophenol nor the addition of the MIP layer provided the required insulating layer for capacitive detection. To resolve this problem the authors used the addition of an octanethiol after the grafting of the MIP layer to 'fill' in the defects and produce a reasonable capacitive device. MIPs have also been grafted to more reliable

insulating layers of hexadecanethiol using absorbed benzophenone initiator for the detection of herbicides (Panasyuk-Delaney et al., 2001), creatinine (Panasyuk-Delaney et al., 2002) and desmetryn (Delaney et al., 2007). This methodology results in a reproducible high quality insulating layer that is a prerequisite capacitive sensing.

Unlike the aforementioned capacitive sensing techniques, the use of MIPs does not rely entirely on the absorption or desorption of an analyte to the sensor surface to produce a change in capacitance. It also relies on the change in dielectric constant within the MIP due to the expulsion of electrolyte from the MIP's porous structure, which causes a change in capacitance, as shown by Delaney and co-workers (Delaney et al., 2007).

5.2.1 Capacitive devices using molecularly imprinted polymers

The first application of molecular imprinting technology in a capacitive device (Panasyuk et al., 1999) highlighted and addressed four key issues required for capacitive detection. These are: i) reducing leakage currents to a minimum, ii) providing a low polymer thickness, iii) ensuring that the capacitive component is significantly greater than the resistive component and iv) ensuring that the solution resistance is negligible in comparison to the capacitive impedance. The solution resistance can easily be lowered by increasing the electrolytes' ionic concentration and the polymer thickness can be controlled by electropolymerisation. The leakage current and high capacitance can both be resolved by 'blocking' the surface, usually with an alkanethiol.

The most common procedure for creating a MIP based capacitive sensor is to electropolymerise o-phenylenediamine (Yin, 2004, Liu et al., 2004, Yin and Xu, 2004) in the presence of the analyte directly onto a gold electrode surface. However, there are two main disadvantages with this method: firstly, Polyphenol-gold binding is not particularly strong and thus the long term stability of these sensors has proven to be poor; secondly, the insulating properties of the electrodes is insufficient, thus there are unwanted redox reactions and background currents.

To attain the required insulating properties for a capacitive device, blocking has been implemented (Cheng et al., 2001, Yang et al., 2005, Gong et al., 2004, Liu et al., 2006, Panasyuk et al., 1999, Yang et al., 2004). This has been achieved by using long chain thiols, usually 1-dodecanethiol, after polymerisation to block the electrode areas that would be otherwise exposed to the electrolyte. To complement blocking and increase

polymer-electrode binding strength, thiols (Yang et al., 2005) and thiolated monomers have also been employed to create MIP layers (Gong et al., 2004, Panasyuk et al., 1999, Yang et al., 2004).

Other approaches without blocking have been investigated by Liao and co-workers (Liao et al., 2004), who demonstrated that satisfactory insulating properties for a capacitive device could be achieved by using a slow scan rate during the electropolymerisation of m-aminophenol onto the electrode surface. Another approach is to use long chain thiols before polymerisation to form the insulating layer and then to graft the polymer to the thiol during photo-polymerisation (Delaney et al., 2007, Panasyuk-Delaney et al., 2002).

The use of a MIP based capacitive device would overcome several of the problems encountered with sensors based on Faradic processes as seen in Chapter 4. From the literature summarised in Table 5.1, possibly the simplest and also one of the most effective ways to produce such a device would be to use an insulating thiol monolayer to anchor a grafted MIP layer. Using this protocol for a capacitive device also lends itself towards a universal method of producing a sensor for various analytes, as theoretically any MIP composition can be polymerised and immobilised onto a sensor surface for convenient label-free detection of target analytes.

Table 5.1 – Summary of MIP-based capacitive devices. (CV – cyclic voltammetry, MBI – mercaptobenzimidazole, DA – Dopamine, SAM – self assembled monolayer, MBA – N,N-methylenediacrylamide, AMPS – 2-acrylamido-2-methyl-1-propane sulfonic acid, *o*-PD – *o*-phenylenediamine)

Analyte	Electrode	Surface preparation	Pre-treatment	Polymerisation	Blocking	Washing	Notes	Ref
Desmetrine & Creatinine	Gold wafer/glass	Piranah Rinse in H ₂ O	Hexadecanethiol in CHCl ₃ soaked in benzophenone in acetone	UV polymerisation: aqueous AMPS and MBA		Incubation in H ₂ O (50°C)	Long chain thiol used to form insulating layer	(Delaney et al., 2007)
Tegafur	Gold wire 0.2 mm diameter	Nitric acid/piranaha H ₂ O wash		Electropolymerisation: <i>m</i> -aminophenol in PBS		HCl and H ₂ O	Produced ultra-thin membrane with slow cyclic scan rate, thus no blocking required for insulation	(Liao et al., 2004)
Pentoxifyverine	Gold wire 0.2 mm diameter	Piranaha rinse in H ₂ O Ethanol wash		Electropolymerisation: <i>o</i> -PD with ion-pair complex, KClO ₄ in PBS		Acetic acid and H ₂ O	Two ion-pair complexes embedded in polymer as selective element	(Yin, 2004)
Transferrin	Glassy carbon 4 mm diameter	Polished in slurry rinsed in ethanol and H ₂ O		Electropolymerisation: <i>o</i> -PD in PBS with KCl		Soaked H ₂ O	Antitransferrin immobilised by copolymerisation and covalent coupling	(Liu et al., 2004)
Cinchonine	Gold wire 0.2mm diameter	Immersed in H ₂ SO ₄ sonicated in ethanol		Electropolymerisation: <i>o</i> -PD in PBS with KClO ₄ and ion-complex		Soaked in dilute acetic acid		(Yin and Xu, 2004)

Table 5.1 – Cont. (CV – cyclic voltammetry, MBI – mercaptobenzimidazole, DA – Dopamine, SAM – self assembled monolayer, MBA – N,N-methylenediacrylamide, AMPS – 2-acrylamido-2-methyl-1-propane sulfonic acid, *o*-PD – *o*-phenylenediamine)

Analyte	Electrode	Surface preparation	Pre-treatment	Polymerisation	Blocking	Washing	Notes	Ref
Glucose	Gold 1mm diameter	Polished in slurry Sonicated in H ₂ O CV in H ₂ SO ₄		Electropolymerisation: <i>o</i> - PD in acetate buffer	1-dodecanethiol	H ₂ O		(Cheng et al., 2001)
Glutathione	Gold disk 2 mm diameter	Polished in slurry Sonicated in H ₂ O CV in H ₂ SO ₄	2- mercaptoethane sulfonate	Electropolymerisation: <i>o</i> - PD in PBS	1-dodecanethiol	Hydrolisation in NaOH solution Cleaned with H ₂ O	SAM used to anchor polymer to surface	(Yang et al., 2005)
Fenvalerate	Gold wire 2 mm diameter	Piranaha Rinsed in H ₂ O	2-MBI	Electropolymerisation: 2- MBI in ethanol alkaline	1- dodecanethiol	Ethanol-water with NaOH	MBI used to replace phenol monomer due to weaker polyphenol-gold binding	(Gong et al., 2004)
Nicotine	Gold disk 10 mm ²	Polished CV in H ₂ SO ₄		Electropolymerisation: poly-DA in PBS	1-dodecanethiol	Alternating H ₂ SO ₄ and H ₂ O	DA oxidation product easily absorbs to gold surface	(Liu et al., 2006)
Phenylalanine	Gold wafer 2.4 mm ²	Piranaha Rinsed in H ₂ O	Mercaptophenol	Electropolymerised: Phenol	Octanethiol	NaH ₂ PO ₄ (50°C)		(Panasyuk et al., 1999)

Table 5.1 – Cont. (CV – cyclic voltammetry, MBI – mercaptobenzimidazole, DA – Dopamine, SAM – self assembled monolayer, MBA – N,N-methylenediacrylamide, AMPS – 2-acrylamido-2-methyl-1-propane sulfonic acid, *o*-PD – *o*-phenylenediamine)

Analyte	Electrode	Surface preparation	Pre-treatment	Polymerisation	Blocking	Washing	Notes	Ref
Mefenacet	Gold disk 2 mm diameter	Polished in slurry sonicated in MeOh and H ₂ O	2-MBI	Electropolymerisation: 2- MBI in ethanol and H ₂ O	1-dodecanethiol	Stirred in ethanol for 40 minutes rinsed in H ₂ O		(Yang et al., 2004)
Creatinine	Thin gold wire 2.4 mm ²	Piranaha rinsed in H ₂ O	Hexadecanethiol in CHCl ₃ Soaked in benzophenone in acetone	UV polymerisation: Aqueous AMPS and MBA		Incubation in H ₂ O (50°C)	Long chain thiol used to form insulating layer	(Panasyuk- Delaney et al., 2002)

5.3 Reproduction of a capacitive MIP device for the detection of creatinine.

The following investigation is the reproduction of a capacitive MIP based device for the detection of creatinine as proposed by Delaney (Panasyuk-Delaney et al., 2002). By reproducing this protocol we gained experience in producing capacitive devices that utilise an insulating thiol layer for both anchoring a selective polymer film and providing the necessary insulating properties required for the operation of such a device.

5.3.1 Methodology

All consumables were supplied by Sigma-Aldrich unless stated otherwise.

5.3.1.1 Custom gold electrodes

Custom planar gold electrodes were created by evaporating gold onto borate glass slides as follows:

The borate glass slides were cut using an CO₂ laser (FenixFlyer, Synrad USA) into 18 mm² working areas and cleaned by soaking them in fresh piranha solution (1:3 mixture of 30% hydrogen peroxide and concentrated sulphuric acid) for 45 minutes. The clean glass was then thoroughly rinsed in deionised water to remove the pirhana solution and dried in a stream of nitrogen.

The clean glass was then placed in a vapour depositor (306 vacuum coating system, Edwards) and 5 nm of chromium was deposited to help bond the following 100 nm of gold, which was further deposited onto the chromium layer. Both layers were deposited at 0.5 nm s⁻¹ and the samples were left to cool in air.

5.3.1.2 Polymer immobilisation protocol

5.3.1.2.1 Electrode surface preparation

The gold electrodes' surfaces were cleaned by immersion in fresh piranha solution (1:3 mixture of 30% hydrogen peroxide and concentrated sulphuric acid) and then thoroughly rinsed in deionised water and dried in a stream of nitrogen.

5.3.1.2.2 Alkanethiol immobilisation

The freshly cleaned gold electrodes were immersed into 5 mM hexadecanethiol in chloroform for a minimum of 12 hours. After the 12 hour period, the thiolated electrodes were briefly rinsed in chloroform and dried in a stream of nitrogen.

5.3.1.2.3 Polymer grafting

The initiator was absorbed by immersing the thiolated gold electrodes in 150 mM benzophenone in acetone for 12 hours. The electrodes were then dried in an oven at 40°C. Following this, 50 µl of de-gassed polymerisation mixture (Table 5.2) was trapped between the initiated gold electrode and a glass cover slip and irradiated with UV from an optical lamp (Cermax xenon, PerkinElmer). The NIP electrodes were prepared in the same fashion, but in the absence of creatinine in the polymerisation mixture.

Table 5.2 – Composition of creatinine-imprinted polymer

Compound	Concentration (mM)
2-Acrylamido-2-methyl-1-propane sulfonic acid	50
N,N-methylenediacrylamide	100
Creatinine	10

5.3.1.2.4 Template removal

The creatinine was removed from the grafted MIP layer by leaving the electrode in a stirred wash solution (1:1 mixture of deionised water and methanol) at 50°C for 1 hour.

5.3.1.3 Analysis techniques

5.3.1.3.1 Contact angle

The static contact angle measurements were taken using a Cam 100 by KSV Instruments Ltd. The measurement was performed by placing a drop of deionised water onto the surface of interest. The contact angle is defined as the angle formed between the solid/liquid interface and the tangent at the liquid/vapour interface where the three

phase boundaries intersect. This angle provides information about the relationship between the cohesive forces of the liquid, and the adhesive forces between the surface and the liquid. When water is used this relationship is directly related to the hydrophobicity of solid surface, for example if the angle tends towards 0° (the adhesive forces are greater than the cohesive forces) then the surface is considered hydrophilic and if the angle is greater than 90° the surface is considered hydrophobic.

5.3.1.3.2 Atomic force microscopy

The AFM analysis was conducted using a PicoScan (Molecular Imaging, USA) in contact mode as described in Section 4.5.1.4.

5.3.1.3.3 Impedance spectroscopy

Impedance spectroscopy was conducted using an ACM AutoACpsp impedance analyser. The impedance was measured over a frequency range of 1 to 1000 Hz with a 32 mV signal amplitude, 0 V offset and an automatic reference resistance in 25 mM phosphate buffer with 100 mM NaCl.

5.3.1.3.4 Impedance monitoring

The impedance of the electrode was monitored using a two electrode system with a Ag/AgCl counter/reference electrode in 25 mM phosphate buffer with 100 mM NaCl as the electrolyte (Figure 5.1). A 10 mV 100 Hz AC potential with a +300 mV offset was passed through the cell. The change in AC potential and phase was monitored using a lock-in-amplifier (Stanford instruments, RS830) as the creatinine and creatine were added to the electrolyte. With the use of a reference resistor and custom software the resistance, reactance and, consequently, the capacitance were calculated and monitored over time.

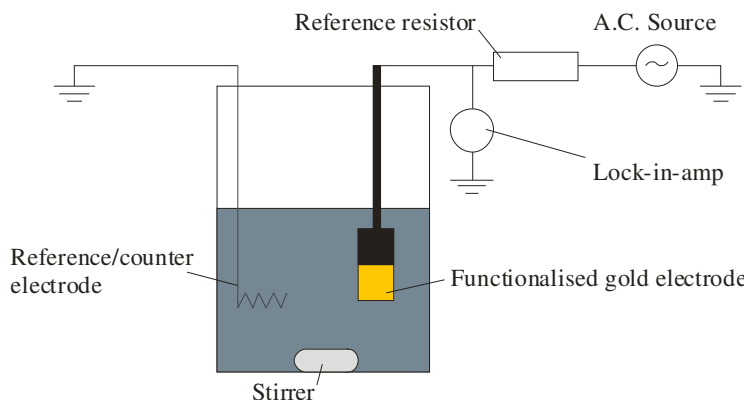


Figure 5.1 – Schematic of experimental setup for two electrode impedance monitoring.

5.3.2 Results of reproduced creatinine specific capacitive device

5.3.2.1 Immobilisation of MIP films using alkanethiol anchor

Each stage of the polymer immobilisation was investigated using contact angle measurement, AFM imaging and impedance spectroscopy. The contact angle (Figure 5.2) demonstrated a distinct change in the surface hydrophobicity at each stage of the polymerisation procedure. The contact angle for bare gold was consistent with angles for pure gold surfaces (no oxide) (Raiber et al., 2005), which demonstrated the effectiveness of the piranha cleaning.

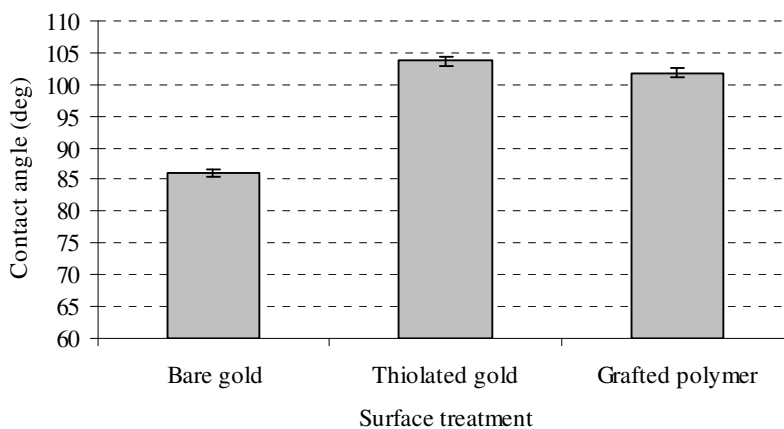


Figure 5.2 – Contact angle of electrode surface at various stages throughout the polymer immobilisation.

The self-assembly of the methyl terminated thiol on the bare gold shows a characteristic increase in hydrophobicity, which is consistent with the literature for methyl terminated monolayers (Martins et al., 2003). The addition of the polymer to the surface causes a slight decrease in the contact angle illustrating that the surface chemistry has once again changed.

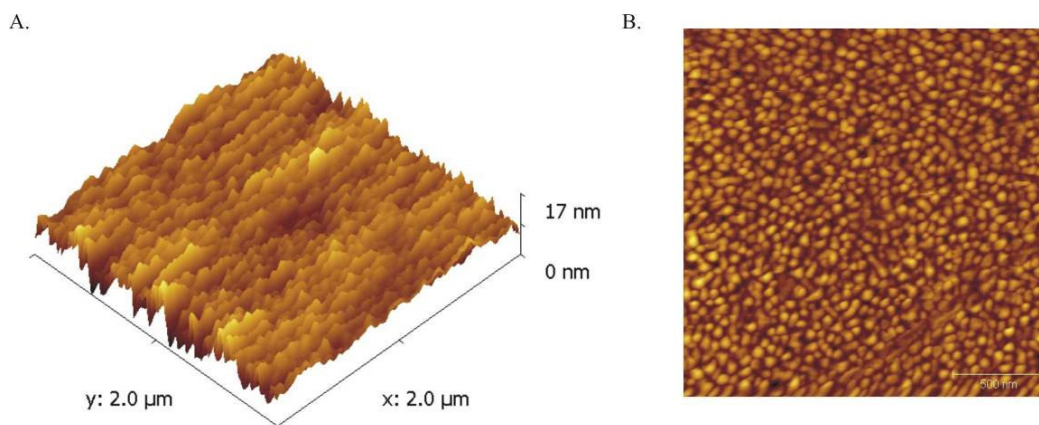


Figure 5.3 – AFM images of A) topography and B) deflection of a bare gold electrode surface.

The AFM images of the bare gold surface (Figure 5.3) show the characteristic grain structure of evaporated gold after piranha cleaning (Wang and Yoon, 2008). The addition of the hexadecanethiol monolayer does not significantly alter the topography of the gold surface although the monolayer causes a small uniform increase in height. However, the change in hydrophobicity of the surface affects the AFM tip when measuring in contact mode and thus reduces the height resolution of the image. Therefore the grains appear slightly larger and smaller in height, see Figure 5.4.

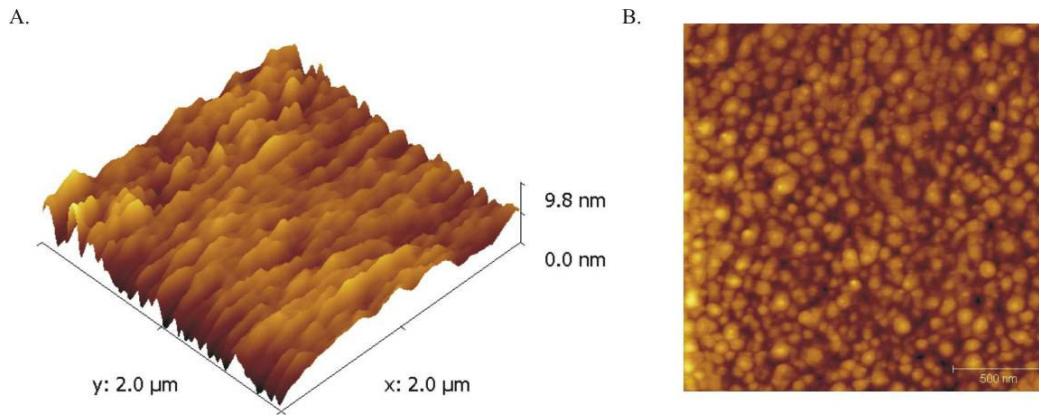


Figure 5.4 – AFM images of A) topography and B) deflection of a thiolated gold electrode surface.

An AFM image of the polymer coating can be seen in Figure 5.5. In this image the gold grains are no longer clearly visible and the rough surface texture of the polymer is now present. To assess the thickness of the polymer the AFM tip was used to remove the polymer from the gold surface (Figure 5.6) and the corresponding profiles demonstrate a thickness of 15 to 20 nm, which is consistent with the literature (Delaney et al., 2007) for this grafting procedure.

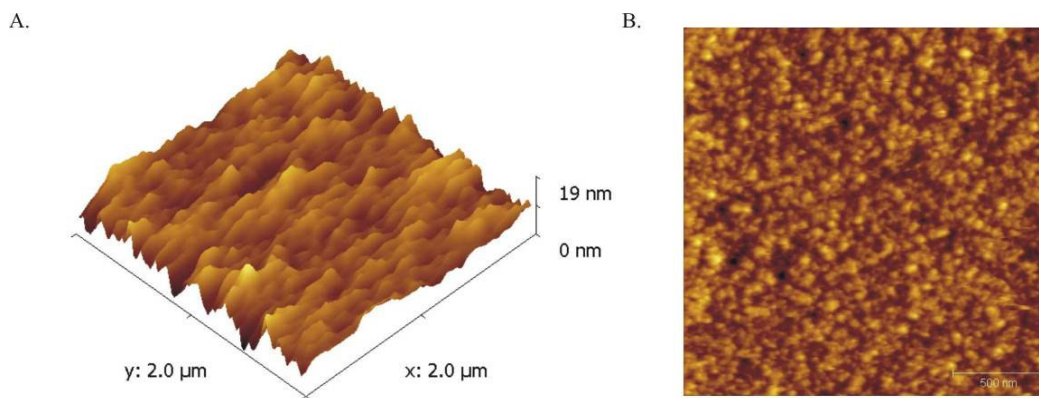


Figure 5.5 – AFM images of A) topography and B) deflection of a NIP coated gold electrode surface.

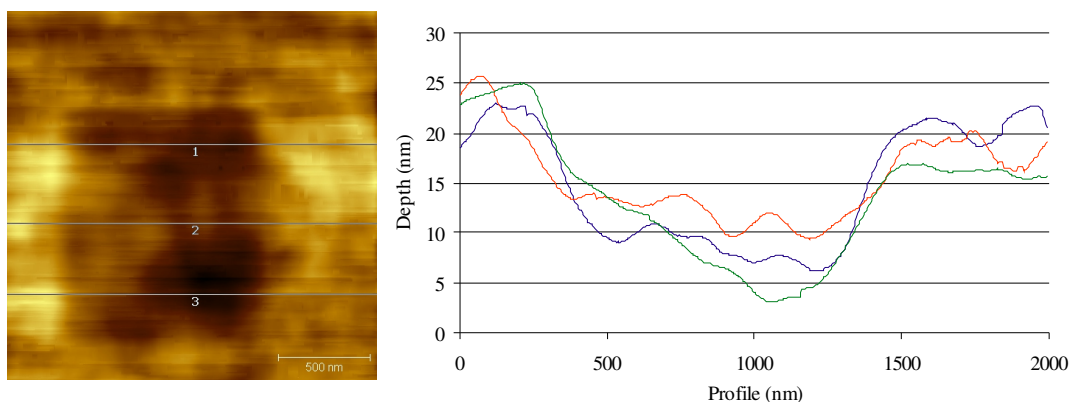


Figure 5.6 – AFM of topography of scratched ($1\ \mu\text{m} \times 1\ \mu\text{m}$) NIP coating and corresponding profile plots. Profile 1 – red, 2 – blue and 3 – green.

The impedance spectrum of the bare gold electrode shows the characteristic of a Randles cell (Figure 5.7 & Figure 5.8). The immobilisation of the thiol layer increases the capacitive component; which is illustrated by the consistently high phase angle, especially above 10 Hz, where previously on the bare gold electrode the phase had rapidly decreased. Also, the additional thiol layer significantly increases the charge transfer resistance. The grafting of the polymer layer causes a slight increase in the impedance relative to the addition of the thiol layer.

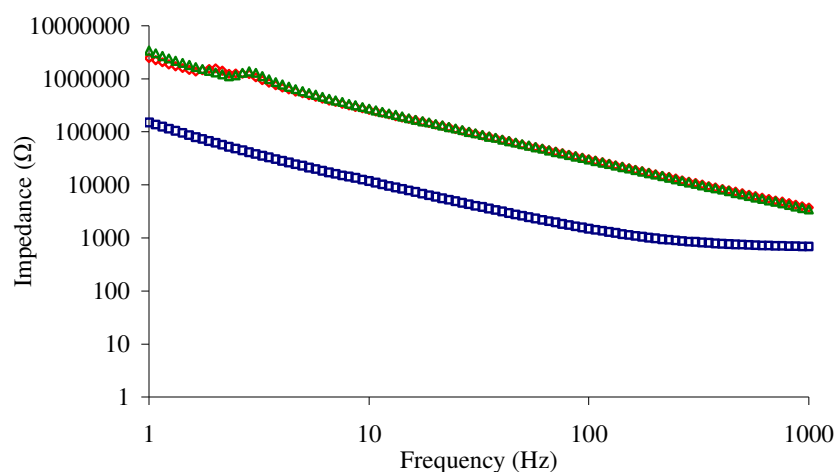


Figure 5.7 – Bode plot demonstrating the variation in impedance during various stages of the grafting polymerisation. Blue – bare gold, red – thiolated gold and green – grafted polymer.

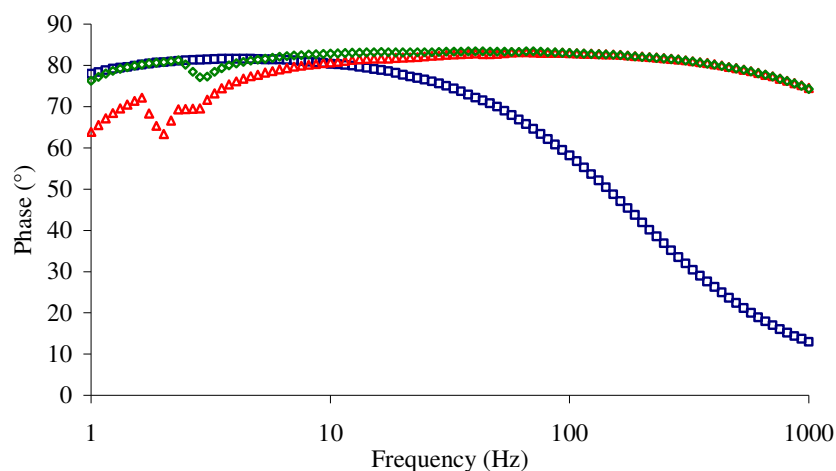


Figure 5.8 – Bode plot demonstrating the variation in phase during various stages of the grafting polymerisation. Blue – bare gold, red – thiolated gold and green – grafted polymer.

5.3.2.2 Response of creatinine specific capacitive devices

Capacitive changes in the polymer grafted layers were measured and the results were seen as a decreasing step change in capacitance, an example of which can be seen in Figure 5.9. Capacitive drift, also visible in Figure 5.9, is probably caused by the adsorption of material at defects on the electrode's surface. This causes long delays in obtaining a steady base line and also limits the sensitivity of the electrode.

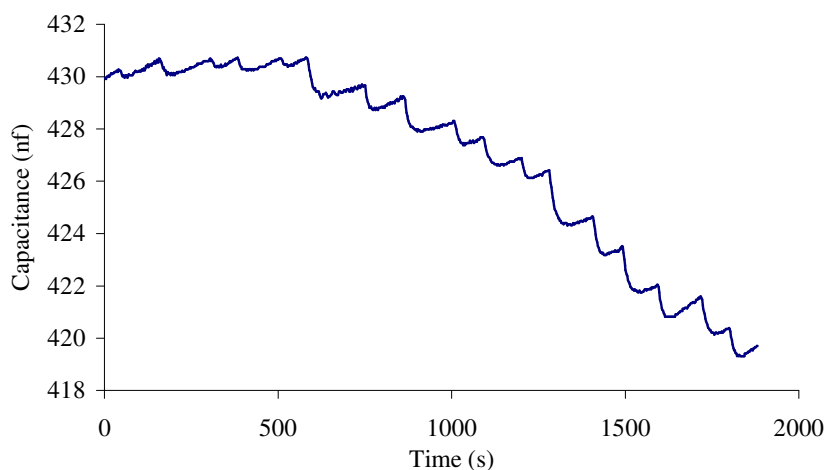


Figure 5.9 – Example sensor response to alternative injections of creatinine and creatine (3 x 200 μ L, 3 x 500 μ L and 3 x 1000 μ L) in 25 mM phosphate buffer with 100 mM NaCl at pH 7.5.

Figure 5.10 and Figure 5.11 show the percentage capacitive change in both NIP and MIP electrodes to creatinine and creatine, respectively. These percentage capacitive changes were calculated as the difference between the capacitance at the point of injection and the capacitance after the step change divided by the initial capacitance.. It can be seen that the addition of creatinine to the MIP coated electrode causes a larger percentage change than its addition to the NIP electrode, therefore demonstrating the high binding capacity of the MIP to creatinine.

Additionally, the capacitive change to creatinine for the MIP electrode is greater than the capacitive change due to creatine, which is contrary to the NIP electrode, thus demonstrating selectivity of the MIP electrode towards creatinine.

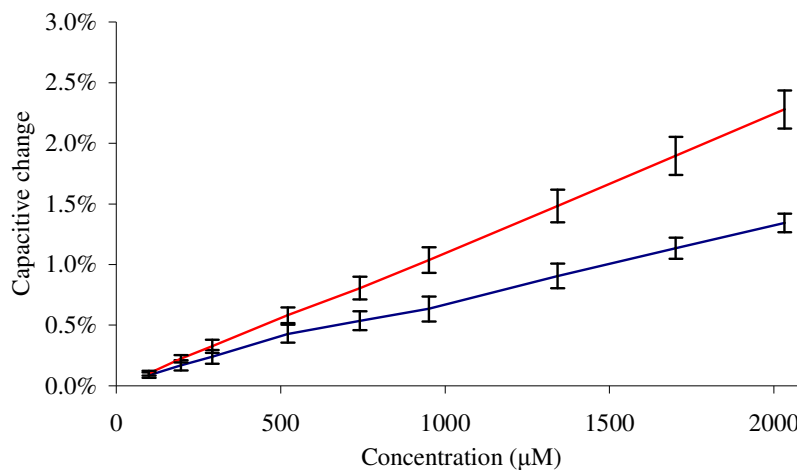


Figure 5.10 – Response of NIP sensor to changes in concentration of creatinine (blue) and creatine (red) from 100 μM to 2000 μM.

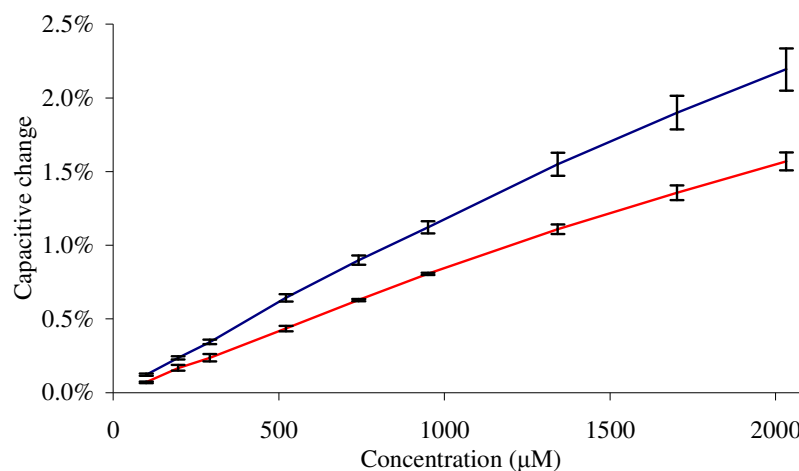


Figure 5.11 – Response of MIP sensor to changes in concentration of creatinine (blue) and creatine (red) from 100 μM to 2000 μM.

5.3.3 Discussion on the performance of the capacitive creatinine devices

The characterisation of the immobilised polymer film in this work is very consistent with the published characterisations performed by Delaney and co-workers (Delaney et al., 2007). The impedance spectroscopy demonstrated Randles cell behaviour with increasing impedance and decreasing capacitance with each stage of the polymerisation process. This is expected as the alkanethiol monolayer will block electroactive species reaching the electrode surface (Hong et al., 1997) and the long chain monolayer has a very high resistance to electron transfer (Xu and Li, 1995). The AFM images of the polymer show an increased roughness with a polymer thickness of approximately 15 nm.

The addition of creatinine to a test solution with a MIP electrode gives a fast decrease in capacitance. Delaney argued that this behaviour was caused by an increase in the dielectric properties of the polymer layer upon the creatinine binding. The response of Delaney's electrodes to the interfering compound creatine was negligible, even for additions of 1 mM creatine (Panasyuk-Delaney et al., 2002). However, in our case we found that the electrodes responded to the addition of creatine, although the capacitive change was smaller than that for the creatinine.

NIP electrodes also responded to additions of both creatinine and creatine although the capacitive change of the sensor to creatine was higher than that of the creatinine. This

suggests that the polymer coating has an affinity for both creatine and creatinine and the higher creatinine response of the MIP is due to the addition of imprinted binding sites that increase the polymer's affinity and specificity and hence response for creatinine.

The reproducibility of the devices was very poor with the initial capacitance varying by up to 200 nF. However, the response of the electrode was always proportional to the initial capacitance. Therefore, the percentage change relative to this initial capacitance was used for comparison. This variation in reproducibility is probably due to defects in the insulating thiol layer and a lack of uniformity of the polymers.

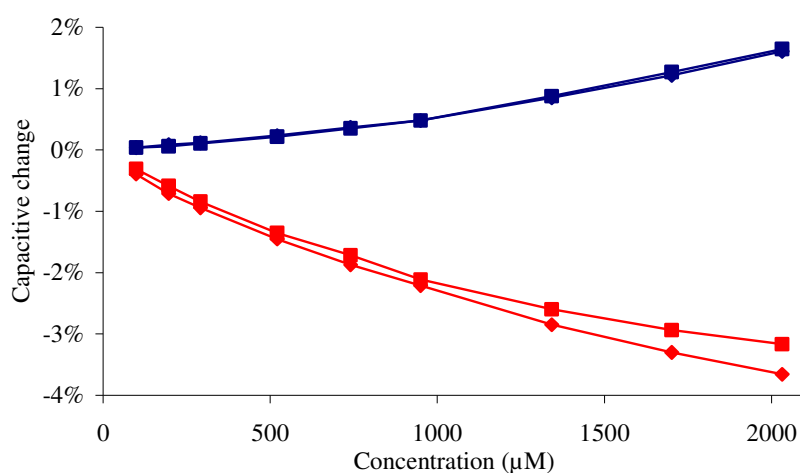


Figure 5.12 – NIP (diamond) and metronidazole-MIP (square) capacitive changes to additions of metronidazole (blue) and imidazole (red).

As the initial construction of the creatinine sensor was relatively successful, the same procedure was repeated for polymers imprinted with metronidazole (described in Chapter 3). The response of these electrodes can be seen in Figure 5.12. It seems that the difference in performance between MIP and NIP sensor is negligible which points to the lack of imprinting effect. The addition of imidazole caused an increase in the capacitance of the sensor (shown as a negative percentage change), this being contradictory to the previous results. This could be explained by the pKa value of imidazole ($pK_a = 7$) (Busch and Knapp, 2004) as opposed to the lower pKa values of metronidazole ($pK_a = 2.62$) (Bardhan et al., 2000), creatine ($pK_a = 3$) (Alekha K. Dash, 2001) and creatinine ($pK_a = 5$) (Khanna and Kurtzman, 2006). As the electrolyte is at pH 7.5, some of the imidazole will be ionised, which could cause an increase in the

dielectric properties of the polymer. It is also possible that the imidazole can cause the polymer to swell (due to repulsion forces between chains with adsorbed template) which would also increase the dielectric properties of the electrode as more electrolyte would be present at the electrode surface.

5.3.4 Conclusion

The reproduction of Delaney's capacitive creatinine sensor proved reasonably successful. Characterisation of the polymer immobilisation was consistent with the literature and the MIP showed an improved response to creatinine when compared to the NIP. However, the MIP also responded to creatine, unlike the electrodes in the literature, and the reproducibility of the devices was poor.

The lack of reproducibility in the devices is most likely due to defects in the insulating monolayer. As the insulating monolayer is essential for the performance of the device, its inconsistency can have a detrimental effect on the sensor's performance. The improvement in reproducibility and quality of this layer should be a priority in further development.

5.4 Investigation of an improved creatinine selective device

Considering the lack of reproducibility of the previous capacitive devices (Section 5.3) and that the quality of the anchoring thiol layer in a capacitive device is essential for sensor performance, further improvements in the quality of the insulating thiol layer was the focus of the following investigation.

5.4.1 Surface pre-treatment for thiol self-assembly

It has been shown that various factors affect the quality and reproducibility of self assembled monolayers (SAM) on gold, these include i) surface contamination (Ron et al., 1998), ii) surface roughness (Creager et al., 1992) and iii) gold oxide formation (Ron and Rubinstein, 1994). The most commonly used procedure for cleaning a gold surface is to immerse the surface in a piranha solution. This highly oxidising solution cleans organic contamination very effectively and has been shown to cause little oxide formation (Guo et al., 1994). However, it has also been shown to recrystallise the surface to a depth of 200 nm (Twardowski and Nuzzo, 2002).

Plasma cleaning for the preparation of a gold surface for self assembly has become a large area of interest for many companies. In particular, the use of oxygen plasma on surface pre-treatment can readily oxidise organic contaminants to remove them from the surface. In addition, etching, for example using piranha solution, has been shown to reduce pin hole defects (Guo et al., 1994), thus increasing the blocking performance of alkanethiols due to the smooth topography.

Raiber and co-workers (Raiber et al., 2005) also reviewed various gold surface treatments to try and attain an optimised method for the removal of SAM layers. They found that hydrogen plasma was capable of removing the SAM layer and it left the surface undistinguishable from a bare gold surface. Oxygen plasma was also used, but it did not remove all the sulphur contaminants and it oxidised the gold surface. However, there should be no sulphur compounds on freshly deposited gold electrodes and it is widely known that alcohols will readily reduce gold oxide (Tremiliosi-Filho et al., 1998).

Therefore, in order to improve the quality of the insulating SAM, an oxygen plasma surface pre-treatment was used before self assembly. Any gold oxide will be reduced by soaking the cleaned surfaces in ethanol and the solvent used for immobilisation will be changed to ethanol as recommended for SAM immobilisation (Schreiber, 2000).

5.4.2 Improved methodology for capacitive detection of creatinine

The following are amendments to the electrode preparation used in Section 5.3.1 to enhance reproducibility and performance of the capacitive devices.

All consumables were supplied by Sigma-Aldrich unless stated otherwise.

5.4.2.1 Gold surface preparation

The evaporated gold surfaces, prepared as described in Section 5.3.1.1, were cleaned using exposure to a 40 W oxygen plasma (K1050X, Emitech UK) for 5 minutes and then immediately immersed in ethanol for 10 minutes to reduce the gold oxide formed during the plasma cleaning.

5.4.2.2 Thiol immobilisation

The ethanol-immersed electrodes from the plasma cleaning were placed into 5 mM hexadecanethiol solutions. The electrodes were left in this solution in the dark at room temperature for 24 hours. They were then rinsed in ethanol and dried in a gentle stream of nitrogen before attaching the initiator.

5.4.2.3 Post polymerisation

After polymerisation the electrodes were immersed in 5 mM hexadecanethiol in ethanol and left for 24 hours to block any defects that may have occurred due to handling and UV exposure.

5.4.3 Results of improved methodology for creatinine detection

The adjustments to the electrode surface preparation and thiol self assembly protocol increased the insulating properties of the electrodes. This can be seen in Figure 5.13 where the phase has a mean value of 88° , demonstrating a nearly purely capacitive system. However, the new electrodes produced had no response to the additions of creatinine

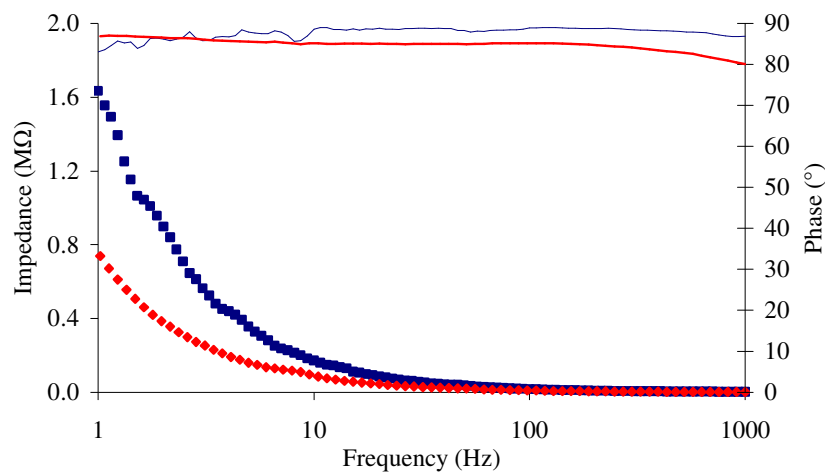


Figure 5.13 – Bode plot of thiol (Blue) and MIP (Red) coated electrodes (impedance – square, phase – diamond) created using the improved self assembly procedure.

5.4.4 Discussion of improved methodology for creatinine detection

The enhancements to the original protocol for preparing a capacitive device, based on an insulating alkanethiol monolayer, have improved the capacitive properties of the electrodes in comparison with the phase calculated from the published literature (79° (Panasyuk-Delaney et al., 2001) and 76° (Panasyuk-Delaney et al., 2002)), which used the previous self-assembly protocol. However, these new devices showed no response to creatinine additions.

It was noted that the electrodes produced using the original protocol had a varied response which was proportional to the initial capacitance of the device. This is demonstrated in Figure 5.14; the response to $100\ \mu\text{M}$ additions of creatinine are compared on three sensors with different initial capacitances. This illustrates that as the initial capacitance decreases, so does the response to additions of creatinine and creatine. Therefore, the improved purely capacitive electrodes, which have a low initial capacitance, will only have a very small response to additions of creatinine.

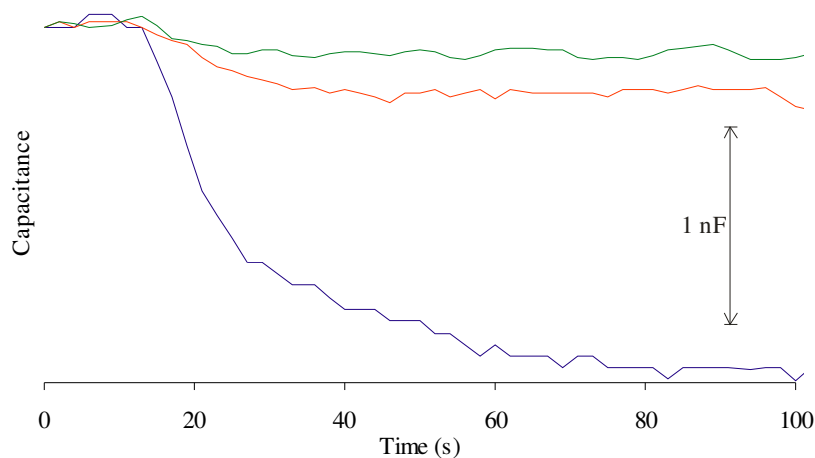


Figure 5.14 – Example response to $100\ \mu\text{M}$ additions of creatinine to three-electrodes prepared using the original protocol with initial capacitances of 500 nF (blue), 293 nF (red) and 119 nF (green).

It was noted by Delaney (Delaney et al., 2007) that some of the electrodes prepared had very low capacitances and extremely high resistances that did not respond to the addition of analyte, was explained by the polymer layer being nonporous. However,

when using the improved methodology, it was a change in the insulating layer, and not the polymer layer which resulted in a similar response.

5.4.4.1 Theoretical discussion of molecularly imprinted capacitive devices

In an attempt to explain the observed results with the improved insulating layer the theoretical model of an electropolymerised capacitive device with and without an insulating anchor layer will be discussed here.

5.4.4.1.1 Modelling electropolymerised capacitive devices

The first molecularly imprinted capacitive device (Panasyuk et al., 1999) was produced using an electropolymerised polymer layer on top of a phenol terminated thiol to anchor the polymer and improve binding strength. This system was modelled as a Randles cell, where the parallel capacitance and resistance are the properties of the chemically sensitive layer (Figure 5.15).

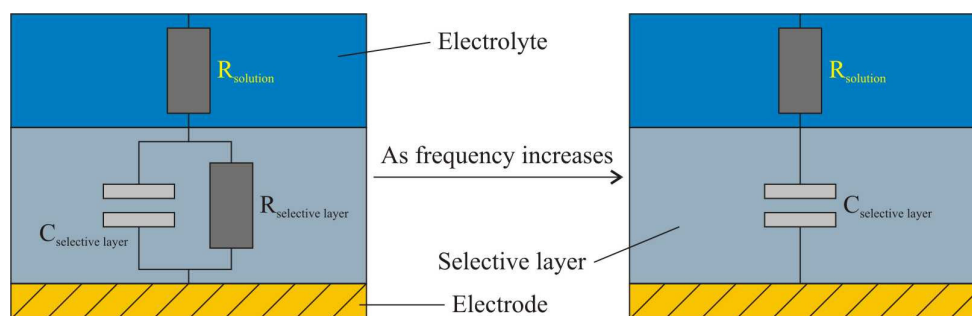


Figure 5.15 – Illustration of capacitive device with the selective layer modelled as a Randles cell.

To attain a more accurate measurement, the majority of the current must favour the capacitive component, thus it must have a low impedance relative to the resistive component. This can be achieved by increasing the applied frequency of the system as shown in Equation 5.1.

$$X = \frac{1}{2\pi f c} \quad \text{Equation 5.1}$$

Where c is the capacitance, X is the reactance and f is the frequency of the applied potential. Thus as the frequency increases the reactance decreases.

So, assuming that the selective polymer layer covers the whole of the electrode's surface and the electrode's surface area (A) is constant, then from Equation 5.2 observed changes in capacitance are dependent on variations in either the polymers thickness (d) and/or the dielectric (ϵ).

$$c = \frac{A\epsilon}{d} \quad \text{Equation 5.2}$$

5.4.4.1.2 Modelling capacitive devices with insulating anchoring layers

The use of an insulating anchor can increase the sensitivity of a capacitive device by reducing the current leakage. One of the simplest ways to achieve this is to create a SAM.

Assuming, as above, that the operating frequency is chosen so that the device is nearly purely capacitive and that the insulating layer and selective polymer are in series (Yang et al., 2005, Liao et al., 2004), then the total capacitance (C_{total}) can be expressed as:

$$\frac{1}{C_{total}} = \frac{1}{C_{thiol}} + \frac{1}{C_{polymer}} \quad \text{Equation 5.3}$$

Where C_{thiol} is the capacitance due to the insulating-thiol layer and $C_{polymer}$ is the capacitance due to the polymer layer.

By considering Equation 5.3, if the thiols' capacitance is large relative to the polymers' capacitance, then the thiols' capacitance becomes insignificant, hence, the total capacitance becomes equivalent to the polymers' capacitance. Which is equivalent to the model described in Section 5.4.4.1.1.

Thus, to acquire an insulating layer with a large capacitance, in accordance to Equation 5.3, the thickness of the layer must be small, which assumes a constant surface area (A) and dielectric (ϵ). This can be further illustrated (Equation 5.4) by combining Equation 5.2 and 5.3 to give the relationship for the total capacitance of the device.

$$C_{total} = A \cdot \frac{\epsilon_{thiol} \epsilon_{polymer}}{\epsilon_{polymer} d_{thiol} + \epsilon_{thiol} d_{polymer}} \quad \text{Equation 5.4}$$

If the polymer coating does not cover the entire surface of the electrode then the response of the device will deteriorate. A model of this shown in Figure 5.16 with the device's total capacitance expressed in Equation 5.5, where θ is the percentage of the surface covered by the polymer. This model is analogous to the models presented in the literature for the capacitive detection of analytes causing desorption of the selective layer (Mirsky et al., 1996, Mirsky et al., 1997).

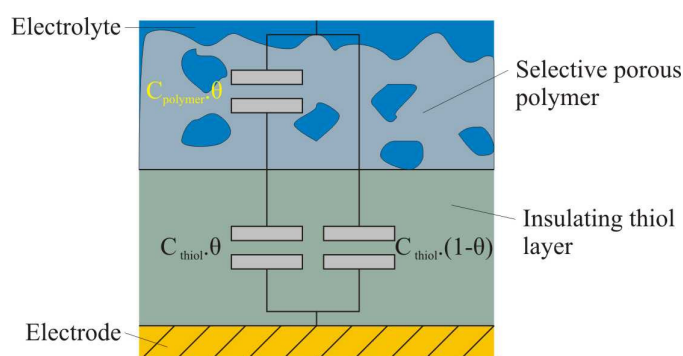


Figure 5.16 – Illustration of capacitive device produced using a thiol insulating layer to anchor a thin polymer film. θ is the percentage of the surface (covered with polymer) which affects the capacitance. This is dependent on polymer coverage and porosity.

$$C_{total} = \left(\frac{1}{C_{thiol} \theta} + \frac{1}{C_{polymer} \theta} \right)^{-1} + C_{thiol} (1 - \theta) \quad \text{Equation 5.5}$$

5.4.4.2 Evaluation of experimental data using the proposed capacitive model

The improved properties of the insulating monolayer are most probably due to a decrease in the monolayer's defects and the better packing of the layer. As the packing of the layer improves, it will become denser and most of the SAM will rearrange itself into a brush formation, which decreases the effective dielectric and increases the thickness of the layer. By considering Equation 5.2, both these changes will result in a lowered capacitance, which possibly explains the decrease in the capacitance of the device when using the improved method of preparation.

Furthermore, by considering Equation 5.4, the decreased dielectric and increased thickness of the insulating layer will be detrimental to the detection limit of the device. This is because, as the effective dielectric decreases so does the effect of any changes in the polymer layer's thickness and as the thickness of the insulating layer increases this is detrimental to any changes in the polymer layer's dielectric. However, even with these changes in the insulating layer, variations in both the dielectric, as proposed by Delaney (Delaney et al., 2007), and thickness, as it is much larger than the monolayer, of the polymer layer should be seen.

A possible explanation for why no response is seen with the new method is that the polymer layer does not cover the entire electrode surface, thus, when considering Equation 5.5, the surface coverage (θ) is less than 1. This implies that as the surface coverage decreases, thus the capacitance of the insulating layer dominates the capacitance of the device.

5.4.4.3 Ideal properties of a capacitive device based on the propose theory

To gain a sensitive response when using a thiol to anchor a selective layer to an electrode, requires the thiol layer to be both insulating and thin, which reduces current leakage and increases the sensitivity of the device respectively. In addition, the selective polymer layer must also be uniform; otherwise the capacitance of the insulating layer will dominate the device.

The other alternative is not to use an insulating anchor as described in Section 5.4.4.1.1., however this will result in high current leakages. Yet, this can be overcome by blocking the surface.

5.4.5 Conclusion of improved methodology for the detection of creatinine

It has been shown that the quality of the insulating thiol layer can be improved with a combination of plasma and ethanol surface pre-treatment and with the thiol being deposited from ethanol solution. However, the capacitive device also requires a uniform polymer coating, as any holes or defects will result in a decreased sensitivity.

5.5 Conclusion of the capacitive detection of creatinine

To explore alternatives to Faradic detection capacitive devices were investigated. It was seen in the literature that a capacitive device prepared using an insulating monolayer to anchor a selectively imprinted polymer provided a simple approach to producing a capacitive electrode. This approach could be easily applied to other MIPs to form a universal platform for sensor development.

The reproduction of the creatinine sensitive electrodes described in the literature was the first goal in investigating these capacitive devices. Variations between MIP and NIP electrodes showed an increase in the capacitive response for the MIP electrode to various concentrations of creatinine. This positive result was further reinforced by the smaller response seen for the interfering compound creatine. However, these results were not as impressive as those published where there was no response to creatine. In addition, although the electrodes worked, their reproducibility was unsatisfactory.

Thus to improve the capacitive response as well as the reproducibility of the electrodes the surface pre-treatment and SAM immobilisation procedure was changed. These changes showed improvements in the impedance of the insulating monolayer, however, these improvements were detrimental to the sensitivity of the electrodes, which is contradictory to the literature.

To explain this unexpected response a model of the capacitive electrodes was derived based on assumptions within the literature. This model described the relationship between the properties of the insulating layer and the decrease in sensitivity. Accordingly, it can be concluded that a uniform polymer layer is as essential as a perfect insulating layer for the performance of a capacitive device.

Chapter 6 - Detection of propofol with the controlled growth of MIP onto a conducting polymer anchor

“That which we persist in doing becomes easier, not that the task itself has become easier, but that our ability to perform it has improved”, Ralph Waldo Emerson (1803 – 1882)

6.1 Introduction

From the work presented in the previous chapters two main issues with regards to MIP-based sensors keep arising; firstly, the lack of control over the polymerisation process and secondly, the electrical insulation caused by the polymer layer when using a faradic detection technique. Two new compounds were introduced to address the problems that incurred during polymer grafting. To increase the level of control over the polymerisation, iniferters were used to initiate and control the polymerisation, and a poly(aniline) anchor was used to increase the connectivity between the electrode and polymer binding sites.

The poly(aniline) anchor was recently developed at Cranfield University (Lakshmi et al., 2009b), thus the following chapter is an initial investigation into the possibility of both an impedance and amperometric sensor, for propofol and creatinine as the target analytes.

6.2 Review of relevant compounds and their chemistry

The following is a review of the new compounds being introduced into the grafting procedure.

6.2.1 Iniferters

Iniferters were created by Otsu (Otsu and Kuriyama, 1984) and are similar to initiators but they are used in ‘living’ radical polymerisations because they can initiate polymerisation, but also act like chain transfer agents and free radical terminators.

Dithiocarbamate-based iniferters form a carbon radical and a dithiocarbamate radical (Figure 6.1). The dithiocarbamate radical is stable and un-reactive, and only the carbon radical is capable of initiating polymerisation as it acts as an active centre for propagation. Termination of the polymerisation can occur by either two carbon radicals reacting or a dithiocarbamate radical reacting with a carbon radical. In the second case, the dithiocarbamate radical can be re-initiated and propagation can continue. It is this property of ‘re-initiation’ that gives iniferters their ‘living’ nature when compared to free radical initiators.

Iniferters are attractive alternatives to free radical initiators because they undergo a more controlled polymerisation (Luo et al., 2002). The increased control comes from the polymerisation being slower, compared to free radical initiators. It has been shown that the initial polymerisation rate can be twelve times slower (Kannurpatti et al., 1996) and polymer growth is linear relative to polymerisation time (de Boer et al., 2000). This can be explained by the termination and re-initiation of the dithiocarbamate radical as opposed to the constant propagation of a carbon radical and the instant termination of a carbon-carbon radical interaction.

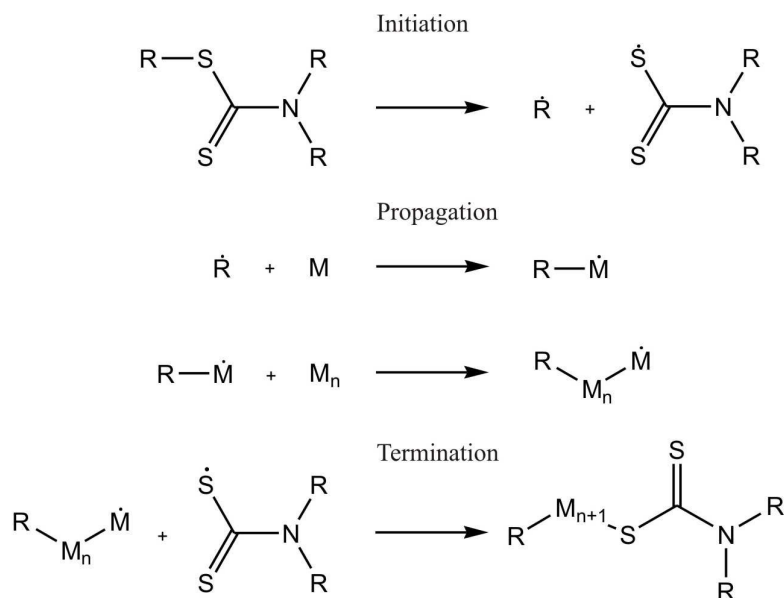


Figure 6.1 – Schematic of dithiocarbamate polymerisation.

6.2.1.1 Polymer grafting

A surface can be functionalised by immobilising iniferters and growing various polymers from the surface. The slower polymerisation, as a consequence of using an iniferter, provides a more controlled polymerisation and ensures accurate variation in the polymer thickness. As the iniferter can be re-initiated, multiple layers consisting of differing constituents can be grown (de Boer et al., 2000). Surface grafting with iniferters has been used to create “thermo responsive phase transition” layers (Matsuda and Ohya, 2005). This was achieved by growing polymer chains of a consistent length from a silane immobilised iniferter. Iniferters have also been successfully used in the preparation of MIPs on silica supports (Ruckert et al., 2002) where their main advantage over immobilised azoinitiators is the lack of bulk polymerisation.

6.2.2 N-phenylethylene diamine methacrylamide (NPEDMA)

N-phenylethylene diamine methacrylamide (NPEDMA) is a monomer designed at Cranfield University, specifically to provide a conductive anchor to which polymer can be grafted from the resulting functional surface. NPEDMA consists of two polymerisable groups, an aniline and a methacrylamide group which can be independently polymerised. The electropolymerisation of NPEDMA results in a poly(aniline) anchor being immobilised on the electrode's surface with a functional surface group capable of further polymerisation.

The poly(NPEDMA) anchor is conductive: as an anchor it provides a low resistive path for the electrochemical study of analytes immobilised in subsequent polymer layers grown on top of the poly(NPEDMA) layer. This is not being possible with most anchors which have a high electrical resistance, for example long chain thiol monolayers.

6.2.2.1 NPEDMA electropolymerisation

The electrochemistry of NPEDMA (Figure 6.2) is presumed to be analogous to that of aniline, where the secondary amine bonded to the benzene ring is oxidised resulting in a radical cation, which has three different structural forms. These various cations are presumed to be unstable, thus further chemical reactions may occur resulting in an autocatalytic reaction (Cui et al., 1993) when the radical cation reacts with NPEDMA.

This is shown in Equation 6.1 and Equation 6.2, where N is NPEDMA, PN is poly(NPEDMA), PN^{ox} is oxidised poly(NPEDMA) and PN^{oli} is oligo(NPEDMA).



The unstable radical cations can also form dimers which can be electrochemically oxidised and reduced (Stuart and Foulkes, 1988), an example of which is shown in Figure 6.2. This electrochemical activity will presumably result in redox peaks at lower potentials than the initial NPEDMA oxidation. Poly(NPEDMA) is formed during chemical reactions between the radical cations and/or their dimers.

6.3 Growing polymer from an electropolymerised NPEDMA layer

The following section describes an investigation into the electropolymerisation of NPEDMA onto an electrode surface. NPEDMA was used as a conductive anchor from which polymer can be grown. The polymerisation was initiated using iniferter attached to the immobilised NPEDMA coating that will allow a controlled polymerisation. Thus, by varying the UV intensity and exposure time, control over the polymerisation can be gained.

6.3.1 Methodology of polymer immobilisation with a NPEDMA anchor

All consumables were supplied by Sigma-Aldrich unless stated otherwise.

6.3.1.1 NPEDMA immobilisation

NPEDMA was synthesised at Cranfield University and dissolved in 50 mM HClO₄ with 10% methanol to a concentration of 2.44 mM. The electropolymerisation was performed using cyclic voltammetry in a three-electrode configuration with a gold working electrode (BASi, UK), a platinum wire counter electrode and a Ag/AgCl reference electrode (BASi, UK) using a microAutoLabII (Eco Chemie, Netherlands) potentiostat. The potential varied between 0 V to 1.1 V at a rate of 50 mV s⁻¹ for 15 scans. The working electrode was mechanically cleaned using aluminium slurry and rinsed in deionised water before each electropolymerisation. After the polymerisation the electrode was rinsed in ethanol and dried in a stream of nitrogen ready for the attachment of the iniferter.

6.3.1.2 Iniferter attachment and polymer growth

The attachment of the iniferter to the NPEDMA coated electrode and the growth of the polymer using the immobilised iniferter for initiation followed the same procedure, the only difference was the solution in which the electrode was submerged.

6.3.1.2.1 Iniferter attachment and polymerisation procedure

The working electrode was submerged into a beaker containing either the iniferter or polymer solution with a glass pipette for degassing. The beaker was sealed with parafilm and the solution was flushed for ten minutes with argon before irradiation with

the UV lamp (CermaX xenon, PerkinElmer). After the UV exposure the electrodes were rinsed in ethanol and dried in a stream of nitrogen.

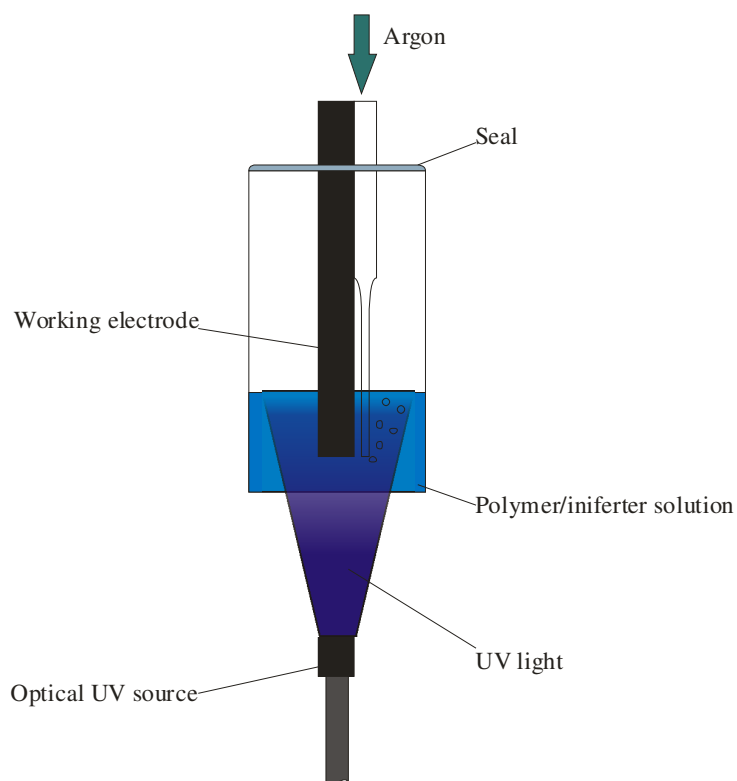


Figure 6.3 – Experimental setup for iniferter attachment and polymer grafting.

6.3.1.2.2 Iniferter solution

The iniferter (*N,N'*diethyldithiocarbamic acid benzyl ester) was purchased from TCI (Oxford, UK) and dissolved in ethanol at 50 mM concentration for the attachment.

6.3.1.2.3 Polymer solution and cleaning

The composition of imprinted polymer used for the selective binding of propofol can be found in Table 6.1. It was designed and tested in a previous study by Cranfield University on behalf of Sphere Medical and was also used in the work described in Chapter 3 for an initial investigation into electrochemical MIP sensors.

Table 6.1 – Propofol polymerisation mixture.

	Substance	Mass (mg)	Role
NIP	Diethylamino ethylmethacrylate	525	Monomer
	Ethleneglycol dimethacrylate	3262	Cross-linker
	Acentonitrile	3925	Porogen
MIP (as above but with template)	Propofol	125	Template

After the polymerisation, the electrodes were cleaned by immersing them in a stirred solution of 50% deionised water and 50% methanol at 50°C for one hour and then dried in a stream of nitrogen and stored in the dark until use.

6.3.1.3 Electrochemical investigatory techniques

6.3.1.3.1 Cyclic voltammetry

The cyclic voltammograms were acquired using a cell with a three-electrode configuration using a functionalised gold working electrode (BASi, UK), a platinum wire counter electrode and a Ag/AgCl reference electrode (BASi, UK). A microAutoLabII (Eco Chemie, Netherlands) potentiostat was used to cycle from -0.5 V to 1 V at a rate of 500 mV s⁻¹ in PBS (pH 7.5) for 3 scans. The third scan of each CV was used for comparison to various electrodes.

6.3.1.3.2 Impedance spectroscopy

All impedance spectroscopy was conducted using an ACM AutoACpSP impedance analyser. The impedance was measured in a frequency range 0.01 Hz - 10000 Hz with a 32 mV signal amplitude, 0 V offset and an automatic reference resistance in a three-electrode configuration with a functionalised gold working electrode (BASi, UK), a platinum wire counter electrode and a Ag/AgCl reference electrode (BASi, UK).

6.3.2 Results of polymer immobilisation with a NPEDMA anchor

6.3.2.1 NPEDMA immobilisation

The cyclic voltammograms of NPEDMA (Figure 6.4) demonstrate its oxidation at a potential around 850 mV, which is similar to the oxidation of aniline (Zhang et al., 2008, Lin et al., 2005). The first scan (blue line) shows the characteristic oxidation peak (I) of the amino oxidation, this peak initially decreases and moves to higher potentials as the scans progress. This change in peak was characteristic of the electropolymerised layers getting thicker and interfering with the oxidation.

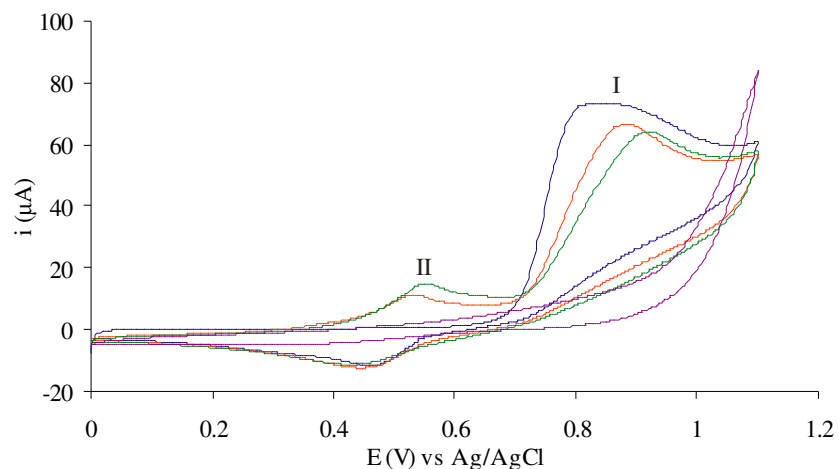


Figure 6.4 – Cyclic voltammetric scans of NPEDMA being electropolymerised (50 mV s^{-1}). Consecutive cyclic scans 1 (blue), 2 (red), 3 (green) and 15 (purple).

The redox couple which occurred during the electropolymerisation (II) was due to dimers of NPEDMA electrochemically reacting, which is typical behaviour of an ECE (electrochemical-chemical-electrochemical) system. This has also been observed by Jin and co-workers during the electropolymerisation of aniline (Jin et al., 2006).

6.3.2.2 Polymer growth

Initially the polymer layer was grown on top of the iniferter for 30 minutes with the UV lamp at a distance of 1 cm, however no response could be gained from these devices. With a reduction in polymerisation time, current could be measured through the immobilised layers, this can be seen in Figure 6.5 where the decrease in polymerisation time leads to increasing current in a cyclic voltammogram.

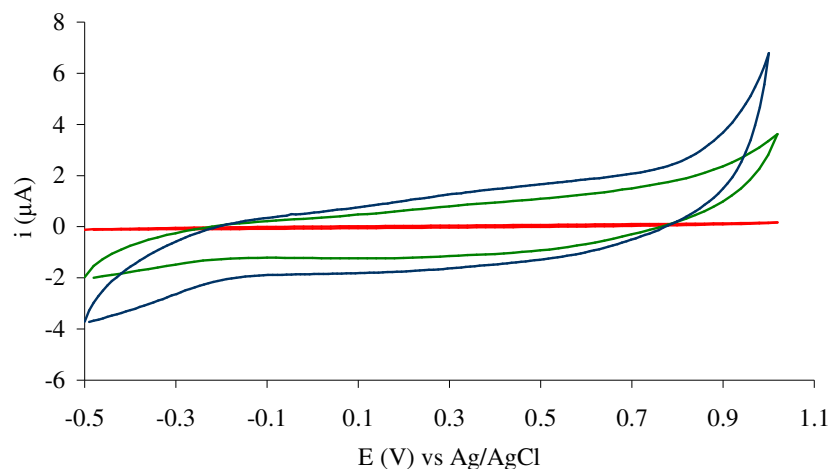


Figure 6.5 – CV of MIP coated electrodes polymerised at a distance of 1 cm from light source for 5 minutes (blue), 10 minutes (green) and 30 minutes (red).

Impedance spectrums (Figure 6.6 and Figure 6.7) of the bare gold electrode conform to Warburg's model of a diffusion related system. With the addition of the NPEDMA layer the overall impedance of the device increases but the Nyquist peak of a characteristic model Randles cell shifts to a lower frequency which shows a decrease in the charge transfer resistance. The growth of the MIP layer on top of the iniferter doubles the impedance of the system compared to a bare gold electrode and the device's response becomes diffusion dependent.

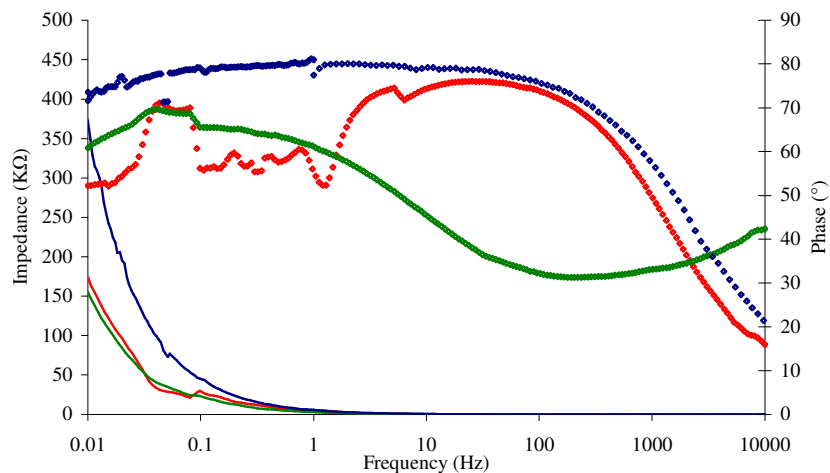


Figure 6.6 – Bode plot of MIP (blue) polymerised for 10 minutes at a distance of 1 cm, NPEDMA (green) and bare (red) gold electrodes in PBS (pH 7.5).

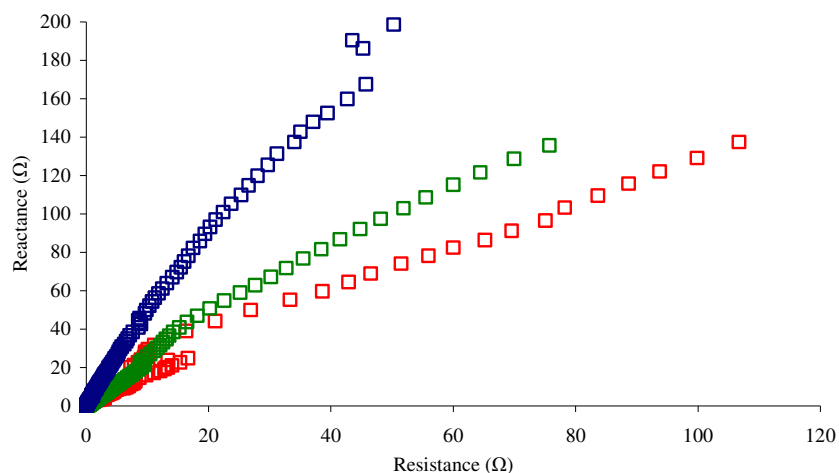


Figure 6.7 – Nyquist plot of MIP (blue) polymerised for 10 minutes at a distance of 1 cm, NPEDMA (green) and bare (red) gold electrodes in PBS (pH 7.5).

The relationships between polymerisation distance (Figure 6.8) and polymerisation time (Figure 6.9) against the resulting current in a cyclic voltammogram show that increasing the polymerisation distance and decreasing the polymerisation time result in a larger current passing through the immobilised layers. This implies that a thicker polymer film would insulate the electrode surface and therefore hinder diffusion.

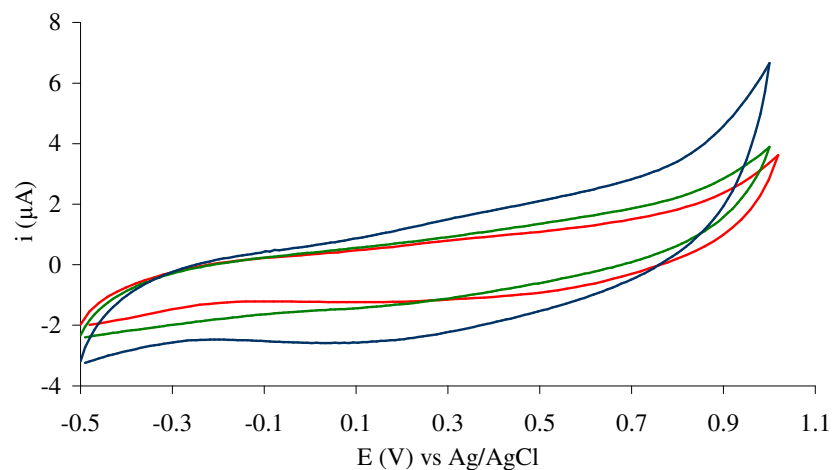


Figure 6.8 – CV of MIP coated electrodes polymerised for a period of 10 minutes at a distance of 3 cm (blue), 2 cm (green) and 1 cm (red).

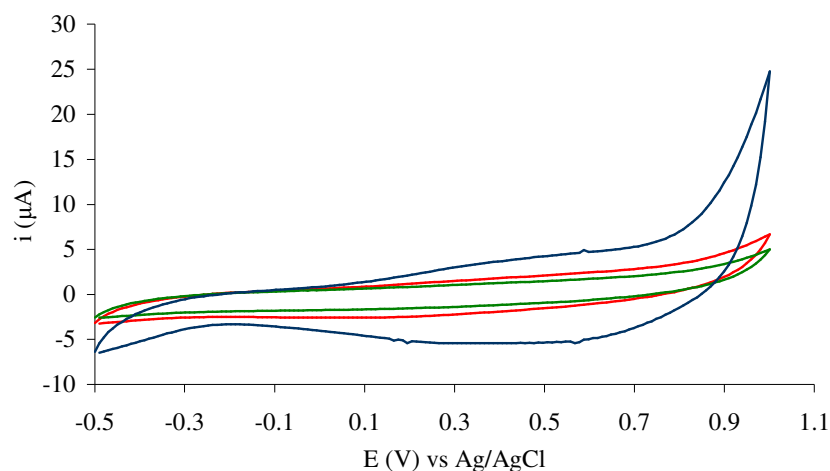


Figure 6.9 – CV of MIP coated electrodes polymerised at a distance of 3 cm for of period of 1 minute (blue), 3 minutes (green) and 10 minutes (red).

6.3.3 Discussion of polymer immobilisation with a NPEDMA anchor

The electropolymerisation of NPEDMA demonstrated the characteristic redox peaks of an aniline electropolymerisation. It appears that there was only one visible redox couple caused by the reduction and oxidation of dimers in the ECE system. It was proposed by Stuart and Foulkes (Stuart and Foulkes, 1988) that the two redox couples in the electropolymerisation of aniline are caused by the dimers benzidine and p-aminodiphenylamine formed after aniline's oxidation. The electrochemical oxidation of an analogous structure to benzidine is shown in Figure 6.2. However, the electrochemical oxidation of the analogous dimer for p-aminodiphenylamine was not achievable as the secondary anime between the phenyl groups became a tertiary anime in the analogous structure. Thus, it was no longer capable of donating protons and forming a double bond with the oxidised phenyl ring. This could explain why only one redox couple was seen in the electropolymerisation of NPEDMA.

The addition of the NPEDMA to the electrode's surface reduces the charge transfer resistance and slightly increases the impedance in PBS (pH 7.5). The growth of polymer on top of the NPEDMA layer results in a more diffusion-orientated system, which was expected as the polymer would behave as a porous insulator.

The current response from a cyclic voltammogram was seen to increase with decreasing polymerisation time and increasing polymerisation distance. This was expected, as both

these changes in polymerisation conditions will result in a decrease in the UV radiation that was incident on the device over some period of time. The polymer's thickness varies proportionally to UV intensity and the exposure time will determine the length of the polymerisation process. The polymer can be viewed as a porous insulating layer, thus the thicker it was, the more the thicker the diffusion layer would become, hence the current would decrease for a constant scan rate.

6.3.4 Conclusion of polymer immobilisation with NPEDMA anchor

Coating an electrode surface with NPEDMA using electropolymerisation has proven to be successful. The electropolymerisation showed similar characteristics to that of an aniline electropolymerisation. The attachment of the iniferter and growth of polymer was also successful and control over the polymerisation by varying the UV exposure time and UV intensity was achieved.

6.4 Impedance detection of creatinine and propofol with NPEDMA anchored MIP

The following section looks at the impedance detection of creatinine and propofol using NPEDMA as a conductive anchor.

6.4.1 Methodology for the impedance detection of creatinine and propofol

All consumables were supplied by Sigma-Aldrich unless stated otherwise.

6.4.1.1 Coating of electrodes with polymers

The various electrode coatings were prepared using the procedure from Section 6.3.1.

6.4.1.2 Impedance detection

The impedance monitoring was achieved by setting up a two-electrode cell with the functionalised working electrode and a Ag/AgCl reference/counter electrode in PBS (pH 7.5) with 10% ACN. A lock-in-amplifier (Stanford instruments, RS830) was used to measure the potential across the cell and the current and impedance were calculated with the aid of a reference resistor (50 k Ω). Propofol dissolved in PBS (pH 7.5) containing 10% ACN was injected into the stirred cell. The same impedance setup was used as previously described in Chapter 5.

6.4.2 Results of the impedance detection of creatinine and NPEDMA

The addition of both creatinine and propofol to the electrolyte caused a negative step change in the capacitance of the electrode as seen in Figure 6.10 and Figure 6.11. The magnitudes of these decreases in capacitance were proportional to the resulting concentrations of analytes in the test solutions. With the addition of polymer, both NIP and MIP onto the NPEDMA surface, the overall change in capacitive response decreased.

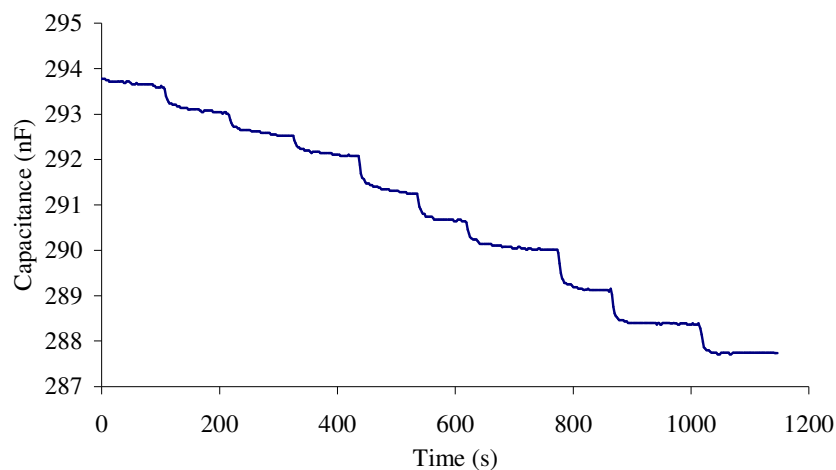


Figure 6.10 – Capacitive step response of a NIP electrode, polymerised for 10 minutes at a distance of 3 cm to additions of creatinine (3 x 200 μL , 3 x 500 μL and 3 x 1000 μL). The resulting calibration curve is shown in Figure 6.12.

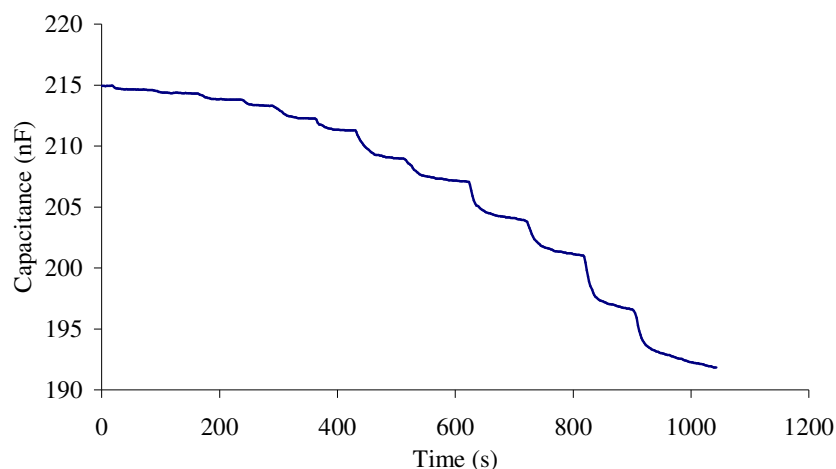


Figure 6.11 – Capacitive step response of a MIP electrode, polymerised for 10 minutes at a distance of 1 cm to additions of propofol (3 x 200 μL , 3 x 500 μL and 3 x 1000 μL). The resulting calibration curve is shown in Figure 6.13.

Comparing the NIP and MIP response (Figure 6.12 and Figure 6.13), the MIP produced a distinctively larger change in capacitance than the NIP for both the creatinine and propofol electrodes. The creatinine-imprinted polymers were also tested against the interfering compound creatine, where both MIP and NIP had similar responses.

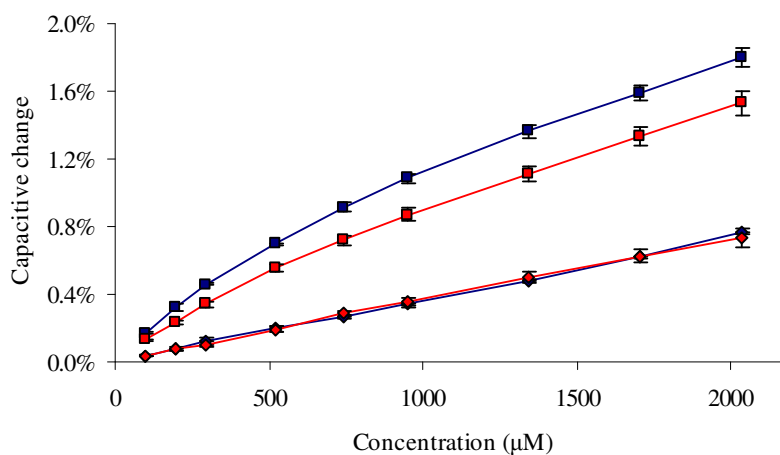


Figure 6.12 – Calibration curves of capacitive NIP (red) and MIP (blue) electrodes in creatinine (square) and creatine (diamond). The NIP and MIP electrodes were polymerised for 10 minutes at a distance of 3 cm.

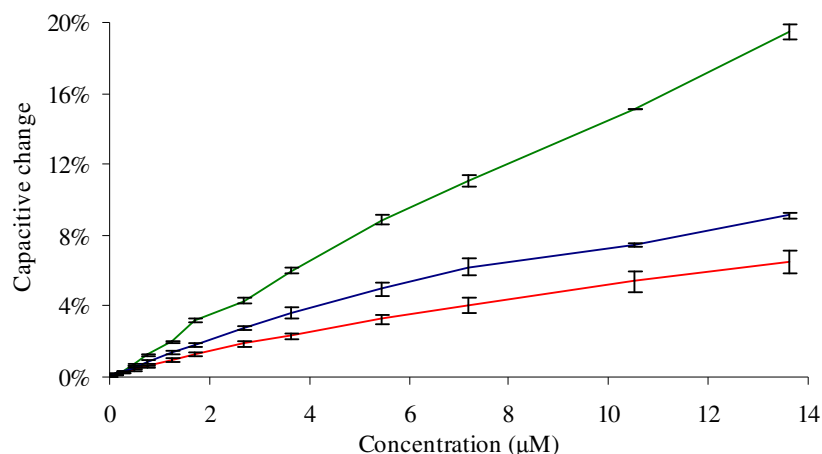


Figure 6.13 – Calibration curves of capacitive NPEDMA (green), NIP (red) and MIP (blue) electrodes. The NIP and MIP electrodes were polymerised for 10 minutes at a distance of 1 cm.

6.4.3 Discussion on the impedance detection of creatinine and propofol

The difference between the MIP and NIP coatings for the detection of creatinine and propofol in the impedance monitoring suggests that the MIP has a larger conformational and/or dielectric change induced by the interaction with the template. This could be due to the greater selectivity of the MIP coating. This hypothesis is also supported by the similarity in response to additions of creatinine by the creatinine MIP and NIP.

The NPEDMA coating gives a larger response, nearly three times that of the MIP. This suggests that the NPEDMA coating interacts with propofol; however, there was no reason for this interaction to have any specificity. Thus, any phenol compound or protein may readily interact with the NPEDMA surface.

6.4.4 Conclusion on the impedance detection of creatinine and propofol

The additions of creatinine and propofol were detected by the impedance monitoring system and there was a distinct difference between the NIP and MIP functionalised electrodes for both of the analytes. This was in accordance with the proposed model of impedance monitoring in Section 5.4.4.1. This approach shows great promise for the detection method for propofol, although it was lacking in sensitivity possible due to current leakage.

6.5 The electrochemical detection of propofol

The following section investigates the Faradic detection of propofol with the aim of attaining some optimised conditions for its amperometric detection.

6.5.1 Methodology for detection of propofol

All consumables were supplied by Sigma-Aldrich unless stated otherwise.

6.5.1.1 Materials

Detection of propofol with bare and NPEDMA coated electrodes was performed in solutions containing 50% acetonitrile or 50% methanol and 50% PBS or 50% of 55 mM HClO₄ in deionised water. The NPEDMA coatings were immobilised using the procedures described in Section 6.3.1.1. The concentration of propofol varied from 0 to 5 mM.

For the fouling investigation, cyclic voltammetry was performed in 1 mM propofol in 55 mM HClO₄ in deionised water or PBS (pH 7.5), containing 10% - 50% of acetonitrile.

The square wave voltammetry was performed in 10 mM KFe(CN)₆ in PBS. Finally, the investigation using square wave voltammetry into the optimal oxidation potential was performed with 1 mM propofol in PBS (pH 7.5) with 10% acetonitrile.

6.5.1.2 Electrochemistry

All of the electrochemical investigations were performed with a three-electrode cell with a gold working electrode (BASi, UK), a platinum wire counter electrode and a Ag/AgCl reference electrode (BASi, UK) on a microAutoLabII (Eco Chemie, Netherlands) potentiostat. The working electrode was cleaned using an aluminium slurry and rinsed in deionised water before each experiment, unless stated otherwise.

6.5.1.2.1 Cyclic voltammetry

The cyclic voltammetry for the detection of propofol and investigations into electrode fouling were performed using the same procedure. This procedure cycled between 0 V and 1.2 V at a rate of 0.5 Vs⁻¹ for 15 cycles.

6.5.1.2.2 Square wave voltammetry

The settings for the square wave voltammetry investigations into the propofol concentration dependence of the sensor signal and the electrode fouling was to scan between 0 V and 1.2 V with an amplitude of 50 mV and a frequency of 100 Hz (approximately 0.5 Vs^{-1}).

6.5.2 Results of the investigation into the detection of propofol

6.5.2.1 Electrochemical detection of propofol and optimisation of the detection conditions

6.5.2.1.1 Detection of propofol on bare gold electrode

The peak response of propofol was investigated using cyclic voltammetry, an example of which can be seen in Figure 6.14. By comparing the voltammograms in the presence of propofol (Figure 6.14, blue lines) to the voltammogram of the supporting electrolyte (Figure 6.14, red line) a definite peak, at 966 mV, can be seen when 5 mM of propofol present. There was also a reduction peak in the voltammogram of PBS at 450 mV, which was lowered in the presence of propofol.

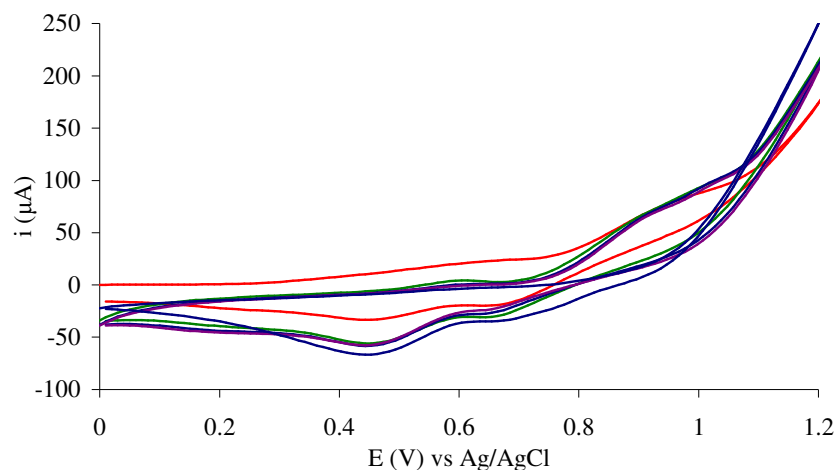


Figure 6.14 – Cyclic voltammogram performed in 50% PBS (pH 7.5) and 50% methanol (blue) and with 5 mM propofol, scans 1 (red), 5 (green), 10 (blue) and 15 (purple).

The oxidation peak potential (Figure 6.15) and current (Figure 6.16) were compared for various electrolytes with a propofol concentration of 5 mM. In all electrolytes tested a

distinct oxidation peak can be seen. When the electrolyte contained methanol, the potential increased from the first to the fifteenth scan. Acetonitrile, on other hand, decreased the potential. The peak oxidation currents for the electrolytes tested were around 60 nA with the highest currents achieved in an electrolyte containing acetonitrile and in PBS (pH of 7.5).

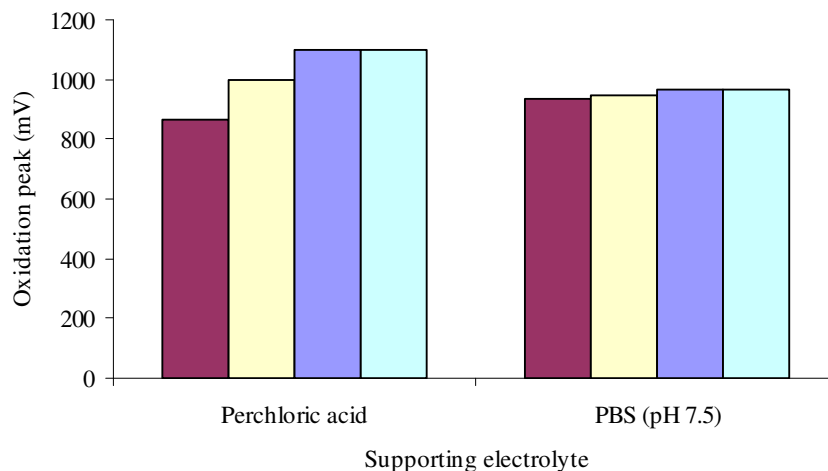


Figure 6.15 – Chart showing the peak oxidation potential of propofol (5 mM) with background subtraction. The potential from the first (red and blue) and fifteen scan (yellow and green) is shown for different electrolytic conditions (HClO_4 or PBS) containing 50% methanol (red and yellow) or 50% acetonitrile (blue and green).

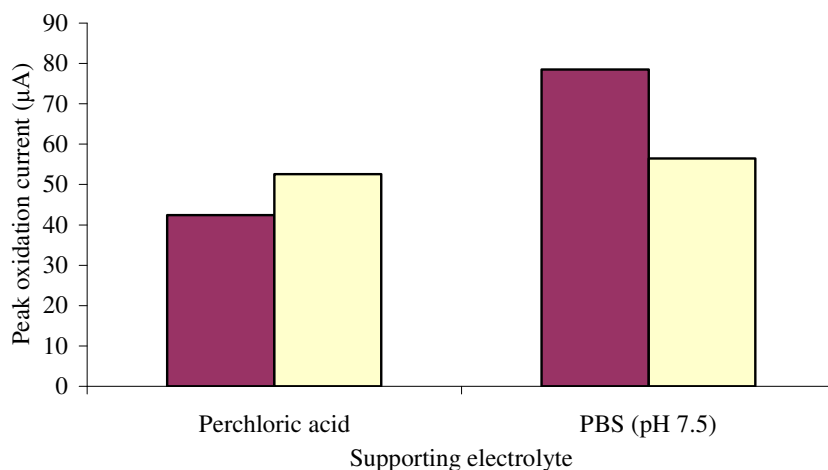


Figure 6.16 – Chart showing the oxidation current of propofol (5 mM) at the peak oxidation current with background subtraction. The current from the first scan is shown for different electrolytic conditions (HClO_4 or PBS) containing either 50% methanol (yellow) or 50% acetonitrile (red).

6.5.2.1.2 Concentration dependence of the propofol oxidation current

To verify that the oxidation peaks previously seen in the presence of propofol were caused by propofol, their concentration dependence was investigated using square wave voltammetry (SWV). As the concentration of propofol was increased, the current response of the oxidation peak also increased for propofol dissolved in 50% acetonitrile with either PBS (Figure 6.17) or HClO₄ (Figure 6.18). For the electrolyte containing HClO₄ there was a decreasing oxidation peak with increasing propofol concentration at 400 mV.

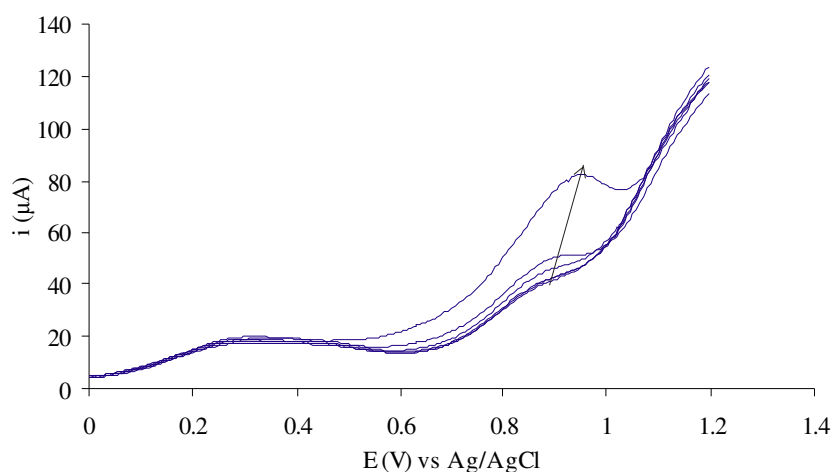


Figure 6.17 – Square wave voltammetry of propofol in 50% ACN and 50% PBS (pH 7.5). Arrow indicates increasing concentrations of propofol (0, 50, 100, 500, 1000, 5000 μM).

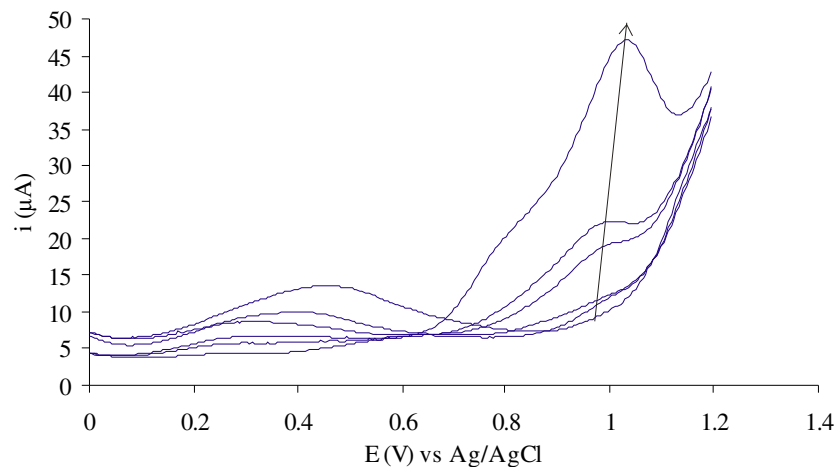


Figure 6.18 – Square wave voltammetry of propofol in 50% ACN and 50% of 55 mM HClO₄ in deionised water. Arrows indicates increasing concentrations of propofol (0, 50, 100, 500, 1000, 5000 µM).

A calibration plot of the responses shown in Figure 6.17 and Figure 6.18 is presented in Figure 6.19. This illustrates that the changes in magnitude of the two plots in Figure 6.19 is caused by the difference in the background current as the trend in the responses is similar for both plots.

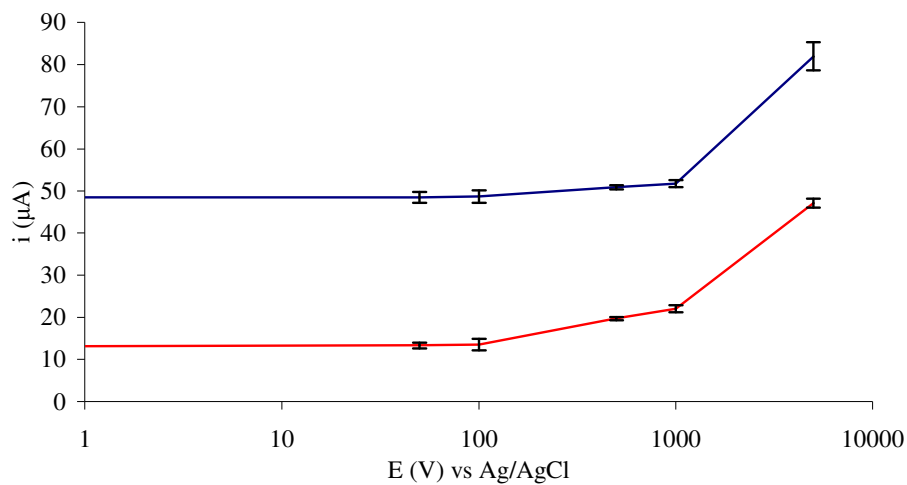


Figure 6.19 – Calibration plot of peak response from SWV of propofol in PBS (blue) at pH 7.5 and HClO₄ (red) on bare gold electrodes.

6.5.2.1.3 Fouling of electrodes by poly(propofol)

It is well known that phenols can be electropolymerised to form poly(phenols). As propofol is a phenol derivative it is assumed that during its oxidation it may polymerise and foul the electrode surface. To investigate this possibility SWV was performed in 10 mM $\text{KFe}(\text{CN})_6$ before and after 15 cyclic scans using gold electrodes in a 1 mM propofol solution with varying supporting electrolytes.

The trend of the response from both the HClO_4 (Figure 6.20) and PBS (Figure 6.21) electrolytes was similar. After the oxidation of propofol, the peak responses from the SWV in $\text{KFe}(\text{CN})_6$ decreased. Upon an increase in the concentration of acetonitrile this reduction in the peak current diminished. The oxidation potential for propofol in the HClO_4 electrolyte drifted to higher values with lower acetonitrile concentrations.

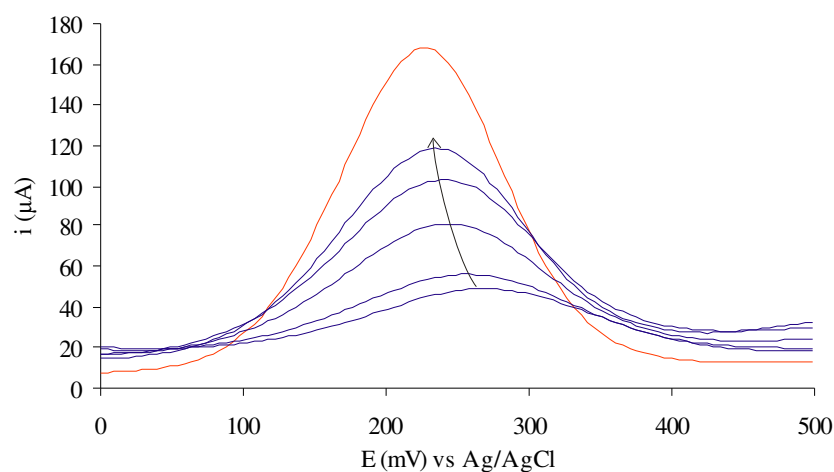


Figure 6.20 – Square wave voltammetry of gold electrode in 10 mM $\text{KFe}(\text{CN})_6$ before (red) and after the oxidation of 1 mM propofol by cyclic voltammetry in 55 mM HClO_4 with varying amounts of acetonitrile (blue). The arrow indicates increasing concentrations of acetonitrile from 10 to 50 %.

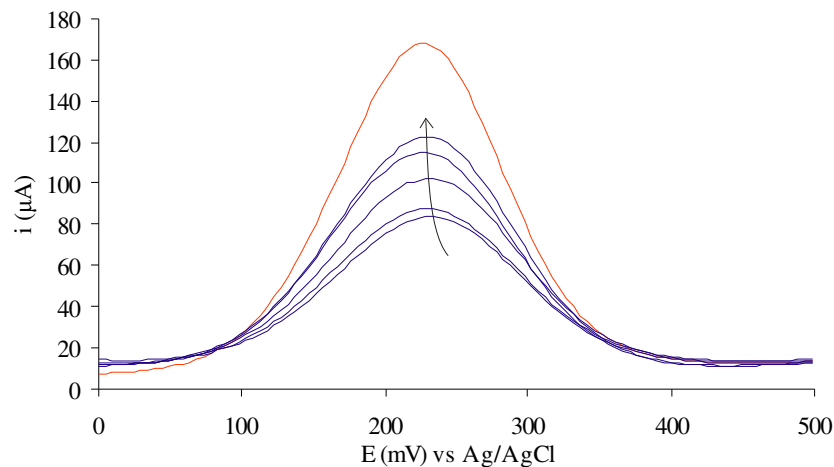


Figure 6.21 – Square wave voltammetry of gold electrode in 10 mM $\text{KFe}(\text{CN})_6$ before (red) and after the oxidation of 1 mM propofol by cyclic voltammetry in PBS (pH 7.5) with varying amounts of acetonitrile (blue). The arrow indicates increasing concentrations of acetonitrile from 10 to 50 %.

During the oxidation of propofol, the variation in acetonitrile concentrations also had other effects on the peak response. Firstly, for the first scan of the cyclic voltammetry (Figure 6.22), the peak potential for the electrolytes with acetonitrile concentrations between 10% to 30% was at approximately 840 mV, while for higher acetonitrile concentrations it was about 977 mV. Secondly, the reduction peak was considerably greater, approximately 36-52 nA, for the lower concentrations of acetonitrile (10% to 30%) as opposed to the 5 nA peak observed for the higher concentrations (Figure 6.23).

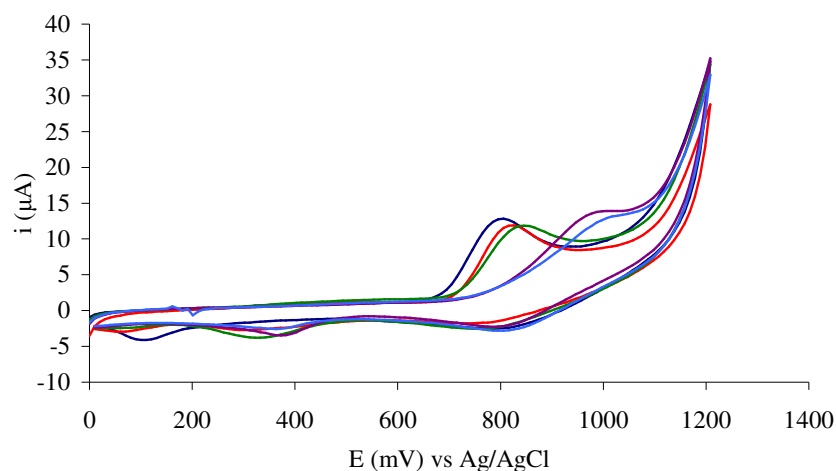


Figure 6.22 – Cyclic voltammetry (scan no. 1 of 15) of 1 mM propofol in 55 mM HClO_4 with 10% (blue), 20% (red), 30% (green), 40% (purple) and 50% (light blue) acetonitrile.

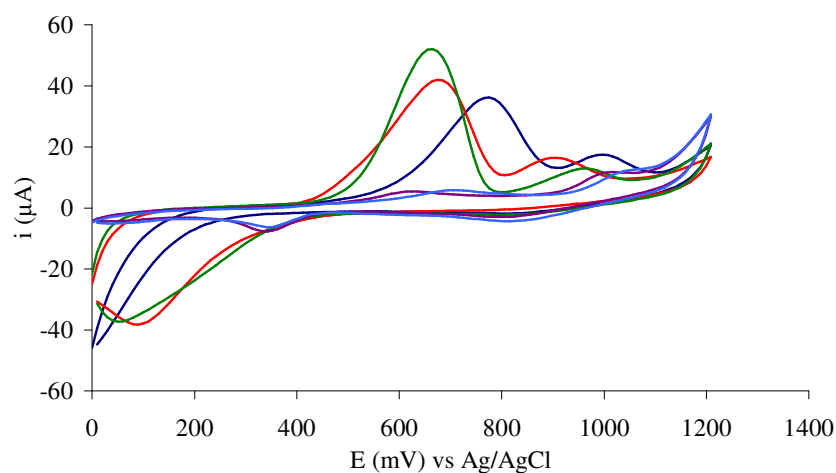


Figure 6.23 – Cyclic voltammetry (scan no. 15) of 1 mM propofol in 55 mM HClO_4 with 10% (blue), 20% (red), 30% (green), 40% (purple) and 50% (light blue) acetonitrile.

6.5.2.2 Detection of propofol on NPEDMA coated electrodes

As the electrodes are coated with the conductive NPEDMA anchor, the electrochemical reactions between propofol and the new electrode surface may have altered. To see if this is the case the detection of propofol was repeated on NPEDMA coated electrodes.

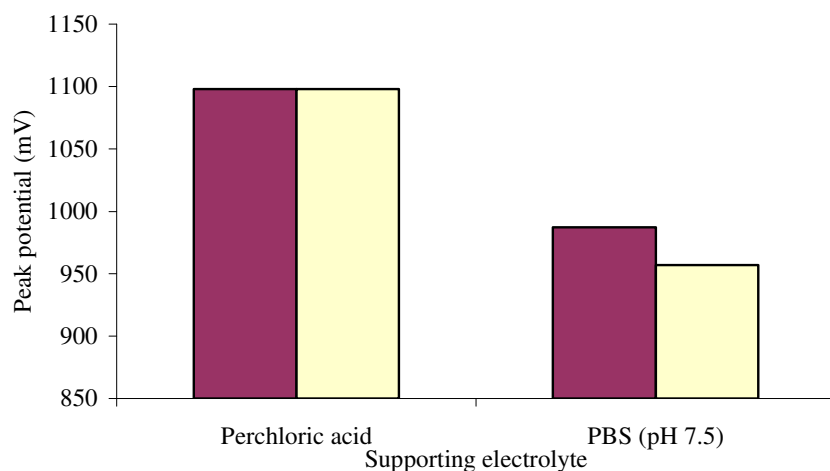


Figure 6.24 – Chart showing the peak oxidation potential of propofol (5 mM) with background subtraction. The potential from the first (red) and last scan (yellow) is shown for different electrolytic conditions (HClO_4 or PBS) containing 50% acetonitrile.

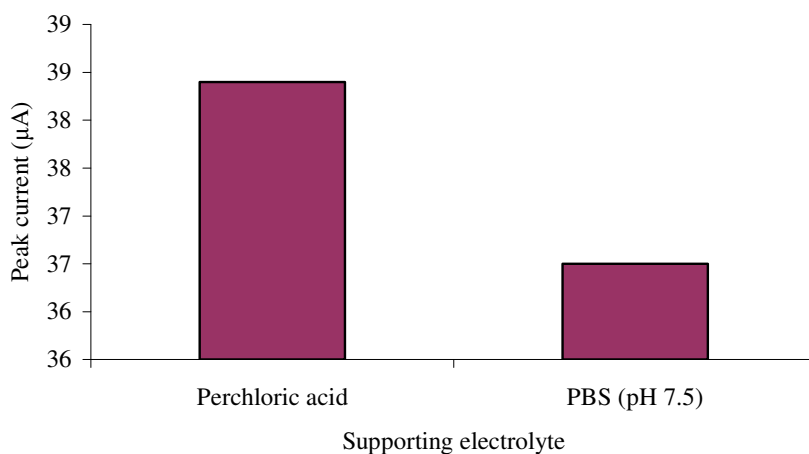


Figure 6.25 – Chart showing the oxidation current of propofol (5 mM) at the peak oxidation current with background subtraction of a NPEDMA coated electrode. The peak current from the first scan is shown for different electrolytic conditions (HClO_4 or PBS) containing 50% acetonitrile.

The results from the detection of propofol on NPEDMA coated electrodes showed similar trends to the gold electrodes (Figure 6.24 and Figure 6.25). The peak potential for the coated electrodes was slightly higher at about 1 V and the corresponding current had decreased to an average of 40 nA as compared to non-modified gold electrodes.

6.5.2.3 Detection of propofol in optimal conditions

From the aforementioned investigations an optimal electrolyte composition was chosen; which consisted of PBS (pH 7.5) with 10% acetonitrile because when methanol was used there was no distinguished oxidation peak. The following work was aimed at optimising the oxidation potential for measuring propofol. This was achieved by comparing square wave voltammograms in the optimal electrolyte with and without propofol.

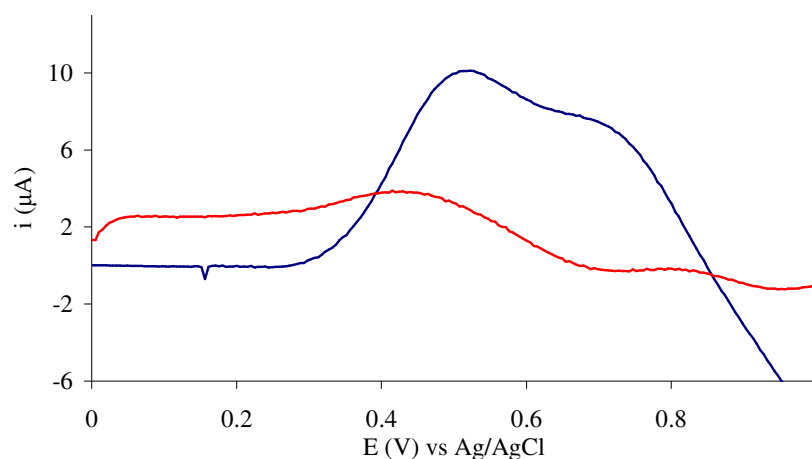


Figure 6.26 – Difference in currents between square wave voltammograms of bare gold electrode (blue) and NPEDMA coated electrode (red) with and without 1 mM propofol in PBS (PH 7.5) with 10% acetonitrile.

Using a bare gold electrode (Figure 6.26) peak oxidation of propofol occurs at 522 mV. For the NPEDAM coated electrode the current response to propofol was greater than the background current, although there are no well defined peaks.

6.5.3 Discussion of the electrochemical detection of propofol

The addition of propofol to the test solution resulted the appearance of in oxidation and reduction peaks (Figure 6.27) at potential values which are consistent with the literature (Pissinis and Marioli, 2007). Propofol undergoes an ECE reaction where the redox couple was only present after the first oxidation at 1 V. It was proposed that this couple cannot be seen when PBS was used as the electrolyte because of its high background Faradic current.

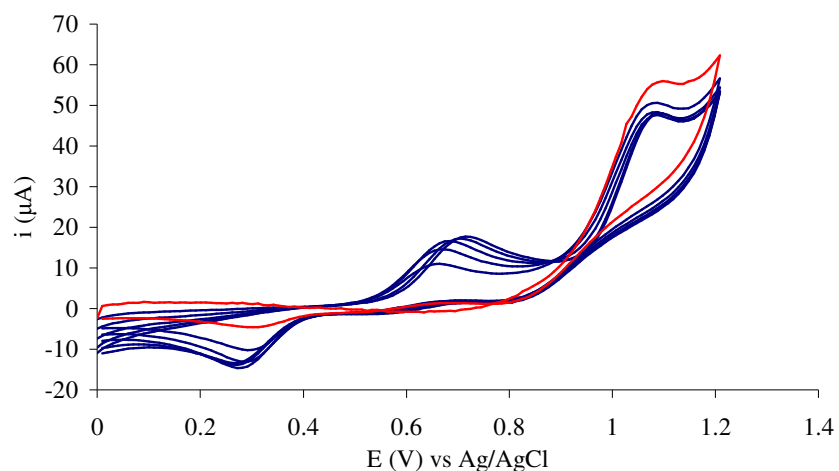


Figure 6.27 – Cyclic voltammetry of 5 mM propofol in 50% acetonitrile and 50% deionised water with 25 mM HClO₄. The first scan is shown in red.

The potential of the propofol oxidation peak was slightly greater than the potentials quoted in the literature (Pissinis and Marioli, 2007, Dowrie et al., 1996), but this variation can be expected as most reported electrochemical investigations regarding propofol have been conducted on graphite electrodes.

The study on the concentration dependence of the propofol oxidation current suggests that the peak response seen in the cyclic voltammetry was due to the presence of propofol and that the difference in current between the HClO₄ and PBS (pH 7.5) electrolyte was due to the difference in the background Faradic currents.

As propofol oxidises, like other phenols, it polymerises to poly(propofol). This polymer can precipitate at the electrode and physically adsorb to the surface. It is suspected that this adsorbed poly(propofol) causes the fouling. The decrease in the peak current from the bare electrode to those electrodes which have oxidised propofol indicated a decrease in electron transfer and demonstrates that fouling has occurred. In addition, the cathodic shift in the peak potential shows a possible decrease in the diffusion flux which can also be related to electrode fouling. Both of these effects are visible in the cyclic voltammograms of propofol and in the SWV in KFe(CN)₆.

As the acetonitrile concentration increases the poly(propofol) will be less inclined to precipitate, hence less fouling will occur. This is a possible explanation for the decrease in fouling observed with increasing acetonitrile concentrations. At low acetonitrile

concentrations there was an increase in the oxidation and reduction peaks associated with propofol dimers. As suggested above, this increase could be explained by the decrease in the solubility of poly(propofol) due to the lower acetonitrile concentrations. Hence, there was a higher concentration of the dimer on the electrode surface and this concentration of dimer increased as more propofol was oxidised.

For a solution with 50% acetonitrile the NPEDMA coated electrodes behaved similar to the bare gold electrodes. However, in methanol there was no distinguished oxidation peak. It is known that methanol will oxidise at relatively low potentials. This fact has been previously used to reduce fouling of propofol on platinum electrodes, via the reaction of the oxidised-methanol and oxidised-phenol, which produces compounds that do not readily adsorb onto the electrode surface (Andreescu et al., 2003). In our case, the oxidised methanol could have reacted with the NPEDMA layer or the resulting compounds from the oxidised components could prevent the detection of propofol.

The increased current at 522 mV was possibly due to the oxidation of propofol. It was previously seen that decreasing the acetonitrile concentration causes the oxidation peak to become more negative.

6.5.4 Conclusion on the electrochemical detection of propofol

Propofol has been successfully oxidised at a gold electrode, and a propofol concentration dependent current for this oxidation has been observed. The oxidation of propofol does cause fouling on the electrode surface and the amount of fouling seems to be dependent on the organic solvent (acetonitrile) concentration within the electrolyte. The addition of a NPEDMA coating it does changes the oxidation potential.

The optimal conditions for detecting propofol on a NPEDMA coated electrode were selected as follows; PBS (pH 7.5) with 10% acetonitrile and an oxidation potential at 522 mV.

6.6 Investigation into the amperometric detection of propofol with a MIP covered electrode

The following section will consider the amperometric detection of propofol using the optimal conditions derived in the study of its electrochemistry.

6.6.1 Methodology for the amperometric detection of propofol

All consumables were supplied by Sigma-Aldrich unless stated otherwise.

6.6.1.1 Polymerising electrodes

The various electrode coatings were prepared using the procedure described in Section 6.3.1.

6.6.1.2 Amperometry

In both experimental setups (see Section 6.3.1.2.1 and 6.3.1.2.2) amperometry was conducted using a three-electrode cell with a gold working electrode (BASi, UK), a platinum wire counter electrode and a Ag/AgCl reference electrode (BASi, UK) on a microAutoLabII (Eco Chemie, Netherlands) at a fixed potential of 522 mV.

6.6.1.2.1 Initial study

The initial amperometric investigation was conducted using in a beaker with a peristaltic pump to circulate and agitate the test solution pumped from a reservoir. Various volumes of propofol were injected into the reservoir and propofol was oxidised at the electrode surface.

6.6.1.2.2 Flow cell

The amperometric detection of propofol was achieved by injecting specific concentrations of propofol into a custom flow cell system. The background electrolyte, PBS (pH 7.5) with 10% acetonitrile, was pumped through the cell using a peristaltic pump (Miniplus3, Gilson, USA) and the propofol was injected using a Valve V-7 (GE Healthcare) injector with a 200 μ L sample loop. See Figure 6.28.

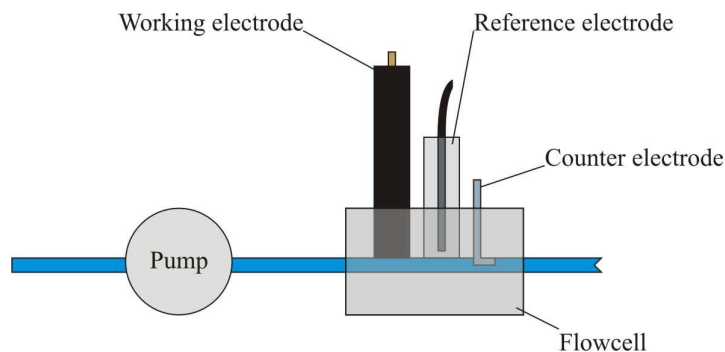


Figure 6.28 – Schematic of experimental setup using a custom flow cell for the amperometric detection of propofol.

6.6.2 Results from the detection of propofol

6.6.2.1 Initial amperometric investigation

The amperometric response of bare (Figure 6.29), immobilised NPEDMA (Figure 6.30) and grafted iniferter (not shown) electrodes show a response to $1\ \mu\text{M}$ additions of propofol. The magnitude of the response increases with increasing concentrations, however these increases are inconsistent as the response constantly decreases with additions of propofol, which was probably an effect of propofol's fouling. The addition of the NPEDMA coating reduces the response by ten fold, thus the noise of system starts to limit the performance of the sensor.

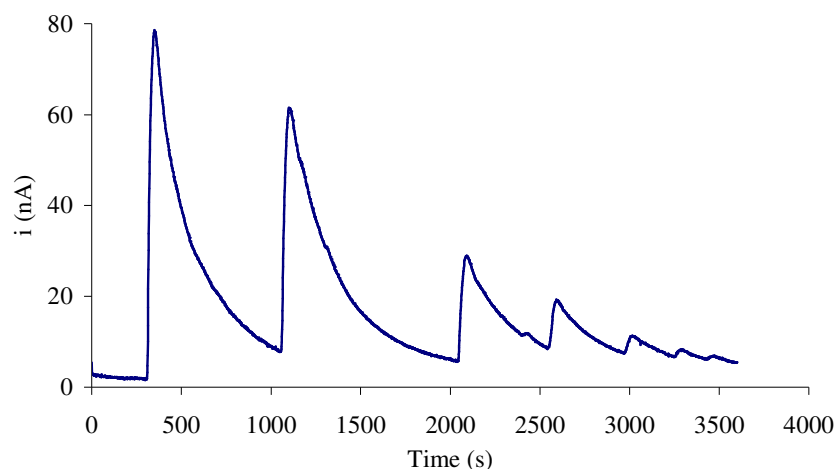


Figure 6.29 – Amperometric response the bare gold electrodes at 522 mV to propofol. Additions of 47.62, 43.29, 20.20, 9.77, 3.85, 1.91, 0.95 μM propofol were made.

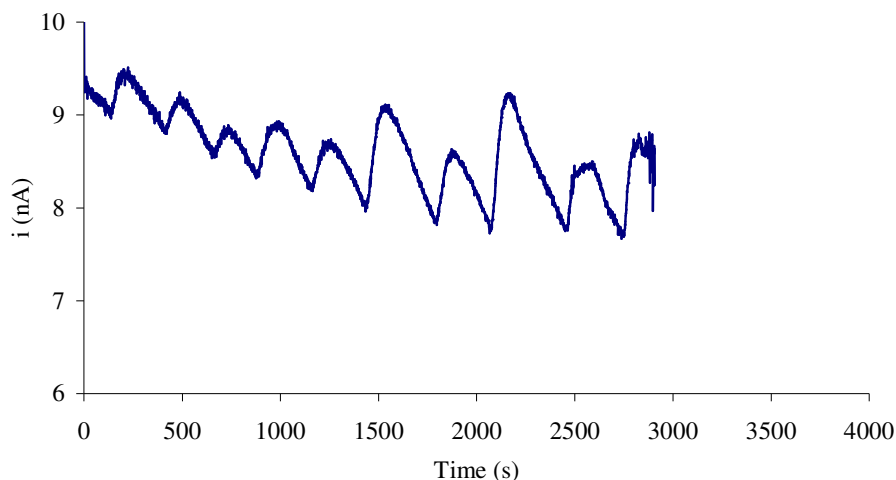


Figure 6.30 – Amperometric response of NPEDMA coated electrodes at 522 mV to propofol. Additions of 1.25, 1.25, 2.48, 2.48, 4.90, 4.85, 11.93, 11.64, 22.46, 21.44, 40.06 μM propofol were made.

A fixed polymerisation distance of 1 cm (Figure 6.5) and a polymerisation time of 30 minutes resulted in electrodes with a very small current response; this was also seen for the amperometric response to propofol. However, with decreasing polymerisation times the current response increases. This was also seen in the amperometric response of these electrodes to propofol (Figure 6.31).

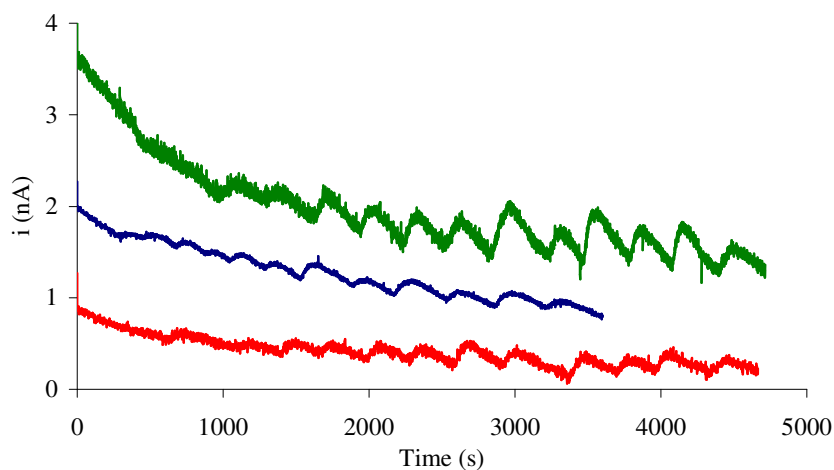


Figure 6.31 – Amperometric response of MIP coated electrodes to various additions of propofol with resulting concentrations of 1.25, 1.25, 2.48, 2.48, 4.90, 4.85, 11.93, 11.64, 22.46, 21.44, 40.06, 36.70 μM . The MIP layers were polymerised at a distance of 1 cm for 10 (blue), 5 (red) and 3 (green) minutes.

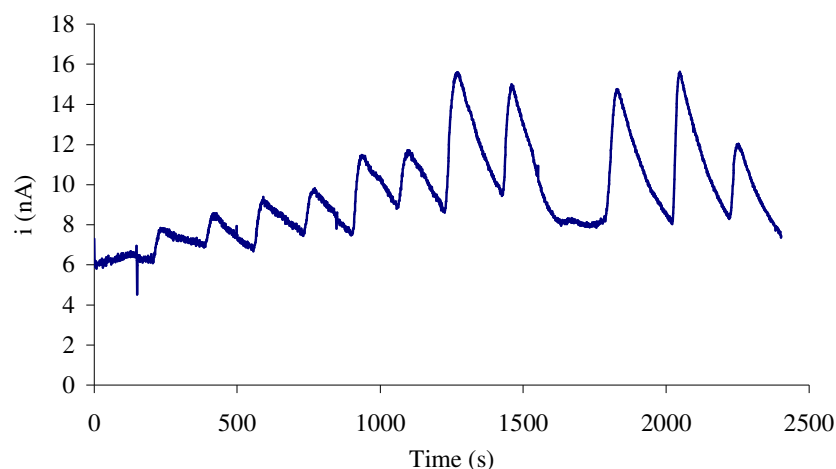


Figure 6.32 – Amperometric response of MIP coated electrodes, polymerised for 1 minute at a distance of 1 cm, to various additions of propofol resulting in a concentration of 1.25, 1.25, 2.48, 2.48, 4.90, 4.85, 11.93, 11.64, 22.46, 21.44, 40.06, 36.70 μM .

Although a response to 1.25 μM of propofol can be seen (Figure 6.31), the addition of the MIP on top of the NPEDMA further reduces the magnitude of the response to propofol. Therefore, further variations in the polymerisation distance (Figure 6.8) and polymerisation time (Figure 6.9) were investigated. From the amperometric response to propofol observed for the different electrodes, an optimum of the polymerisation condition was found to be a polymerisation distance of 3 cm and a polymerisation time of 1 minute (Figure 6.32).

6.6.2.2 Amperometry with a flow cell

6.6.2.2.1 Selective detection of propofol

The responses of the polymer coated electrodes to injections of propofol are shown as calibration curves (Figure 6.33) for polymerisation times from 1 to 3 minutes. This illustrates that the NIP electrode has a similar linear response which was practically independent of the polymerisation time. However, the MIP electrodes show a decrease in peak current with increasing polymerisation times.

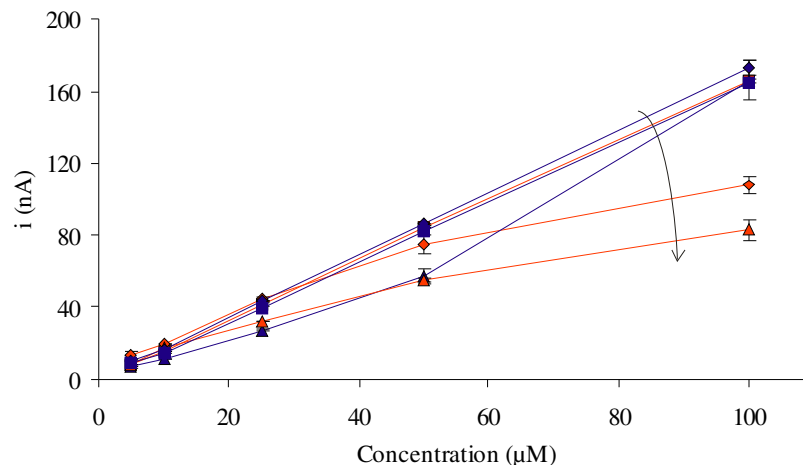


Figure 6.33 – Calibration plot of amperometric response of NIP (blue) and MIP (red) electrodes to injections of propofol in PBS (pH 7.5) with 10% acetonitrile. The polymers layer were prepared at a distance of 3 cm for 1 (square), 2 (diamond) and 3 (triangle) minutes. The arrow indicates increasing polymerisation times.

The decrease in response with increasing polymerisation time seems to be an effect of the electrode exposure to propofol; for example at higher concentrations each injection of propofol has a smaller response than the previous injection. This can be clearly seen in Figure 6.34 for a 3 minute polymerised MIP as the peak current for the last four injections of 100 μM of propofol decreases from injection to injection. This was particularly obvious when compared to the very reproducible response of the 1 minute polymerised MIP seen in Figure 6.35.

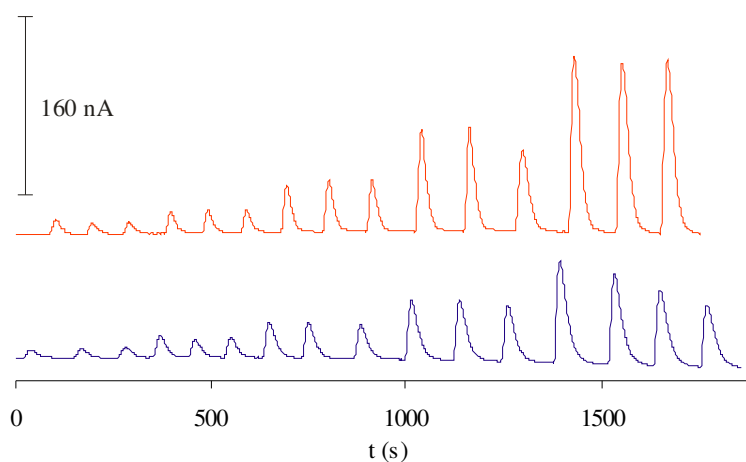


Figure 6.34 – Amperometric response of MIP (blue) and NIP (red) electrodes polymerised for 3 minutes to injections of propofol (5 μM , 10 μM , 25 μM , 50 μM and 100 μM).

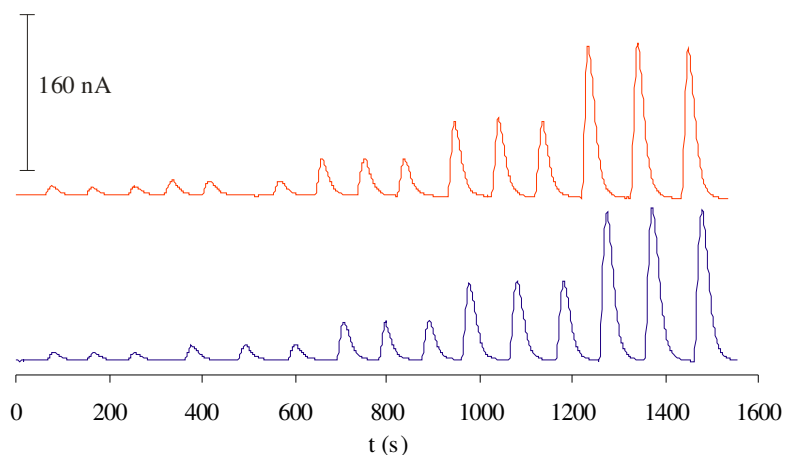


Figure 6.35 – Amperometric response of MIP (blue) and NIP (red) electrodes polymerised for 1 minute to injections of propofol (5 μM , 10 μM , 25 μM , 50 μM and 100 μM).

6.6.2.2.2 Reduction in flow rate

The response of the electrode will be dependent on the diffusion of propofol through the polymer to the electrode surface. To analyse the impact of the diffusion process the flow rate was decreased to $7 \mu\text{Ls}^{-1}$ from $26 \mu\text{Ls}^{-1}$. The following calibration plots result from these investigations at this slower flow rate.

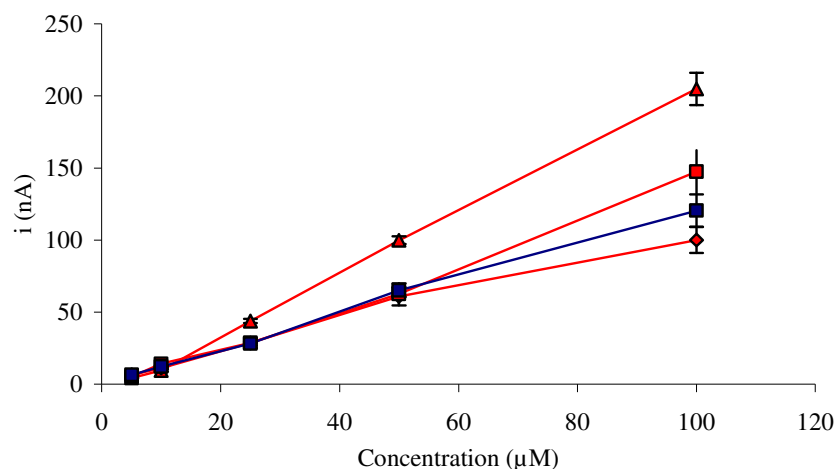


Figure 6.36 – Calibration plot of amperometric response to NIP coated electrodes with a flow rate of $7 \mu\text{Ls}^{-1}$. Polymerised for 1 minute (blue) and 3 minutes (red) at a distance of 3 cm (square), 5 cm (diamond) and 10 cm (triangle).

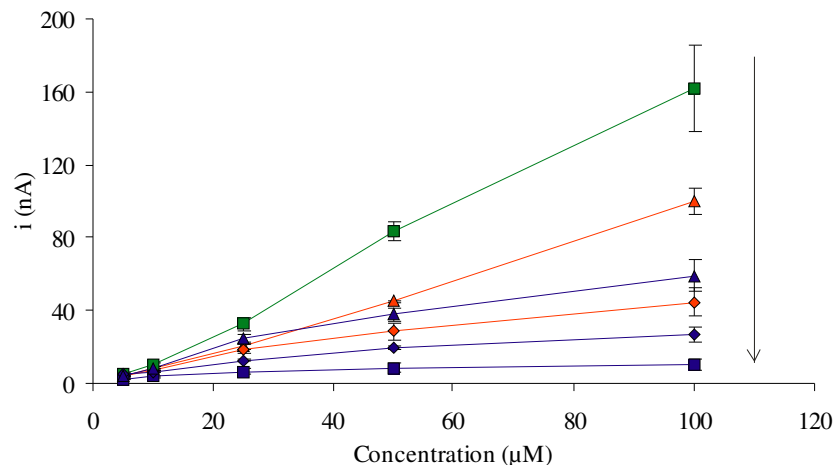


Figure 6.37 – Calibration plot of amperometric response to MIP coated electrodes with a flow rate of $7 \mu\text{Ls}^{-1}$. Polymerised for 1 minute (green), 2 minutes (red) and 3 minutes (blue) at a distance of 3 cm (square), 5 cm (diamond) and 10 cm (triangle). The arrow shows increasing UV exposure.

For all the NIP electrodes, including those tested at the faster flow rate, the amperometric response to injections of propofol was very similar (Figure 6.33 and Figure 6.36). However, the amperometric response of the MIP electrodes was dependent on polymerisation time and distance (Figure 6.37). With decreasing polymerisation time and increasing polymerisation distance, the magnitude for the peak current tends towards the NIP response, even at a slower flow rate.

6.6.2.2.3 Interfering substances

It was observed in the previous results that with the right polymerisation conditions, there was a large difference between the responses from the MIP and the NIP electrodes. To see if the MIP coated electrodes have any selectivity, and to assess if other electrochemical interfering compounds will be rejected, the amperometric response to ascorbic acid was investigated.

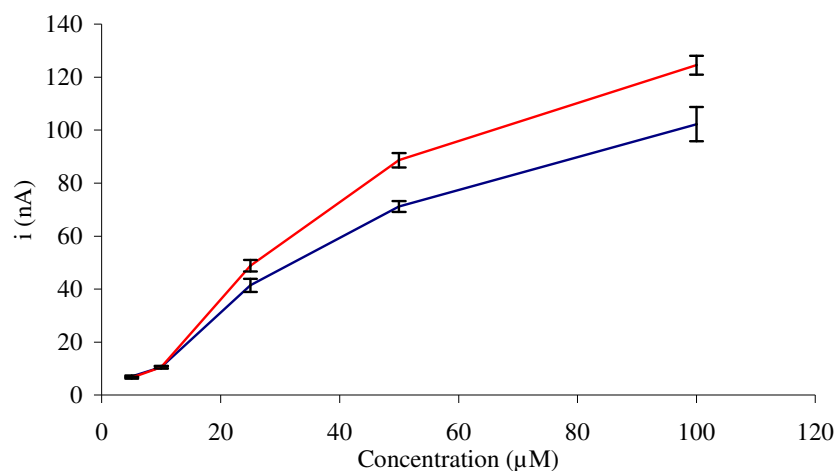


Figure 6.38 – Calibration plot of amperometric response of ascorbic acid injections at $7 \mu\text{Ls}^{-1}$ on MIP (blue) and NIP (red) electrodes polymerised for 1 minute at a distance of 3 cm.

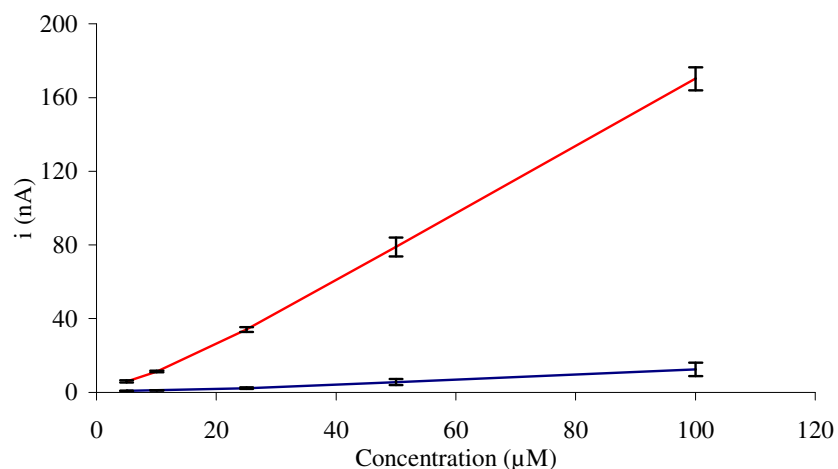


Figure 6.39 – Calibration plot of amperometric response of ascorbic acid injections at $7 \mu\text{Ls}^{-1}$ on MIP (blue) and NIP (red) electrodes polymerised for 3 minutes at a distance of 3 cm.

Upon injections of ascorbic acid over the MIP and NIP polymer electrodes, both polymerised for 1 minute (Figure 6.38), there was little difference between the peak current responses. However, the electrodes polymerised for 3 minutes responded to ascorbic acid very differently than the electrodes polymerised for 1 minute with the MIP response about 10 times smaller than the NIP response.

6.6.3 Discussion of the selective detection of propofol

6.6.3.1 Initial amperometric investigation

The amperometric response of the bare and immobilised NPEDMA and iniferter electrodes to 1 μM of propofol demonstrates that propofol can be detected at 522 mV in PBS (pH 7.5) with 10% acetonitrile. However, these additional coatings when compared to a bare gold electrode decrease the magnitude of the current by approximately ten fold.

From the 30 minute MIP polymerisation there was no response. As the UV exposure was lowered either by decreasing polymerisation time or by increasing the polymerisation distance, the sensor response increased. This suggests that increased UV exposure leads to a lower response.

The amount of UV can be directly related to the amount of polymer formed. Hence, less polymer ensures a greater response. This was expected as the polymer has no foreseeable conducting properties, thus it insulates the electrode surface.

The amperometric response did demonstrate the effects of fouling, as the sensor response to an injection of propofol was not consistent. This is less important for the final product where the electrodes are in a flow cell and not permanently exposed to propofol. Also, it should be noted that this also implies that the amperometric response was a step change as the concentration of propofol permanently increases.

6.6.3.2 Flow cell amperometry

The NIP electrodes, irrespective of the polymerisation time, showed a similar response. This implies increasing thickness of NIP polymer does not affect the diffusion of propofol to the surface of the electrode where it is oxidised. There was only a slight decrease in the baseline of the NIP electrode which could possibly be attributed to propofol fouling. However, the decrease in the MIP response was probably due to strong propofol binding onto the surface of polymer preventing more propofol reaching the electrode. Further washing was performed on the MIP electrodes exposed to propofol but no change was seen.

As there was little difference in response for the electrodes polymerised for 1 minute at different flow rates this suggests that the response was not diffusion controlled. However, a decrease in the MIP sensor response was seen when using the slower flow rate with the MIP electrodes polymerised for 3 minutes, which suggests that the response was diffusion related for the thicker polymer. It is supposed that the slower flow rate in this case gave more time for the propofol to diffuse through the MIP and strongly bind to the imprinted cavities. This in turn hinders further diffusion of propofol and reduces the amount of oxidation at the electrode surface, hence reducing the signal from the electrode. Another explanation could be that at slower flow rates the boundary layer between the fluid and the polymer is larger, therefore less propofol diffuses across the boundary layer.

Ascorbic acid is considered to be one of the main electrochemically interfering compounds in blood. Thus, an investigation into the response of the electrodes to injections of ascorbic allowed an assessment of the sensor's specificity. As the sensor responded to ascorbic acid injections in a similar manner as to propofol injections it can be concluded that ascorbic acid will interfere with the propofol detection using these electrodes.

As a consequence of the aforementioned results, the large variation in MIP response for the 3 minute polymerised electrode cannot be considered a sole property of an injection of propofol. This would imply that the presence of propofol during the 3 minute polymer coating significantly changes the conformation of the resulting polymer. As this change affects both ascorbic acid and propofol it was likely that the porosity of the polymer was lacking, so both compounds cannot diffuse to the electrodes surface. This could be due to propofol getting polymerised into the cross-linked matrix, thus resulting in a polymer coating with a higher density than the NIP.

6.6.4 Conclusion on detection of propofol

The magnitude of the amperometric response to propofol was related to the variations in the test solutions' concentration. However, increasing the polymer layer thickness on the electrode surface decreased the magnitude of the response to an extent where the noise of the system dominated the sensor response.

The use of a flow cell increased the sensitivity of propofol detection with the response to 5 μM concentrations being easily seen, thus it should be possible to detect lower concentrations using their approach.

The limited exposure of the electrode to propofol has decreased the fouling effects previously seen, although the long-term lifetime of such a device is still unclear.

The strong binding of propofol to the thicker MIP layers implies that for the longer term operation of such an amperometric system, a thin MIP layer is required or a washing procedure would be needed that can remove the bound propofol.

The polymerised electrodes respond to injections of ascorbic acid in a similar manner to injections of propofol. Hence, ascorbic acid will be an interferant to the detection of propofol.

6.7 Chapter conclusion

The goal of this chapter was to address two key issues, i) the lack of control over the polymerisation process and ii) the electrical insulation of the polymer anchor. The proposed solution to these issues was to introduce two new compounds, an iniferter to give controlled initiation of the polymerisation and NPEDMA to form a conductive poly(aniline-based) anchor.

The electropolymerisation and adsorption of NPEDMA proved to be a very repeatable process and the characterisation of this immobilised layer demonstrated that poly(NPEDMA) had a high conductivity. Further characterisation of the iniferter and polymer layers showed significant changes in the electrodes response, this confirming their immobilisation. The growth of the polymer from the iniferter, which was immobilised onto the NPEDMA layer, would be controlled by both the UV exposure time and the distance of UV source from the electrode surface.

Propofol detection on bare gold and on NPEDMA coated electrodes was possible. It was seen to undergo an ECE reaction and the poly(propofol) formed could adsorb onto and foul the electrode surface. However, this fouling was dependent on the acetonitrile concentration in the supporting electrolyte and was less apparent on the NPEDMA electrodes.

The initial investigations into the detection of propofol, both amperometric and impedance, proved successful. Using amperometry, there was a concentration dependent response, however, the noise from the experimental setup limited the detection. The impedance response demonstrated a clear concentration dependence and there was a significant difference between the NIP and MIP.

Using a custom-made flow cell improved the amperometric response of the polymer coated electrodes. This resulted in a reproducible response with a detection limit of less than 5 μM . By altering the polymerisation conditions, the MIP coated electrodes could be optimised. However, the MIP and NIP electrodes were also both found to respond to ascorbic acid. This suggests that the difference in peak currents is possibly due to polymer barrier properties.

Chapter 7 - General conclusion and further work

“The rule is perfect: in all matters of opinion our adversaries are insane.” Mark Twain (1835 - 1910)

7.1 General conclusion

The ability to improve the monitoring of clinical parameters within a critical care environment would assist healthcare professionals as well as improve patient outcomes. This thesis addressed this challenge by incorporating MIP-based technology with electrochemical transducers to selectively monitor the concentration of clinically relevant parameters. Three different target analytes were investigated, which were; i) metronidazole, a 5-nitroimidazole drug with antibiotic properties, ii) creatinine, which is used to evaluate muscle disorders and renal dysfunction, and iii) propofol, an anesthetic agent used worldwide in both medical and veterinary practices.

For each of these three analytes, a different imprinted polymer composition was used. For creatinine, the MIP composition was based on a previously developed protocol proposed by Delaney and co-workers (Panasyuk-Delaney et al., 2002), while for propofol and metronidazole MIPs were computationally designed at Cranfield University. All of the MIP tests demonstrated an increased binding capacity to their imprinted target when compared to the NIP.

The MIP for metronidazole was computationally designed using SybylTM (Tripos, US) and tested by SPE techniques with UV detection. The immobilisation of the MIP onto transducers' surfaces using UV initiation proved relatively inefficient and provided inconsistent results. However, by using thermal initiation the polymer could be successfully grafted to the surface. The detection of metronidazole was not as successful as other analytes, although a concentration dependent current could be seen, the required sensitivity was not reached. This lack of sensitivity was mainly due to the

large cathodic potential at which metronidazole reduces, which pushed the limits of the application for platinum transducers.

An investigation into the capacitive detection of creatinine was undertaken following the method described by Delaney (Delaney et al., 2007) and co-workers. The proposed procedure was simple with the pre-polymerisation complex formed in water, allowing this approach to be used as a universal method for producing sensing devices for therapeutic substances. Although precise reproduction of previously described results proved to be difficult due to lack of consistency and control over the grafting procedure, the developed sensors did possess the ability to detect creatinine. We managed to successfully demonstrate that MIP electrodes had a greater response to creatinine as compared to NIP coated electrodes and that the response to a compound with a similar structure, such as creatine, was greatly decreased.

In an attempt to improve the reproducibility of the published procedure, the electrode pre-treatment was modified to increase the density of the intermediate thiol layer. These alterations improved the insulating properties of thiol monolayer and also improved the reproducibility of the devices. Contrary to the proposed theory, these changes decreased the sensitivity of the detection. Taking these results into account, a model for capacitive electrodes with an anchored selective polymer was derived to explain this response.

Subsequently, based on the previous results, it was apparent that three key issues needed to be addressed in order to develop a high performance sensor: i) detection via Faradic currents and impedance is best served with a conductive polymer anchor, ii) the reproducibility and control of the grafted polymer needs to be improved to enhance reproducibility of the results, and iii) the analyte needs to be detectable within the potential window of the system for Faradic detection. In the following set of experiments we began to address these key issues. The first key issue was fulfilled using an innovative dual-polymerisable monomer (NPEDMA) designed and synthesised at Cranfield University. Using iniferters to initiate and control the polymerisation addressed the second issue. To address the third issue we changed the target compound to propofol, which can be easily detected at a relatively low potential.

The MIP for propofol was computationally designed and tested earlier at Cranfield University. In this work MIP was grafted in a controlled environment using an iniferter, which was anchored to a conductive NPEDMA layer. The successful detection of propofol, both capacitively and amperometrically was achieved with a MIP sensor. Using the NPEDMA-iniferter combination, capacitive detection of propofol and creatinine was demonstrated successfully.

The amperometric detection of propofol had a low detection limit ($< 5 \mu\text{M}$) and with the controlled polymerisation, the electrode responses were reproducible. Differences were observed between the MIP and NIP responses. However, the same differences were also seen for the interfering substance ascorbic acid, suggesting that the differences between the MIP and NIP are due to non-specific binding.

Following on from the results of this thesis, it is possible to conclude that a universal methodology for the production of MIP sensors will be difficult to achieve. Nonetheless, several key aspects for the construction of MIP sensors can, however, be proposed: firstly, the choice of detection method for a given analyte is intrinsically linked to the analyte and the detection system, and thus no matter how well a MIP functions, if the bound analyte is not detectable, the device will not function. Secondly, a low impedance path between the transducer and bound analyte is required for Faradic detection. Finally, in order to attain reproducible devices, control over the polymer grafting is essential.

7.2 Suggestions for further work

The proposed future work should be focused on improving understanding of the NPEDMA-iniferter anchor and on developing more effective capacitive and amperometric detection methodologies.

The development of the NPEDMA-iniferter-based anchor should be continued to ensure better control over the immobilisation of iniferter. It is expected that developments in Cranfield Health would produce different aniline derivative with a covalently attached iniferter. This will dramatically simplify the grafting procedure and also increase the density of surface radicals needed for initiation of polymerisation process.

Monitoring the concentration of an analyte using the capacitive scheme proved successful and a selective MIP was demonstrated. However, the sensitivity achieved with this technique was not within the required clinical range, and the electrodes were not tested in a flow cell, which is more characteristic for the final product. Therefore, to improve the sensitivity, an investigation into the optimal MIP and polymerisation conditions should be carried out.

The amperometric detection of propofol proved very successful with a good sensitivity and reproducibility, yet it lacked in selectivity. Therefore, further improvement of polymer composition, possibly adding PEG layers or other coatings impenetrable to ascorbic and uric acids would be necessary.

Reference

- ABDEL-HAMID, I., IVNITSKI, D., ATANASOV, P. & WILKINS, E. (1998) Fast Amperometric Assay for *E. coli* O157:H7 Using Partially Immersed Immuno-electrodes. *Electroanalysis*, 10, 758-763.
- ADAMS, E., ROELANTS, W., DE PAEPE, R., ROETS, E. & HOOGMARTENS, J. (1998) Analysis of gentamicin by liquid chromatography with pulsed electrochemical detection. *Journal of Pharmaceutical and Biomedical Analysis*, 18, 689-698.
- AL-GHAMDI, A. H., AL-SHADOKHY, M. A. & AL-WARTHAN, A. A. (2004) Electrochemical determination of Cephalothin antibiotic by adsorptive stripping voltammetric technique. *Journal of Pharmaceutical and Biomedical Analysis*, 35, 1001-1009.
- ALEKHA K. DASH, D. W. M., HAN HUAI-YAN, JOE CARNAZZO, JEFFREY R. STOUT, (2001) Evaluation of creatine transport using Caco-2 monolayers as an *in vitro* model for intestinal absorption. *Journal of Pharmaceutical Sciences*, 90, 1593-1598.
- ANDREA, P., MIROSLAV, S., SILVIA, S. & STANISLAV, M. (2001) A solid binding matrix/molecularly imprinted polymer-based sensor system for the determination of clenbuterol in bovine liver using differential-pulse voltammetry. *Sensors and Actuators, B: Chemical*, 76, 286-294.
- ANDREESCU, S., ANDREESCU, D. & SADIK, O. A. (2003) A new electrocatalytic mechanism for the oxidation of phenols at platinum electrodes. *Electrochemistry Communications*, 5, 681-688.
- BAJPAI, L., VARSHNEY, M., SEUBERT, C. N. & DENNIS, D. M. (2004) A new method for the quantitation of propofol in human plasma: efficient solid-phase extraction and liquid chromatography/APCI-triple quadrupole mass spectrometry detection. *Molecularly Imprinted Polymers in Separation Science*, 810, 291-296.
- BANKS, C. E. & COMPTON, R. G. (2006) New electrodes for old: From carbon nanotubes to edge plane pyrolytic graphite. *Analyst*, 131, 15-21.
- BARDHAN, K. D., BAYERDORFFER, E., VAN ZANTEN, S. J. O. V., LIND, T., MEGRAUD, F., DELCHIER, J. C., HELLBLUM, M., STUBBEROD, A., BURMAN, C. F., GROMARK, P.-O. & ZEIJLON, L. (2000) The HOMER Study: The Effect of Increasing the Dose of Metronidazole When Given with Omeprazole and Amoxicillin to Cure *Helicobacter pylori* Infection. *Helicobacter*, 5, 196-201.
- BARTLETT, P. N., GHONEIM, E., EL-HEFNAWY, G. & EL-HALLAG, I. (2005) Voltammetry and determination of metronidazole at a carbon fiber microdisk electrode. 66, 869.
- BATRA, D. & SHEA, K. J. (2003) Combinatorial methods in molecular imprinting. *Current Opinion in Chemical Biology*, 7, 434-442.

- BELTAGI, A. M. (2003) Determination of the antibiotic drug pefloxacin in bulk form, tablets and human serum using square wave cathodic adsorptive stripping voltammetry. *Journal of Pharmaceutical and Biomedical Analysis*, 31, 1079-1088.
- BENONI, G., CUZZOLIN, L., GILLI, E., SCHINELIA, M., MAZZI, G., BARTOLONI, A. & PASETTO, A. (1990) Pharmacokinetics of propofol: influence of fentanyl administration. *European Journal of Pharmacology*, 183, 1457-1458.
- BERBERICH, J. A., CHAN, A., BODEN, M. & RUSSELL, A. J. (2005) A stable three-enzyme creatinine biosensor. 3. Immobilization of creatinine amidohydrolase and sensor development. *Acta Biomaterialia*, 1, 193-199.
- BERGER, A. J., ITZKAN, I. & FELD, M. S. (1997) Feasibility of measuring blood glucose concentration by near-infrared Raman spectroscopy. *Spectrochimica Acta Part A: Molecular and Biomolecular Spectroscopy*, 53, 287-292.
- BOUBRIAK, O. A., SOLDATKIN, A. P., STARODUB, N. F., SANDROVSKY, A. K. & EL'SKAYA, A. K. (1995) Determination of urea in blood serum by a urease biosensor based on an ion-sensitive field-effect transistor. *Sensors and Actuators B: Chemical*, 27, 429-431.
- BROWN, D. V. & MEYERHOFF, M. E. (1991) Potentiometric enzyme channeling immunosensor for proteins. *Biosensors and Bioelectronics*, 6, 615-622.
- BUSCH, M. S. A. & KNAPP, E.-W. (2004) Accurate pK_a Determination for a Heterogeneous Group of Organic Molecules. *ChemPhysChem*, 5, 1513-1522.
- CADUFF, A., HIRT, E., FELDMAN, Y., ALI, Z. & HEINEMANN, L. (2003) First human experiments with a novel non-invasive, non-optical continuous glucose monitoring system. *Biosensors and Bioelectronics*, 19, 209-217.
- CHENG, Z., WANG, E. & YANG, X. (2001) Capacitive detection of glucose using molecularly imprinted polymers. *Biosensors and Bioelectronics*, 16, 179-185.
- CHIANELLA, I., KARIM, K., PILETSKA, E. V., PRESTON, C. & PILETSKY, S. A. (2006) Computational design and synthesis of molecularly imprinted polymers with high binding capacity for pharmaceutical applications-model case: Adsorbent for abacavir. *Analytica Chimica Acta*, 559, 73-78.
- CODMAN. (2001) Neurotrend: Cerebral tissue monitoring system. <http://www.jnjgateway.com>.
- COONEY, C. G. & TOWE, B. C. (1997) Intravascular carbon dioxide monitoring using micro-flow colorimetry. *Biosensors and Bioelectronics*, 12, 11-17.
- COONEY, C. G. & TOWE, B. C. (2000) A miniaturized pH and pCO_2 intravascular catheter using optical monitoring and a dual concentric-flow microdialysis approach. *Sensors and Actuators B: Chemical*, 62, 177-181.
- CORTINA, M., ESPLANDIU, M. J., ALEGRET, S. & DEL VALLE, M. (2006) Urea impedimetric biosensor based on polymer degradation onto interdigitated electrodes. *Sensors and Actuators B: Chemical*, 118, 84-89.
- CREAGER, S. E., HOCKETT, L. A. & ROWE, G. K. (1992) Consequences of microscopic surface roughness for molecular self-assembly. *Langmuir*, 8, 854-861.

- CUI, C. Q., ONG, L. H., TAN, T. C. & LEE, J. Y. (1993) Extent of incorporation of hydrolysis products in polyaniline films deposited by cyclic potential sweep. *Electrochimica Acta*, 38, 1395-1404.
- DARAIN, F., PARK, S. U. & SHIM, Y. B. (2003) Disposable amperometric immunosensor system for rabbit IgG using a conducting polymer modified screen-printed electrode. *Biosensors and Bioelectronics*, 18, 773-780.
- DAVIES, M. P., DE BIASI, V. & PERRETT, D. (2004) Approaches to the rational design of molecularly imprinted polymers. *Analytica Chimica Acta*, 504, 7-14.
- DE BOER, B., SIMON, H. K., WERTS, M. P. L., VAN DER VEGTE, E. W. & HADZIOANNOU, G. (2000) "Living" Free Radical Photopolymerization Initiated from Surface-Grafted Iniferter Monolayers. *Macromolecules*, 33, 349-356.
- DELANEY, T. L., ZIMIN, D., RAHM, M., WEISS, D., WOLFBEIS, O. S. & MIRSKY, V. M. (2007) Capacitive Detection in Ultrathin Chemosensors Prepared by Molecularly Imprinted Grafting Photopolymerization. *Anal. Chem.*, 79, 3220-3225.
- DOBAY, R., HARSANYI, G. & VISY, C. (1999) Detection of uric acid with a new type of conducting polymer-based enzymatic sensor by bipotentiostatic technique. *Analytica Chimica Acta*, 385, 187-194.
- DONG, W., YAN, M., ZHANG, M., LIU, Z. & LI, Y. (2005) A computational and experimental investigation of the interaction between the template molecule and the functional monomer used in the molecularly imprinted polymer. *Analytica Chimica Acta*, 542, 186-192.
- DOWRIE, R. H., EBLING, W. F., MANDEMA, J. W. & STANSKI, D. R. (1996) High-performance liquid chromatographic assay of propofol in human and rat plasma and fourteen rat tissues using electrochemical detection. *J Chromatogr B Biomed Appl*, 678, 279-88.
- EGGENSTEIN, C., BORCHARDT, M., DIEKMANN, C., BERND, G., DUMSCHAT, C., CAMMANN, K., KNOLL, M. & FRIEDRICH, S. (1999) A disposable biosensor for urea determination in blood based on an ammonium-sensitive transducer. *Biosensors and Bioelectronics*, 14, 33-41.
- ELLMERER, M., SCHAUPP, L., TRAJANOSKI, Z., JOBST, G., MOSER, I., URBAN, G., SKRABAL, F. & WACH, P. (1998) Continuous measurement of subcutaneous lactate concentration during exercise by combining open-flow microperfusion and thin-film lactate sensors. *Biosensors and Bioelectronics*, 13, 1007-1013.
- ESPADAS-TORRE, C., OKLEJAS, V., MOWERY, K. & MEYERHOFF, M. E. (1997) Thromboresistant Chemical Sensors Using Combined Nitric Oxide Release/Ion Sensing Polymeric Films. *J. Am. Chem. Soc.*, 119, 2321-2322.
- EUBEL, R. A., WIUM, C. A., HAWTREY, A. O. & COETZEE, J. (1990) Electrochemical determination of 2,6-diisopropylphenol after high-performance liquid chromatography of extracts from serum. *Journal of Chromatography B: Biomedical Sciences and Applications*, 526, 293-295.

- FARRINGTON, K. & REGAN, F. (2007) Investigation of the nature of MIP recognition: The development and characterisation of a MIP for Ibuprofen. *Biosensors and Bioelectronics*, 22, 1138-1146.
- FERANCOVA, A., KORGOVA, E., BUZINKAIOVA, T., KUTNER, W., STEPANEK, I. & LABUDA, J. (2001) Electrochemical sensors using screen-printed carbon electrode assemblies modified with the [beta]-cyclodextrin or carboxymethylated [beta]-cyclodextrin polymer films for determination of tricyclic antidepressive drugs. *Analytica Chimica Acta*, 447, 47-54.
- FERREIRA, V. S., ZANONI, M. V. B. & FOGG, A. G. (1997) Cathodic Stripping Voltammetric Determination of Ceftazidime in Urine at a Hanging Mercury Drop Electrode. *Microchemical Journal*, 57, 115-122.
- FROST, M. C. & MEYERHOFF, M. E. (2002) Implantable chemical sensors for real-time clinical monitoring: progress and challenges. 6, 633-641.
- GANTER, M. T., HOFER, C. K., ZOLLINGER, A., SPAHR, T., PASCH, T. & ZALUNARDO, M. P. (2004) Accuracy and performance of a modified continuous intravascular blood gas monitoring device during thoracoscopic surgery. *Journal of Cardiothoracic and Vascular Anesthesia*, 18, 587-591.
- GERRITSEN, M., JANSEN, J. A. & LUTTERMAN, J. A. (1999) Performance of subcutaneously implanted glucose sensors for continuous monitoring. *The Netherlands Journal of Medicine*, 54, 167-179.
- GFRERER, R. J., BRUNNER, G. A., TRAJANOSKI, Z., SCHAUPP, L., SENDLHOFER, G., SKRABAL, F., JOBST, G., MOSER, I., URBAN, G., PIEBER, T. R. & WACH, P. (1998) Novel system for real-time ex vivo lactate monitoring in human whole blood. *Biosensors and Bioelectronics*, 13, 1271-1278.
- GHINAMI, C., GIULIANI, V., MENARINI, A., ABALLE, F., TRAVAINI, S. & LADISA, T. (2007) Electrochemical detection of tobramycin or gentamicin according to the European Pharmacopoeia analytical method. *Journal of Chromatography A*, 1139, 53-56.
- GONG, F. C., ZHANG, X. B., GUO, C. C., SHEN, G. L. & YU, R. Q. (2003) Amperometric metronidazole sensor based on the supermolecular recognition by metalloporphyrin incorporated in carbon paste electrode. *Sensors*, 3, 91.
- GONG, J.-L., GONG, F.-C., KUANG, Y., ZENG, G.-M., SHEN, G.-L. & YU, R.-Q. (2004) Capacitive chemical sensor for fenvalerate assay based on electropolymerized molecularly imprinted polymer as the sensitive layer. *Analytical and Bioanalytical Chemistry*, 379, 302-307.
- GUMBRECHT, W., SCHELTER, W., MONTAG, B., RASINSKI, M. & PFEIFFER, U. (1990) Online blood electrolyte monitoring with a ChemFET microcell system. *Sensors and Actuators B: Chemical*, 1, 477-480.
- GUO, L.-H., FACCI, J. S., MCLENDON, G. & MOSHER, R. (1994) Effect of Gold Topography and Surface Pretreatment on the Self-Assembly of Alkanethiol Monolayers. *Langmuir*, 10, 4588-4593.

- GUTIERREZ, M., ALEGRET, S. & DEL VALLE, M. (2007) Potentiometric bioelectronic tongue for the analysis of urea and alkaline ions in clinical samples. *Biosensors and Bioelectronics*, 22, 2171-2178.
- HARWOOD, G. W. J. & POUTON, C. W. (1996) Amperometric enzyme biosensors for the analysis of drugs and metabolites. *Advanced Drug Delivery Reviews*, 18, 163-191.
- HAUPT, K. & MOSBACH, K. (2000) Molecularly Imprinted Polymers and Their Use in Biomimetic Sensors. *Chem. Rev.*, 100, 2495-2504.
- HEINZE, J. (1993) Ultramicroelectrodes in electrochemistry. *Angewandte Chemie (International Edition in English)*, 32, 1268-1288.
- HENG, L. Y. & HALL, E. A. H. (2001) Assessing a photocured self-plasticised acrylic membrane recipe for Na⁺ and K⁺ ion selective electrodes. 443, 25-40.
- HENZE, D., BOMPLITZ, M., RADKE, J. & CLAUSEN, T. (2004) Reliability of the NeuroTrend sensor system under hyperbaric conditions. 132, 45-56.
- HERNANDEZ, L., ZAPARDIEL, A., PEREZ LOPEZ, J. A. & BERMEJO, E. (1988) Measurement of nanomolar levels of psychoactive drugs in urine by adsorptive stripping voltammetry. *Talanta*, 35, 287-292.
- HERREJON, A., INCHAURRAGA, I., PALOP, J., PONCE, S., PERIS, R., TERRADEZ, M. & BLANQUER, R. (2006) Usefulness of Transcutaneous Carbon Dioxide Pressure Monitoring to Measure Blood Gases in Adults Hospitalized for Respiratory Disease. *Archivos de Bronconeumologia*, 42, 225-229.
- HIANIK, T., SNEJDARKOVA, M., SOKOLIKOVA, L., MESZAR, E., KRIVANEK, R., TVAROZEK, V., NOVOTNY, I. & WANG, J. (1999) Immunosensors based on supported lipid membranes, protein films and liposomes modified by antibodies. *Sensors and Actuators, B: Chemical*, 57, 201-212.
- HILLBERG, A. L., BRAIN, K. R. & ALLENDER, C. J. (2005) Molecular imprinted polymer sensors: Implications for therapeutics. *Molecularly Imprinted Polymers: Technology and Applications*, 57, 1875-1889.
- HONG, S., JAMES, E. M., CARL, J. S., HARRY, B. M., JR. & WILLIAM, R. H. (1997) Blocking behavior of self-assembled monolayers on gold electrodes. *Journal of Solid State Electrochemistry*, V1, 148.
- HU, S. Q., WU, Z. Y., ZHOU, Y. M., CAO, Z. X., SHEN, G. L. & YU, R. Q. (2002) Capacitive immunosensor for transferrin based on an o-aminobenzenthiole oligomer layer. *Analytica Chimica Acta*, 458, 297-304.
- HUANG, K.-J., LUO, D.-F., XIE, W.-Z. & YU, Y.-S. Sensitive voltammetric determination of tyrosine using multi-walled carbon nanotubes/4-aminobenzenesulfonic acid film-coated glassy carbon electrode. *Colloids and Surfaces B: Biointerfaces*, In Press, Corrected Proof.
- HWANG, E., PAPPAS, D., MATHEW, G., JEEVARAJAN, A. S. & ANDERSON, M. M. (2005) Paratrend Sensor Evaluation.

- IGUCHI, S., MITSUBAYASHI, K., UEHARA, T. & OGAWA, M. (2005) A wearable oxygen sensor for transcutaneous blood gas monitoring at the conjunctiva. *Sensors and Actuators B: Chemical*, 108, 733-737.
- JIN, M., YU, Z. & XIA, Y. (2006) Electrochemical and spectroelectrochemical studies on aniline in organic medium and its antiknock mechanism. *Russian Journal of Electrochemistry*, 42, 964-968.
- KAIMORI, S., KITAMURA, T., ICHINO, M., HOSOYA, T., KURUSU, F., ISHIKAWA, T., NAKAMURA, H., GOTOH, M. & KARUBE, I. (2006) Structural development of a minimally invasive sensor chip for blood glucose monitoring. *Analytica Chimica Acta*, 573-574, 104-109.
- KAINE, L. A. & WOLNIK, K. A. (1994) Forensic investigation of gentamicin sulfates by anion-exchange ion chromatography with pulsed electrochemical detection. *Journal of Chromatography A*, 674, 255-261.
- KANNURPATTI, A. R., LU, S., BUNKER, G. M. & BOWMAN, C. N. (1996) Kinetic and Mechanistic Studies of Iniferter Photopolymerizations. *Macromolecules*, 29, 7310-7315.
- KAPETANOVIC, V., DIMITROVSKA, A. & ZIVANOV-STAKIC, D. (1992) Differential pulse polarographic determination of cefoxitin. *Farmaco*, 47, 1429-1435.
- KELLY, S., COMPAGNONE, D. & GUILBAULT, G. (1998) Amperometric immunosensor for lactate dehydrogenase LD-1. *Biosensors and Bioelectronics*, 13, 173-179.
- KHANNA, A. & KURTZMAN, N. A. (2006) Metabolic alkalosis. *Journal of Nephrology*, 19, 10.
- KIM, N., PARK, I.-S. & KIM, D.-K. (2004) Characteristics of a label-free piezoelectric immunosensor detecting *Pseudomonas aeruginosa*. *Sensors and Actuators B: Chemical*, 100, 432-438.
- KNICHEL, M., HEIDUSCHKA, P., BECK, W., JUNG, G. & GOEPEL, W. (1995) Utilization of a self-assembled peptide monolayer for an impedimetric immunosensor. *Sensors and Actuators, B: Chemical*, B28, 85-94.
- KOBOS, R. K. (1987) ENZYME-BASED ELECTROCHEMICAL BIOSENSORS. *TrAC - Trends in Analytical Chemistry*, 6, 6-9.
- KRAUSE, C., MIRSKY, V. M. & HECKMANN, K. D. (1996) Capacitive detection of surfactant adsorption on hydrophobized gold electrodes. *Langmuir*, 12, 6059-6064.
- KRIZ, D. & MOSBACH, K. (1995) Competitive amperometric morphine sensor based on an agarose immobilised molecularly imprinted polymer. *Analytica Chimica Acta*, 300, 71-75.
- KULAPINA, E. G., BARAGUZINA, V. V. & KULAPINA, O. I. (2004) Ionometric determination of gentamicin and kanamycin in biological fluids and ready-to-use medicinal forms. *Pharmaceutical Chemistry Journal*, 38, 513-516.
- LA-SCALEA, M. A., SERRANO, S. H. P. & GUTZ, I. G. R. (1999) Voltammetric Behaviour of Metronidazole at Mercury Electrodes. *J. Braz. Chem. Soc.* [online]. 10, 127 - 135.

- LAKSHMI, D., BOSSI, A., WHITCOMBE, M., CHIANELLA, I., FOWLER, S., SUBRAHMANYAM, S., PILETSKA, E. & PILETSKY, S. (2009a) An Electrochemical Sensor for Catechol and Dopamine Based on a Catalytic Molecularly Imprinted Polymer-Conducting Polymer Hybrid Recognition Element. *Analytical Chemistry*, In Press.
- LAKSHMI, D., WHITCOMBE, M. J., DAVIS, F., CHIANELLA, I., PILETSKA, E. V., GUERREIRO, A., SUBRAHMANYAM, S., BRITO, P. S., FOWLER, S. A. & PILETSKY, S. A. (2009b) Chimeric Polymers Formed from a Monomer Capable of Free-Radical, Oxidative and Electrochemical Polymerisation. *Chemical Communications*, In Press.
- LAM, Y.-Z. & ATKINSON, J. K. (2007) Biomedical sensor using thick film technology for transcutaneous oxygen measurement. *Medical Engineering & Physics*, 29, 291-297.
- LE NOIR, M., PLIEVA, F., HEY, T., GUIEYSSE, B. & MATTIASSON, B. (2007) Macroporous molecularly imprinted polymer/cryogel composite systems for the removal of endocrine disrupting trace contaminants. *Journal of Chromatography A*, 1154, 158-164.
- LEE, Y.-C., CHO, B.-W., KIM, C.-S., KOH, K.-N. & SOHN, B.-K. (2000) A ISFET cartridge for electrolyte measurement by micromachinery. *Sensors and Actuators B: Chemical*, 65, 336-339.
- LI, C., WANG, C., WANG, C. & HU, S. (2005) Construction of a novel molecularly imprinted sensor for the determination of O,O-dimethyl-(2,4-dichlorophenoxyacetoxyl)(3'-nitrophenyl)methinephosphonate. *Analytica Chimica Acta*, 545, 122-128.
- LIAO, H., ZHANG, Z., LI, H., NIE, L. & YAO, S. (2004) Preparation of the molecularly imprinted polymers-based capacitive sensor specific for tegafur and its characterization by electrochemical impedance and piezoelectric quartz crystal microbalance. *Electrochimica Acta*, 49, 4101-4107.
- LIN, C. Y., HUNG, Y. C., LIU, C. M., LO, C. F., LIN, Y. C. & LIN, C. L. (2005) Synthesis, electrochemistry, absorption and electro-polymerization of aniline-ethynyl metalloporphyrins. *Dalton Transactions*, 396-401.
- LIU, K., WEI, W.-Z., ZENG, J.-X., LIU, X.-Y. & GAO, Y.-P. (2006) Application of a novel electrosynthesized polydopamine-imprinted film to the capacitive sensing of nicotine. *Analytical and Bioanalytical Chemistry*, 385, 724-729.
- LIU, Y., WANG, F., TAN, T. & LEI, M. (2007) Study of the properties of molecularly imprinted polymers by computational and conformational analysis. *Analytica Chimica Acta*, 581, 137-146.
- LIU, Z., HUANG, S., JIANG, D., LIU, B. & KONG, J. (2004) A Novel Capacitive Immunosensor Using Electropolymerized Insulating Poly (o-phenylenediamine) Film on a Glass Carbon Electrode for Probing Transferrin. *Analytical Letters*, 37, 2283 - 2301.

- LIYONG ZHANG, G. C., CONG FU, (2002) Molecular selectivity of tyrosine-imprinted polymers prepared by seed swelling and suspension polymerization. *Polymer International*, 51, 687-692.
- LOWINSOHN, D. & BERTOTTI, M. (2007) Flow injection analysis of blood l-lactate by using a Prussian Blue-based biosensor as amperometric detector. *Analytical Biochemistry*, 365, 260-265.
- LU, S., WU, K., DANG, X. & HU, S. (2004) Electrochemical reduction and voltammetric determination of metronidazole at a nanomaterial thin film coated glassy carbon electrode. 63, 653.
- LUO, N., BRIAN HUTCHISON, J., ANSETH, K. S. & BOWMAN, C. N. (2002) Synthesis of a novel methacrylic monomer iniferter and its application in surface photografting on crosslinked polymer substrates. *Journal of Polymer Science, Part A: Polymer Chemistry*, 40, 1885-1891.
- LUTGERS, H. L., HULLEGIE, L. M., HOOGENBERG, K., SLUITER, W. J., DULLAART, R. P. F., WIENTJES, K. J. & SCHOONEN, A. J. M. (2000) Microdialysis measurement of glucose in subcutaneous adipose tissue up to three weeks in Type 1 diabetic patients. *The Netherlands Journal of Medicine*, 57, 7-12.
- LY, S. Y. & KIM, Y. K. (2006) Assay of glucose in urine and drinking water with voltammetric working sensors of infrared photo diode electrode. *Sensors and Actuators A: Physical*, 127, 41-48.
- MAHONY, J. O., NOLAN, K., SMYTH, M. R. & MIZAIKOFF, B. (2005) Molecularly imprinted polymers--potential and challenges in analytical chemistry. *Analytica Chimica Acta*, 534, 31-39.
- MANDAL, P. C. (2004) Reactions of the nitro radical anion of metronidazole in aqueous and mixed solvent: a cyclic voltammetric study. 570, 55.
- MANYANGA, V., KREFT, K., DIVJAK, B., HOOGMARTENS, J. & ADAMS, E. (2008) Improved liquid chromatographic method with pulsed electrochemical detection for the analysis of gentamicin. *Journal of Chromatography A*, 1189, 347-354.
- MARTINS, M. C. L., FONSECA, C., BARBOSA, M. A. & RATNER, B. D. (2003) Albumin adsorption on alkanethiols self-assembled monolayers on gold electrodes studied by chronopotentiometry. *Biomaterials*, 24, 3697-3706.
- MATSUDA, T. & OHYA, S. (2005) Photoiniferter-Based Thermoresponsive Graft Architecture with Albumin Covalently Fixed at Growing Graft Chain End. *Langmuir*, 21, 9660-9665.
- MEYERHOFF, M. E. (1993) In vivo blood-gas and electrolyte sensors: Progress and challenges. *TrAC Trends in Analytical Chemistry*, 12, 257-266.
- MIRSKY, V. M., KRAUSE, C. & HECKMANN, K. D. (1996) Capacitive sensor for lipolytic enzymes. *Thin Solid Films*, 284-285, 939-941.
- MIRSKY, V. M., MASS, M., KRAUSE, C. & WOLFBEIS, O. S. (1998) Capacitive Approach to Determine Phospholipase A2 Activity toward Artificial and Natural Substrates. *Analytical Chemistry*, 70, 3674-3678.

- MIRSKY, V. M., RIEPL, M. & WOLFBEIS, O. S. (1997) Capacitive monitoring of protein immobilization and antigen-antibody reactions on monomolecular alkylthiol films on gold electrodes. *Biosensors and Bioelectronics*, 12, 977-989.
- MIYAHARA, Y., TSUKADA, K., MIYAGI, H. & SIMON, W. (1991) Urea sensor based on an ammonium-ion-sensitive field-effect transistor. *Sensors and Actuators B: Chemical*, 3, 287-293.
- MOHAMED, R., MOTTIER, P., TREGUIER, L., RICHOSZ-PAYOT, J., YILMAZ, E., TABET, J. C. & GUY, P. A. (2008) Use of molecularly imprinted solid-phase extraction sorbent for the determination of four 5-nitroimidazoles and three of their metabolites from egg-based samples before tandem LC-ESIMS/MS analysis. *Journal of Agricultural and Food Chemistry*, 56, 3500-3508.
- MYLES, P. S., BUCKLAND, M. R., WEEKS, A. M., BUJOR, M. & MOLONEY, J. (1999) Continuous arterial blood gas monitoring during bilateral sequential lung transplantation. *Journal of Cardiothoracic and Vascular Anesthesia*, 13, 253-257.
- NAVARRO-VILLOSLADA, F., ORELLANA, G., MORENO-BONDI, M. C., VICK, T., DRIVER, M., HILDEBRAND, G. & LIEFEITH, K. (2001) Fiber-Optic Luminescent Sensors with Composite Oxygen-Sensitive Layers and Anti-Biofouling Coatings. *Anal. Chem.*, 73, 5150-5156.
- NICHOLLS, I. A. (1998) Towards the rational design of molecularly imprinted polymers. *Journal of Molecular Recognition*, 11, 79-82.
- O'MAHONY, J., MOLINELLI, A., NOLAN, K., SMYTH, M. R. & MIZAIKOFF, B. (2005) Towards the rational development of molecularly imprinted polymers: ¹H NMR studies on hydrophobicity and ion-pair interactions as driving forces for selectivity. *Biosensors and Bioelectronics*, 20, 1884-1893.
- O'MAHONY, J., MOLINELLI, A., NOLAN, K., SMYTH, M. R. & MIZAIKOFF, B. (2006) Anatomy of a successful imprint: Analysing the recognition mechanisms of a molecularly imprinted polymer for quercetin. *Biosensors and Bioelectronics*, 21, 1383-1392.
- OGOREVC, B. & GOMISCEK, S. (1991) Electrochemical analysis of cephalosporin antibiotics. *Journal of Pharmaceutical and Biomedical Analysis*, 9, 225-236.
- OGOREVC, B., KRASNA, A., HUDNIK, V. & GOMISCEK, S. (1991) Adsorptive stripping voltammetry of selected cephalosporin antibiotics and their direct determination in urine. *Mikrochimica Acta*, 103, 131-144.
- OLIVEIRA BRETT, A. M., SERRANO, S. H. P., GUTZ, I. & LA-SCALEA, M. A. (1997a) Electrochemical reduction of metronidazole at a DNA-modified glassy carbon electrode. *13th International Symposium on Bioelectrochemistry and Bioenergetics*, 42, 175-178.
- OLIVEIRA BRETT, A. M., SERRANO, S. H. P., GUTZ, I. G. R. & LA-SCALEA, M. A. (1997b) Comparison of the Voltammetric Behavior of Metronidazole at a DNA-Modified Glassy Carbon Electrode, a Mercury Thin Film Electrode and a Glassy Carbon Electrode. *Electroanalysis*, 9, 110.

- OTSU, T. & KURIYAMA, A. (1984) Living mono- and biradical polymerizations in homogeneous system synthesis of AB and ABA type block copolymers. *Polymer Bulletin*, 11, 135-142.
- OZKAN, S. A., OZKAN, Y. & SİŞENTUĞRK, Z. (1998) Electrochemical reduction of metronidazole at activated glassy carbon electrode and its determination in pharmaceutical dosage forms. *Journal of Pharmaceutical and Biomedical Analysis*, 17, 299-305.
- PANASYUK-DELANEY, T., MIRSKY, V. M., ULBRICHT, M. & WOLFBEIS, O. S. (2001) Impedometric herbicide chemosensors based on molecularly imprinted polymers. *Analytica Chimica Acta*, 435, 157-162.
- PANASYUK-DELANEY, T., MIRSKY, V. M. & WOLFBEIS, O. S. (2002) Capacitive creatinine sensor based on a photografted molecularly imprinted polymer. *Electroanalysis*, 14, 221-224.
- PANASYUK, T. L., MIRSKY, V. M., PILETSKY, S. A. & WOLFBEIS, O. S. (1999) Electropolymerized Molecularly Imprinted Polymers as Receptor Layers in Capacitive Chemical Sensors. *Anal. Chem.*, 71, 4609-4613.
- PFEIFFER, D., MOLLER, B., KLIMES, N., SZEPONIK, J. & FISCHER, S. (1997) Amperometric lactate oxidase catheter for real-time lactate monitoring based on thin film technology. *Biosensors and Bioelectronics*, 12, 539-550.
- PILETSKY, S. A., KARIM, K., PILETSKA, E. V., DAY, C. J., FREEBAIRN, K. W., LEGGE, C. & TURNER, A. P. F. (2001) Recognition of ephedrine enantiomers by molecularly imprinted polymers designed using a computational approach. *Analyst*, 126, 1826-1830.
- PILETSKY, S. A., PILETSKA, E. V., CHEN, B., KARIM, K., WESTON, D., BARRETT, G., LOWE, P. & TURNER, A. P. F. (2000) Chemical grafting of molecularly imprinted homopolymers to the surface of microplates. Application of artificial adrenergic receptor in enzyme-linked assay for β -agonists determination. *Analytical Chemistry*, 72, 4381-4385.
- PILETSKY, S. A., PILETSKAYA, E. V., PANASYUK, T. L., EL'SKAYA, A. V., LEVI, R., KARUBE, I. & WULFF, G. (1998) Imprinted membranes for sensor technology: opposite behavior of covalently and noncovalently imprinted membranes. *Macromolecules*, 31, 2137-2140.
- PILETSKY, S. A., PILETSKAYA, E. V., SERGEYEVA, T. A., PANASYUK, T. L. & EL'SKAYA, A. V. (1999) Molecularly imprinted self-assembled films with specificity to cholesterol. *Sensors and Actuators, B: Chemical*, 60, 216-220.
- PILETSKY, S. A., TURNER, N. W. & LAITENBERGER, P. (2006) Molecularly imprinted polymers in clinical diagnostics-Future potential and existing problems. *Medical Engineering and Physics*, 28, 971-977.
- PISSINIS, D. E. & MARIOLI, J. M. (2007) Electrochemical detection of 2,6-diisopropylphenol (propofol) in reversed phase HPLC at high pH. *Journal of Liquid Chromatography and Related Technologies*, 30, 1787-1795.

- PLUMMER, G. F. (1987) Improved method for the determination of propofol in blood by high-performance liquid chromatography with fluorescence detection. *Journal of Chromatography: Biomedical Applications*, 421, 171-176.
- RAIBER, K., TERFORT, A., BENNDORF, C., KRINGS, N. & STREHBLow, H.-H. (2005) Removal of self-assembled monolayers of alkanethiolates on gold by plasma cleaning. *Surface Science*, 595, 56-63.
- RHEMREV-BOOM, M. M., KORF, J., VENEMA, K., URBAN, G. & VADGAMA, P. (2001) A versatile biosensor device for continuous biomedical monitoring. *Biosensors and Bioelectronics*, 16, 839-847.
- RICKERT, J., GOPEL, W., BECK, W., JUNG, G. & HEIDUSCHKA, P. (1996) A 'mixed' self-assembled monolayer for an impedimetric immunosensor. *Biosensors and Bioelectronics*, 11, 757-768.
- RIEPL, M., MIRSKY, V. M., NOVOTNY, I., TVAROZEK, V., REHACEK, V. & WOLFBEIS, O. S. (1999a) Optimization of capacitive affinity sensors: Drift suppression and signal amplification. *Analytica Chimica Acta*, 392, 77-84.
- RIEPL, M., MIRSKY, V. M. & WOLFBEIS, O. S. (1999b) Electrical control of alkanethiols self-assembly on a gold surface as an approach for preparation of microelectrode arrays. *Mikrochimica Acta*, 131, 29-34.
- ROLFE, P. (1988) Review of chemical sensors for physiological measurement. *Journal of Biomedical Engineering*, 10, 138-145.
- RON, H., MATLIS, S. & RUBINSTEIN, I. (1998) Self-Assembled Monolayers on Oxidized Metals. 2. Gold Surface Oxidative Pretreatment, Monolayer Properties, and Depression Formation. *Langmuir*, 14, 1116-1121.
- RON, H. & RUBINSTEIN, I. (1994) Alkanethiol Monolayers on Preoxidized Gold. Encapsulation of Gold Oxide under an Organic Monolayer. *Langmuir*, 10, 4566-4573.
- RUCKERT, B., HALL, A. J. & SELLERGRÉN, B. (2002) Molecularly imprinted composite materials via iniferter-modified supports. *Journal of Materials Chemistry*, 12, 2275-2280.
- SALVADOR, J. P., ESTEVEZ, M. C., MARCO, M. P. & SANCHEZ-BAEZA, F. (2007) A new methodology for the rational design of molecularly imprinted polymers. *Analytical Letters*, 40, 1294-1306.
- SANT, W., POURCIEL-GOUZY, M. L., LAUNAY, J., DO CONTO, T., COLIN, R., MARTINEZ, A. & TEMPLE-BOYER, P. (2004) Development of a creatinine-sensitive sensor for medical analysis. *Sensors and Actuators B: Chemical*, 103, 260-264.
- SCHEIPERS, A., WAMUS, O., SUNDERMEIER, C., ESHOLD, J., WEI, T., GITTER, M., RO, B. & KNOLL, M. (2001) Potentiometric ion-selective silicon sensors for the on-line monitoring of blood electrolytes. 439, 29.
- SCHNAKENBERG, U., LISEC, T., HINTSCHE, R., KUNA, I., UHLIG, A. & WAGNER, B. (1996) Novel potentiometric silicon sensor for medical devices. *Sensors and Actuators B: Chemical*, 34, 476-480.

- SCHOENFISCH, M. H., MOWERY, K. A., RADER, M. V., BALIGA, N., WAHR, J. A. & MEYERHOFF, M. E. (2000) Improving the Thromboresistivity of Chemical Sensors via Nitric Oxide Release: Fabrication and in Vivo Evaluation of NO-Releasing Oxygen-Sensing Catheters. *Anal. Chem.*, 72, 1119-1126.
- SCHREIBER, F. (2000) Structure and growth of self-assembling monolayers. *Progress in Surface Science*, 65, 151-256.
- SHAHROKHIAN, S., KARIMI, M. & KHAJEHSHARIFI, H. (2005) Carbon-paste electrode modified with cobalt-5-nitrosalophen as a sensitive voltammetric sensor for detection of captopril. *Sensors and Actuators B: Chemical*, 109, 278-284.
- SHEPPARD, N. F., MEARS, D. J. & GUISEPPI-ELIE, A. (1996) Model of an immobilized enzyme conductimetric urea biosensor. *Biosensors and Bioelectronics*, 11, 967-979.
- SHERVEDANI, R. K., MEHRJARDI, A. H. & ZAMIRI, N. (2006) A novel method for glucose determination based on electrochemical impedance spectroscopy using glucose oxidase self-assembled biosensor. *Bioelectrochemistry*, 69, 201-208.
- SINGH, N., CUI, X., BOLAND, T. & HUSSON, S. M. (2007) The role of independently variable grafting density and layer thickness of polymer nanolayers on peptide adsorption and cell adhesion. 28, 763-771.
- SKOOG, D. A. (2000) *Analytical chemistry: an introduction*, Saunders College.
- SMITH, I., WHITE, P. F., NATHANSON, M. & GOULDSON, R. (1994) Propofol: An update on its clinical use. *Anesthesiology*, 81, 1005-1043.
- SOLE, S., ALEGRET, S., CESPEDES, F., FABREGAS, E. & DIEZ-CABALLERO, T. (1998) Flow Injection Immunoanalysis Based on a Magnetoimmunosensor System. *Analytical Chemistry*, 70, 1462-1467.
- SPURLOCK, L. D., JARAMILLO, A., PRASERTHDAM, A., LEWIS, J. & BRAJTER-TOTH, A. (1996) Selectivity and sensitivity of ultrathin purine-templated overoxidized polypyrrole film electrodes. *Analytica Chimica Acta*, 336, 37-46.
- STUART, A. & FOULKES, F. (1988) Study of ECE reactions with multiple parallel chemical steps using linear scan voltammetry. *Electrochimica Acta*, 33, 1411-1424.
- SUBRAHMANYAM, S., PILETSKY, S. A., PILETSKA, E. V., CHEN, B., KARIM, K. & TURNER, A. P. F. (2001) 'Bite-and-Switch' approach using computationally designed molecularly imprinted polymers for sensing of creatinine. *Biosensors and Bioelectronics*, 16, 631-637.
- SULEIMAN, A. A. & XU, Y. (1998) An Amperometric Immunosensor for Cocaine. *Electroanalysis*, 10, 240-243.
- SUZUKI, H., ARAKAWA, H. & KARUBE, I. (2001) Fabrication of a sensing module using micromachined biosensors. *Biosensors and Bioelectronics*, 16, 725-733.
- TREMILIOSI-FILHO, G., GONZALEZ, E. R., MOTHEO, A. J., BELGSIR, E. M., LÉGER, J. M. & LAMY, C. (1998) Electro-oxidation of ethanol on gold: analysis of the reaction products and mechanism. *Journal of Electroanalytical Chemistry*, 444, 31-39.

- TURA, A., SBRIGNADELLO, S., BARISON, S., CONTI, S. & PACINI, G. (2007) Impedance spectroscopy of solutions at physiological glucose concentrations. *Biophysical Chemistry*, 129, 235-241.
- TURKEWITSCH, P., WANDEL, B., DARLING, G. D. & POWELL, W. S. (1998) Fluorescent Functional Recognition Sites through Molecular Imprinting. A Polymer-Based Fluorescent Chemosensor for Aqueous cAMP. *Analytical Chemistry*, 70, 2025-2030.
- TWARDOWSKI, M. & NUZZO, R. G. (2002) Chemically Mediated Grain Growth in Nanotextured Au, Au/Cu Thin Films: Novel Substrates for the Formation of Self-Assembled Monolayers. *Langmuir*, 18, 5529-5538.
- VAN ES, R. M., SETFORD, S. J., BLANKWATER, Y. J. & MEIJER, D. (2001) Detection of gentamicin in milk by immunoassay and flow injection analysis with electrochemical measurement. *Analytica Chimica Acta*, 429, 37-47.
- VEL KRAWCZYK, T. K., TROJANOWICZ, M. & LEWENSTAM, A. (1994) Enzymatic flow-injection determination of urea in blood serum using potentiometric gas sensor with internal nonactin based ISE. *Talanta*, 41, 1229-1236.
- VERRELLI, G., FRANCIOSO, L., PAOLESSE, R., SICILIANO, P., DI NATALE, C., D'AMICO, A. & LOGRIECO, A. (2007) Development of silicon-based potentiometric sensors: Towards a miniaturized electronic tongue. *Sensors and Actuators B: Chemical*, 123, 191-197.
- VOSTIAR, I., TKAC, J., STURDIK, E. & GEMEINER, P. (2002) Amperometric urea biosensor based on urease and electropolymerized toluidine blue dye as a pH-sensitive redox probe. *Bioelectrochemistry*, 56, 113-115.
- WANG, J. (1999) Amperometric biosensors for clinical and therapeutic drug monitoring: a review. *Journal of Pharmaceutical and Biomedical Analysis*, 19, 47-53.
- WANG, J. (2000) *Analytical Electrochemistry*, Wiley-VCH.
- WANG, J. (2006) *Analytical electrochemistry*, John Wiley & Sons, Inc.
- WANG, J. & YOON, R.-H. (2008) AFM Forces Measured between Gold Surfaces Coated with Self-Assembled Monolayers of 1-Hexadecanethiol. *Langmuir*, 24, 7889-7896.
- WANG, W., GAO, S. & WANG, B. (1999) Building fluorescent sensors by template polymerization: The preparation of a fluorescent sensor for d-Fructose. *Organic Letters*, 1, 1209-1212.
- WANG, Z., ZHOU, H. & ZHOU, S. (1993) Study on the determination of metronidazole in human serum by adsorptive stripping voltammetry. 40, 1073.
- WEI, S., JAKUSCH, M. & MIZAIKOFF, B. (2006) Capturing molecules with templated materials-Analysis and rational design of molecularly imprinted polymers. *Analytica Chimica Acta*, 578, 50-58.
- WEN, T. C., SIVAKUMAR, C. & GOPALAN, A. (2002) In-situ spectroelectrochemical evidences for the copolymerization of o-toluidine with diphenylamine-4-sulphonic acid by UV-visible spectroscopy. *Spectrochimica Acta - Part A Molecular and Biomolecular Spectroscopy*, 58, 167-177.

- WIENJES, K. J., VONK, P., VONK-VAN KLEI, Y., SCHOONEN, A. J. M. & KOSSEN, N. W. (1998) Microdialysis of glucose in subcutaneous adipose tissue up to 3 weeks in healthy volunteers. *Diabetes Care*, 21, 1481-1488.
- WILLIAMS, R. A. & BLANCH, H. W. (1994) Covalent immobilization of protein monolayers for biosensor applications. *Biosensors and Bioelectronics*, 9, 159-167.
- WISNIEWSKI, N. & REICHERT, M. (2000) Methods for reducing biosensor membrane biofouling. *Colloids and Surfaces B: Biointerfaces*, 18, 197-219.
- WODERER, S., HENNINGER, N., GARTHE, C.-D., KLOETZER, H. M., HAJNSEK, M., KAMECKE, U., GRETZ, N., KRAENZLIN, B. & PILL, J. (2007) Continuous glucose monitoring in interstitial fluid using glucose oxidase-based sensor compared to established blood glucose measurement in rats. *Analytica Chimica Acta*, 581, 7-12.
- WU, L. & LI, Y. (2004) Study on the recognition of templates and their analogues on molecularly imprinted polymer using computational and conformational analysis approaches. *Journal of Molecular Recognition*, 17, 567-574.
- WU, Y., ROJAS, A. P., GRIFFITH, G. W., SKRZYPCHAK, A. M., LAFAYETTE, N., BARTLETT, R. H. & MEYERHOFF, M. E. (2007) Improving blood compatibility of intravascular oxygen sensors via catalytic decomposition of S-nitrosothiols to generate nitric oxide in situ. *Sensors and Actuators B: Chemical*, 121, 36-46.
- XU, J. & LI, H. (1995) The Chemistry of Self-Assembled Long-Chain Alkanethiol Monolayers on Gold. *Journal of Colloid and Interface Science*, 176, 138-149.
- YANG, L., WEI, W., XIA, J. & TAO, H. (2004) Artificial Receptor Layer for Herbicide Detection Based on Electrosynthesized Molecular Imprinting Technique and Capacitive Transduction. *Analytical Letters*, 37, 2303 - 2319.
- YANG, L., WEI, W., XIA, J., TAO, H. & YANG, P. (2005) Capacitive Biosensor for Glutathione Detection Based on Electropolymerized Molecularly Imprinted Polymer and Kinetic Investigation of the Recognition Process. *Electroanalysis*, 17, 969-977.
- YANG, Y., ZHANG, S. F., KINGSTON, M. A., JONES, G., WRIGHT, G. & SPENCER, S. A. (2000) Glucose sensor with improved haemocompatibility. *Biosensors and Bioelectronics*, 15, 221-227.
- YAO, J., LI, X. & QIN, W. (2008) Computational design and synthesis of molecular imprinted polymers with high selectivity for removal of aniline from contaminated water. *Analytica Chimica Acta*, 610, 282-288.
- YIN, F. (2004) Capacitive sensors using electropolymerized o-phenylenediamine film doped with ion-pair complex as selective elements for the determination of pentoxifyverine. *Talanta*, 63, 641-646.
- YIN, F. & XU, X. (2004) Construction and Analytical Application of a Novel Ion-Selective Capacitive Sensor for Determination of Cinchonine. *Analytical Letters*, 37, 3129-3147.

- YOON, H. J., SHIN, J. H., LEE, S. D., NAM, H., CHA, G. S., STRONG, T. D. & BROWN, R. B. (2000) Solid-state ion sensors with a liquid junction-free polymer membrane-based reference electrode for blood analysis. *Sensors*, *64*, 8.
- ZHANG, H., ANNICH, G. M., MISKULIN, J., OSTERHOLZER, K., MERZ, S. I., BARTLETT, R. H. & MEYERHOFF, M. E. (2002) Nitric oxide releasing silicone rubbers with improved blood compatibility: preparation, characterization, and in vivo evaluation. *Biomaterials*, *23*, 1485-1494.
- ZHANG, L., ZHANG, C. & LIAN, J. (2008) Electrochemical synthesis of polyaniline nano-networks on p-aminobenzene sulfonic acid functionalized glassy carbon electrode. Its use for the simultaneous determination of ascorbic acid and uric acid. *Biosensors and Bioelectronics*, *24*, 690-695.
- ZHI, Y., HU, J., WU, Z. & LI, Q. (1998) Study on the voltammetric behavior of metronidazole and its determination at a Co/GC modified electrode. *Analytical Letters*, *31*, 429.
- ZUMAN, P., KAPETANOVIC, V. & ALEKSIC, M. (2000) Recent developments in electroanalytical chemistry of cephalosporins and cefamycins. *Analytical Letters*, *33*, 2821.

Publications

- LAKSHMI, D., BOSSI, A., WHITCOMBE, M., CHIANELLA, I., FOWLER, S., SUBRAHMANYAM, S., PILETSKA, E. & PILETSKY, S. (2009a) An Electrochemical Sensor for Catechol and Dopamine Based on a Catalytic Molecularly Imprinted Polymer-Conducting Polymer Hybrid Recognition Element. *Analytical Chemistry*, In Press.
- LAKSHMI, D., WHITCOMBE, M. J., DAVIS, F., CHIANELLA, I., PILETSKA, E. V., GUERREIRO, A., SUBRAHMANYAM, S., BRITO, P. S., FOWLER, S. A. & PILETSKY, S. A. (2009b) Chimeric Polymers Formed from a Monomer Capable of Free-Radical, Oxidative and Electrochemical Polymerisation. *Chemical Communications*, In Press.
- KYPRIANOU, D., GUERREIRO, A. R., CHIANELLA, I., PILETSKA, E. V., FOWLER, S. A., KARIM, K., WHITCOMBE, M. J., TURNER, A. P. F. & PILETSKY, S. A. (2009) New reactive polymer for protein immobilisation on sensor surfaces. *Biosensors and Bioelectronics*, 24, 1365-1371.

